THE INFLUENCE OF NITROGEN ON THE PLASTICITY OF DIAMOND

being a thesis submitted for the degree of

Doctor of Philosophy

at the University of Hull

by

Robert David Daniel, MEng (Hons)

September 2000

Abstract

The aim of this work has been to use the soft impressor technique to investigate the plastic deformation of single crystal diamond and in particular to determine the effect that single substitutional nitrogen has on plasticity.

Traditionally hardness tests in the form of Vickers or Knoop rigid indenters have been used to investigate the mechanical properties of materials which cannot be fabricated into tensile or three point bend test specimens. The high stress concentrations created by these types of test introduce a large degree of brittle failure in ultra-hard, covalently bonded materials. The soft impressor technique, on the other hand, allows large pressures to be applied without large stress concentrations. The result is that plastic deformation can be more readily induced into super hard materials such as diamond. This work has shown that not only can diamond be readily plastically deformed but that traces of nitrogen impurities within the lattice have a significant effect on the conditions necessary to produce dislocations.

For this work, several different soft impressors were used to produce a range of pressures in the temperature range 800° to 1400°C. A selection of synthetic (HPHT) diamonds with various nitrogen concentrations were impressed and compared with impressions placed in natural type IIa specimens containing no nitrogen but heavily dislocated. Numerous analytical techniques were used to determine the level of deformation produced and gain a better understanding of the effect of nitrogen related defects.

The first two chapters of this thesis review, first plasticity and then diamond, with reference to those properties/characteristics relevant to this topic. The third chapter discusses the principle of the soft impressor technique and the methodologies used. In the fourth chapter, models by which single crystal diamond plastically deforms are introduced, together with results that have extended the brittle-ductile transition schematic produced by Brookes, E.J. (1992). Results on the effect of dwell time and the phenomenon of impression creep are also presented. The fifth chapter identifies the predominant defects associated with substitutional nitrogen in HPHT diamond and presents profiles of impressions for diamonds with different 'grown-in' defect levels. The results are discussed and conclusions are made, in conjunction with suggestions for further work in chapter 6.

Acknowledgements

First of all I would like to thank my family (the MMs, the Ls and the blokes) for their support, and especially Mapi and Granddad for their vigilance.

Secondly, Dr Jill Brookes for her undying devotion to detail, her unending patience, and for giving me this opportunity in the first place.

Thirdly, the department (Engineering Design and Manufacture): Chris Ingleby whose technical expertise and know-how would be sorely missed and Gary Robinson without whom there wouldn't be so many nice pictures. Also my colleagues who have had the unenviable task of putting up with me both during my initiation period and the dark days of "writing-up".

Fourthly, thank you to all those at DeBeers, Charters and DTC for the money and for finally giving me the samples I wanted and then helping me understand my results. In addition I would like to thank all those people who have answered my many questions, you all helped to produce this thesis.

Finally, thank you to Rudolph and Femke for your equipment, your advice and for living somewhere outside Hull.

Table of Contents

Chapter 6: Discussion and Conclusions

Chapter 1

INTRODUCTION TO PLASTICITY

1.1 Introduction

There are two types of deformation that a material can undergo, elastic and plastic. Elastic deformation is where a material will change shape under the influence of a force, but upon the removal of the force the original form is returned, *e.g.* an elastic band. Plastic deformation is where the shape change produced by the force remains after the removal of that force. Both types of deformation have been known about and used for millennia. Elasticity, for instance, was used very effectively by the ancient Greeks to build bows and catapults, which rely heavily on the elastic properties of the wood from which they are made. The plastic properties of materials were probably the first to be put to use. Ever since man started to mould materials into the desired shape rather than making tools by chipping lumps off pieces of flint, he has been inadvertently making use of plasticity. However, only with the advent of the theory of crystallinity could the theory of plastic deformation really begin to be understood.

The theory of plasticity can be split up into two interdependent parts. The first part is the macroscopic view and deals with the consequences of plasticity such as ductility, work hardening and creep. The second part is the microscopic view, where the theory of dislocations and their interactions become important. In engineering, the main emphasis is on the stresses exerted on components under certain conditions and the consequences of those stresses. However, these calculations/predictions are meaningless without a measure of the strength of the material(s) used to make the component. The strength characteristics of a material can be gained by looking at its stress/strain diagram. The microscopic plastic deformation of a material becomes important when it is used to explain features on the stress/strain diagram, such as yield point or a brittle ductile transition temperature. Experimentation reported within this thesis has concentrated solely on the stress/strain diagram of single crystal diamond. Therefore, discussion will be confined to topics relevant to face centred cubic (f.c.c.) single crystals.

1.2 The Effects of Plastic Deformation

The most obvious consequence of the plasticity of a material is a change in shape without significant fracture. In engineering, the plasticity of a material is used to explain phenomena such as ductility, work hardening and creep. Each of these is an essential property to understand when using materials in modern-day engineering. The advent of cost effect manufacture has forced engineers to design and build with economy in mind. Techniques such as stress analysis have allowed design engineers to push the mechanical properties of materials to their limits in order to reduce the cost of manufacture by reducing the amount of material used. For this type of engineering to succeed, it is essential to fully understand the responses of the materials to stresses. In many respects, however, macroscopic investigations into the plastic behaviour of materials can be misleading or contradictory. This is because the level of plastic deformation depends on the type of experiment, its conditions and the criteria the experimentalist uses to quantify plasticity.

Ductility:

The ductility of a material is a measure of the response of a material to external forces, based on the ratio between brittle failure and plastic deformation. A material is said to be brittle if it fails catastrophically via a cleavage mechanism, whereas it is said to be ductile if it changes shape under the influence of an applied force. In reality, all materials possess both brittle and ductile characteristics, the degree to which each characteristic is dominant over the other depends on the experimental conditions. For instance glass is widely recognised to be a brittle material, however Joos (1957) showed experimentally that glass could behave in a plastic manner. In addition, when the experimental temperature of the glass was raised, its tendency to brittle behaviour was reduced until such point when it became molten. The influence of temperature on ductility has led to the concept of a brittle-ductile transition temperature (BDTT).

The BDTT is the temperature at which a material, under load, ceases to behave in a brittle manner and becomes ductile/plastic. In a single crystal, this temperature is solely the temperature at which dislocation activity is possible. The identification of the BDTT is dependent on the definition and experimental conditions. It is possible for a crystal to fail in a brittle manner but still show signs of plasticity. The identification of the BDTT is reliant on the definition of the point at which brittle behaviour ceases and plasticity begins. To an engineer, the BDTT represents the point at which dislocations affect the properties

of the material. To a physicist, the BDTT is at the point when the very first signs of dislocation activity are observed. The effect of the type of experiment can clearly be seen in work on the plasticity of silicon. Originally, it was thought that dislocation activity in silicon was limited to temperatures above 600°C when subjecting a single crystal to compression tests at constant strain rates. However, when a confining hydrostatic force was applied to suppress cleavage fracture, the temperature at which dislocations could be induced was reduced to about 300°C (Castaing *et al*, 1981). This suggests that a material can never be fundamentally brittle *i.e.* if an experiment was designed to inhibit crack formation, it would be possible to initiate dislocations at any temperature, in any material.

Work hardening and creep:

The phenomena of work hardening and creep are of great interest to the materials engineer. The degree to which a material will deform under a given set of conditions is increasingly important to understand, especially with the advent of high temperature, high tolerance applications such as those demanded in the aerospace industry. Work hardening is the phenomena whereby a material is observed to become harder the more it is deformed. On the other hand, creep is the continued plastic deformation of the material whilst under load. In many respects, work hardening and creep are the same phenomenon, looked at from a different perspective. Both deal with continued plastic deformation of a material, only creep looks at how and why the material continues to deform whilst work hardening concentrates on reasons why it slows down. In each case they are dependent on the production and subsequent interaction of dislocations.

As a crystal is plastically deformed, the stress necessary to continue to move the dislocations that cause the deformation increases. This is known as work hardening. The causes behind this in single crystals were first considered by Taylor in 1934, where he suggested that work hardening was due to internal stresses created by the dislocations themselves. Since then, a great deal of work has been done on this phenomenon, but very little progress has been made. This is because to understand why a crystal has work hardened, one must first know what the dislocation structure of a plastically deformed crystal is. Then one must know how much strain is needed to create that structure and finally calculate the stress needed to propagate slip. This is a fairly easy task if the deformation is restricted to a single slip system, at a finite temperature and the stress field is uniform. In most cases, however, this situation does not exist.

The stress/strain relationship for F.C.C. metals was devised by Friedel *et al* (1955) and for single crystal germanium by Alexander (1961). As seen in figure 1.1 there are three stages to the work hardening of F.C.C. crystals. Stage I is characterised by an initial rapid hardening that levels out. Stage II is a region of rapid work hardening where the slope of the line is constant, regardless of conditions. Stage III is temperature dependent and is where the hardening rate is significantly reduced.

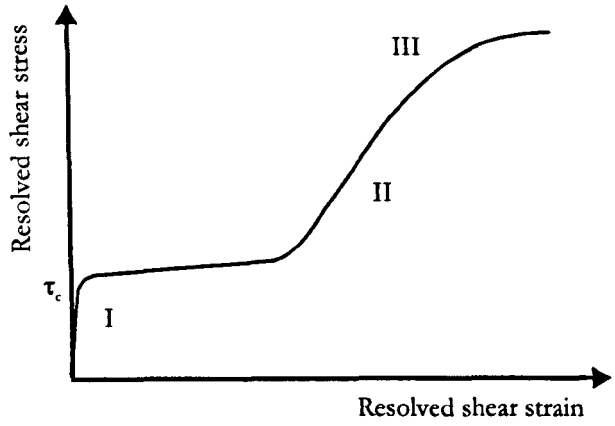

Figure 1.1. Graph showing the three stages of work hardening in F.C.C. single crystals.

The work hardening in stage I is, in part, due to the interaction between newly formed dislocation loops and the Frank network. A Frank network is the net of dislocations grown into the crystal that have relaxed during annealing processes to form a randomly oriented network of low energy dislocations. An expanding dislocation loop will have to intersect some of Frank network dislocations (known as trees) as it moves. The intersection of the trees produces jogs in the loop, which slows its movement, therefore hardening the crystal. Hardening in stage I is also characteristic of a material that is deforming via an easy glide or laminar flow mechanism as opposed to a complicated one (Cottrell, 1953). Easy glide is when a material slips only on one slip system, thereby producing long parallel slip lines on the surface. As these slip lines are produced by favourably positioned Frank-Read sources, the continuation of deformation should extend the length and height (of the cut the surface) of each dislocation rather than produce more. The parallel dislocations react elastically with one another, either by their proximity to one another or by slight inhomogeneities. This interaction can slow the movement and change the direction of the dislocations, which can cause a hardening of the crystal. The hardening due to elastic interaction between dislocations in laminar flow is much greater than that of the jog formation, however, neither are sufficient to explain the rapid hardening seen in stage II.

The rapid work hardening seen in stage II is caused by turbulent plastic flow. Turbulent plastic flow occurs when the crystal is not restricted to flow on a single slip system. If several slip systems are active, then there is a greater opportunity for the dislocations to interact with one another to form jogs, kinks and ultimately sessile dislocations. The sessile dislocations form barriers to any subsequent dislocations, causing pile up. As the stress increases, the dislocations are increasingly stressed but are unable to move, thereby reducing the amount of strain.

Stage III is the point on the graph when the rate of work hardening is significantly reduced. The crystal may still work harden but not as quickly. This sudden reduction in the work hardening rate is seen as the point at which secondary cross slipping is observed. The cross-slipping mechanism allows the dislocations to avoid the sessile dislocations, which relieves the piled up dislocations. Cross slipping in itself, however, produces Frank-Read sources, which increases the dislocation density and the production of sessile dislocations. The added number of sessile dislocations produces extra barriers to slip. Stage III is therefore a competitive process between stress relief via cross slipping and increased barrier production. The onset of stage III behaviour is thermally activated. As the temperature is increased, the stress at which it starts is reduced, *i.e.* the stage II region is reduced. In some cases, if the temperature at deformation is low enough, stage III may never be observed and stage II hardening is seen until the crystal twins or fractures.

Creep is the time dependent plastic deformation of a material. This phenomenon is most readily seen when a cylindrical specimen of soft material with a low homologous temperature (*i.e.* lead) is uniaxialy loaded in tension. The temperature and load are kept constant and the extension of the specimen is recorded over time. A typical creep curve for metals, polymers and ceramics (given the correct homologous temperatures) can be seen in figure 1.2. It can be seen that as in the work hardening scenario, there are three distinct sections; not including the initial plastic strain of the material as the load is applied. The first section is known as primary or transient creep, where a rapid deceleration of the strain rate occurs. This is due to the same dislocation interactions that cause work hardening in stages I and II. The second stage, known as steady state creep, is denoted by a region on the graph where the strain rate is constant. This is analogous to stage III on the work hardening diagram and is attributed to the competitive process of increased strain due to cross slipping and diffusion mechanisms against work hardening due to increased dislocation interaction. The third stage or tertiary creep is characterised by the accelerated

strain rate due to decreased material surface area (but the same applied load) as the specimen begins to catastrophically fail.

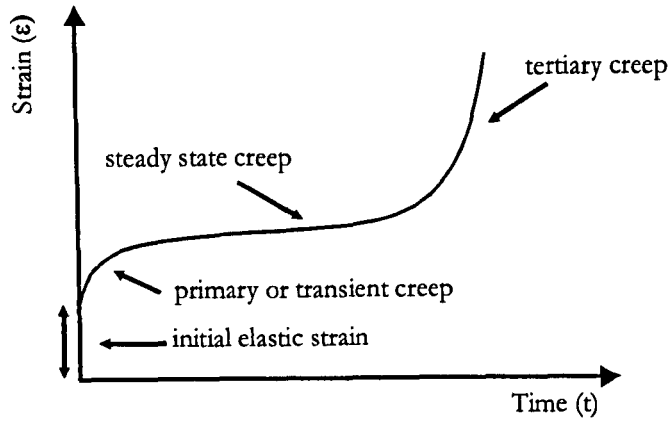

Figure 1.2. A typical creep curve for a material in uniaxial tension.

Creep can also be measured when loading the specimen in compression. A useful way of achieving compression creep data is through indentation testing. Hargreaves (1928) was the first to notice that creep occurred in metals when increasing the contact time of spherical indenters. Since then the method of analysing creep data via rigid indenters has been considerably developed. The main consideration of these techniques is that, as the indenter deforms the surface, the area over which the load is applied is increased, which has the effect of decreasing the applied stress. This is in direct contradiction to tensile creep testing where the flow of the specimen tends to reduce the area of material, which has the effect of increasing the applied stress. This fundamental difference in creep testing means that tensile creep tests will tend to exhibit a region where the strain rate increases dramatically before catastrophic failure (tertiary creep). Whereas tertiary creep in compressive tests, on the other hand, will tend to show a decrease in the strain rate. This is due to the fact that a stage will be reached whereby the projected area of the indenter is so large that the applied pressure is no longer sufficient to cause dislocation movement through the highly deformed zone. If failure is observed, it would be denoted by the appearance of cracks, caused by dislocation interaction stress concentrations.

In general, as the creep of a single crystal relies on dislocation motion, creep is dependent on the experimental temperature. At low temperatures (>0.5Tm) dislocations are less mobile, therefore creep is unlikely. However, at temperatures above 0.5Tm the glide of dislocations is possible, which produces primary creep. At higher temperatures the climb and cross slipping of dislocations becomes possible, which produces steady state creep (stage II).

1.3 Slip

The study of stress/strain characteristics of some single crystals has been extensive and has led to great advances in the understanding of plasticity on a macroscopic level. However, to be able to fully understand these results a closer look at the deformation on a microscopic level is needed.

When looking at a well-prepared crystalline surface, the most obvious evidence of plastic deformation will be that of slip lines or bands. This type of plasticity is known as translational slip and is where one part of a crystal lattice has moved with respect to another, under an applied shear force, but produced no net change in the crystal order (figure 1.3). This can be seen when a tensile force is applied to a well-oriented crystal (Elam, 1936, Schmid and Boas, 1950). A closer look at slip bands revealed that only certain discrete planes of the crystal were deformed and the size of the undeformed sections or glide packets, were dependent on the conditions of deformation (Andrade 1940). Taylor and Elam (1926) showed that the slip band itself is not restricted to a flat plane. This type of deformation has been seen in crystalline iron, mercury (Greenland, 1937) and silver chloride (Nye, 1949) and has become known as pencil glide.

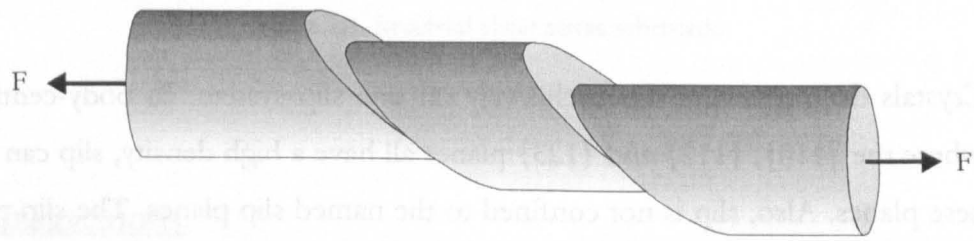

Figure 1.3. Translational slip in a single crystal, under a tensile stress.

The long-range order of crystals means that slip is generally confined to certain planes and directions, called slip systems. This anisotropy in slip is derived from the order in which the atoms are laid down in the crystal lattice. The most easily sheared direction is generally the one where the distance between the neighbouring atoms is the shortest. Equally, the most easily sheared plane of atoms is the one with the densest packing. In diamond cubic structures, the slip direction is $<1\bar{1}0>$ and the plane {111}, whereas in hexagonal close-packed crystals (HCP) $<2\bar{1}\bar{1}0>$, {0001} are the easy shear direction and plane. The symmetry of crystals means that for a given crystal and direction of force, there may not be just one active slip plane but several, all from within the same family of slip planes.

Slip should occur at the point of greatest shear stress, although with crystals this point may not coincide with the slip plane and direction of the crystal. Therefore, the point where slip initiates may not be the point that has the greatest magnitude of shear rather, the point at which the shear force exceeds the critical value for initiation of slip in that slip plane (Schmid, 1924). This has led to the theory of resolved shear stress, which states that if a cylindrical crystal is subjected to a uniaxial tensile load (F) (figure 1.4), the force component in the direction of slip is:

$$F\cos(\lambda)$$

If the area of the slip plane is (A), (λ) is the angle between the load axis and the slip direction and the angle between the load axis and the slip plane normal is (ϕ), then the resolved shear stress is:

$$\tau = \frac{F}{A} \cdot \cos(\phi) \cdot \cos(\lambda)$$

The stress to cause the initiation of slip on any plane for a given material and conditions is known as the critical resolved shear stress.

Crystals do not always slip exclusively on one slip system. In body-centred cubic crystals where the {110}, {112} and {123} planes all have a high density, slip can occur on any of these planes. Also, slip is not confined to the named slip planes. The slip planes are simply the planes on which slip is most likely to occur, as it is the one with the lowest resolved shear stress. It is possible to initiate slip on planes other than the recognised slip plane by increasing the resolved shear stress on them to levels high enough to initiate slip *i.e.* the critical resolved shear stress. In this way, the slipping of a crystal on a slip plane may distort the stress field around the slipped regions enough to produce critical resolved shear stresses high enough to initiate slip on different slip systems. It is also important to note that other slip systems may become active at elevated temperatures.

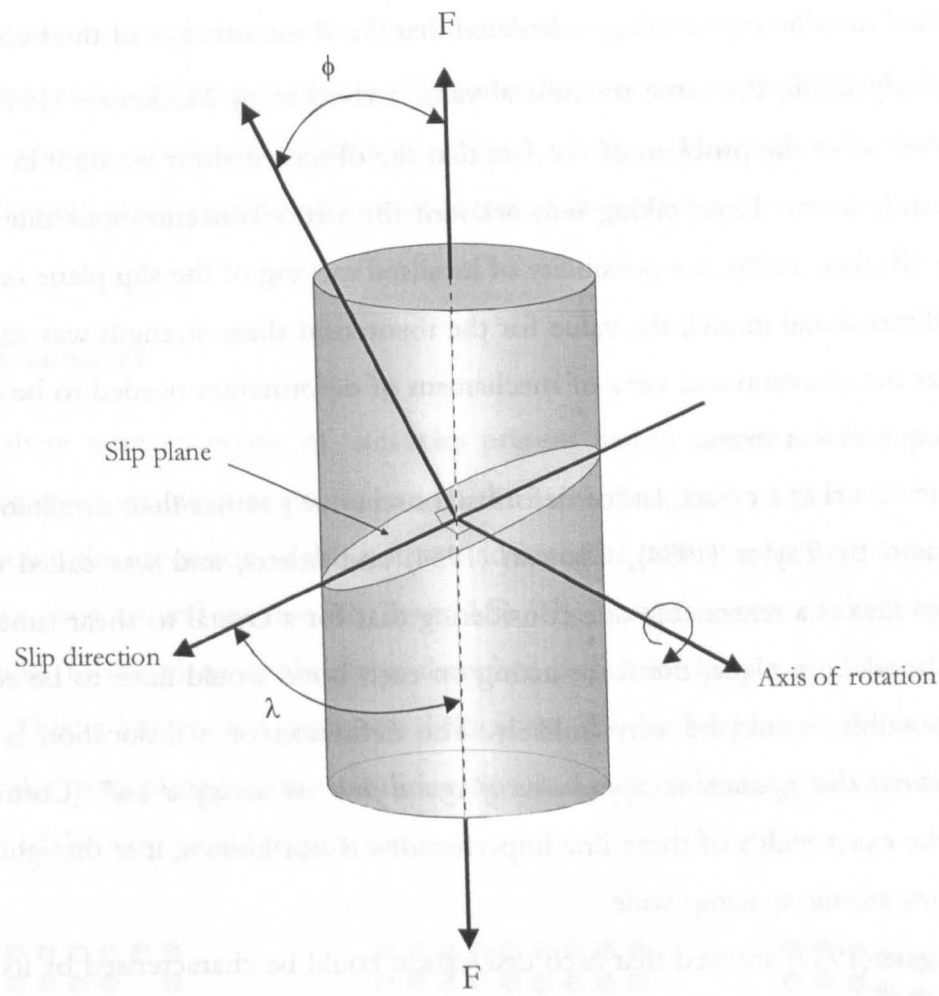

Figure 1.4. Resolved shear stress schematic.

1.4 Dislocations

Frenkel (1926) estimated the theoretical shear strength of a crystalline structure. He assumed that if one row of atoms was sheared over another by a known amount, the theoretical shear strength (τ_m) was approximately $\mu/2\pi$, where (μ) is the shear modulus. This was based on the energy needed to simultaneously break all of the bonds and then remake them. The problem with this view was that the shear strength (τ_m) measured experimentally was several orders of magnitude lower than this. For example, the experimental shear strength of annealed zinc or aluminium crystals was $\sim 10^{-4}\mu$ (Cottrell, 1953). Even refinements to Frenkel's work by Mackenzie (1949), who reduced the theoretical shear strength (τ_m) to $\mu/30$, failed to produce a value which was close to that observed.

Bragg and Nye (1947) and later Bragg and Lomer (1949) used a soap bubble model to calculate the shear strength of a crystal. The bubbles took the form of a two-dimensional

close packed metallic crystal. They calculated that the shear strength of the bubble raft was approximately $\mu/30$, the same theoretical value arrived at by Mackenzie (1949). This did not however solve the problem of the fact that the observed shear strength in real crystals is significantly lower. Even taking into account the stress concentrations due to thermal vibrations (Becker, 1925), the possibility of localised melting of the slip plane or errors due to a two-dimensional model, the value for the theoretical shear strength was still too high. It was clear the conventional view of mechanism of deformation needed to be changed to one that required less stress.

The idea that a crystal lattice deforms consecutively rather than simultaneously was first theorised by Taylor (1934), Orowan (1934) and others, and was called dislocation theory. This idea is a reasonable one considering that for a crystal to shear simultaneously on all the bonds in a plane, the force acting on each bond would have to be equal. This, although possible, would be very unlikely. The definition of a dislocation is "*a line of imperfect material that separates a slipped area of crystal from an unslipped one*" (Cottrell, 1953). Although the exact width of these line imperfections is not known, it is thought that they are only a few atomic spacings wide.

Burgers (1939) showed that each dislocation could be characterised by its direction and strength, and the vector (b) has now become known as the *Burgers vector*. Due to the ordered nature of crystals and the forces that hold the atoms together, any amount of slip must have discrete values, *i.e.* from one equilibrium position to another. Each crystal lattice will have a different set of discrete values depending on their lattice structure and the distance between neighbouring atoms. The smallest amount of slip that will leave the crystal lattice with its original order (an identity translation) is when the Burgers vector (b) is in the direction of a lattice vector and is one lattice spacing in strength. This is known as a unit dislocation. It is possible that a lattice structure has positions of equilibrium which are less than that of one lattice spacing, producing a Burgers vector less than unity, *e.g.* a partial dislocation. A Burgers vector that has strength higher than unity is unstable and will dissociate into separate dislocations with different vectors, thereby lowering its energy (Frank, 1949).

There are two main types of dislocation, the edge dislocation (Taylor and Orowan, 1934) and the screw dislocation (Burgers, 1939), each defined by their Burgers vectors. The edge dislocation has its Burgers vector perpendicular to its dislocation line whereas the screw dislocation has a parallel Burgers vector.

In reality, dislocations are rarely perfectly straight. A dislocation line can only terminate at a free surface or a node. Therefore, if a dislocation initiated in the bulk of a

crystal is unable to do this it must bend around itself to produce a circle, *i.e.* no free ends. The roughly circular dislocation line has the same Burgers vector throughout, therefore it must have regions which are defined as screw and edge. The regions in between the alternate edge and screw regions are known as mixed dislocations.

The prismatic dislocation:

If there were an excess of vacancies present within a crystal lattice, it would be possible for these vacancies to precipitate on the same close packed plane to form a hole. At some point, the expansion of this hole would exceed a critical value and collapse leaving a dislocation loop around the outside (figure 1.5). The Burgers vector of the loop would be perpendicular to the plane of the loop, therefore the entire loop would be pure edge in character. This is known as a prismatic dislocation. As the Burgers vector of the loop is perpendicular to its plane, a prismatic dislocation can only glide along its axis. Shrinkage or expansion of the loop would require climb.

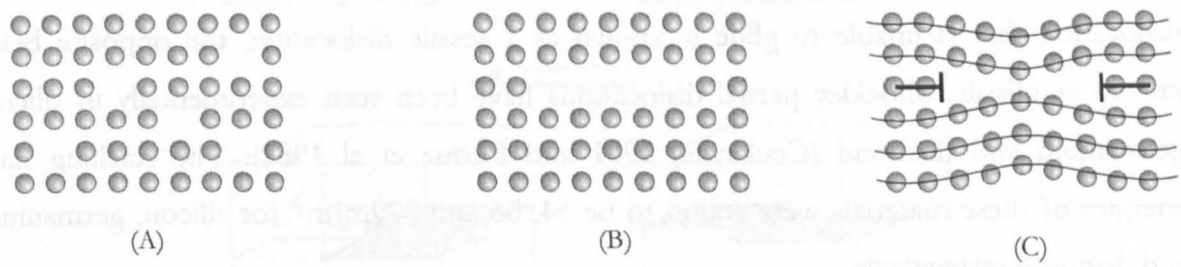

Figure 1.5. Diagram showing a prismatic dislocation.

The partial dislocation:

A partial dislocation is where the imperfection in the crystal is not of any great magnitude but rather a slight misalignment within the crystal. They are usually associated with stacking faults, which are "*low energy internal surface imperfections*" (Barrett 1952). The boundary within the crystal of a stacking fault is a partial dislocation. The shape of a partial dislocation can take many forms and each form has different properties. The properties of each form become important when considering the motion of partial dislocations and their interaction with other partial or full dislocations.

The easiest way to visualise a partial dislocation is by using the face centred cubic (f.c.c.) crystal structure. By taking the densely packed layers and stacking them up one upon the other, it becomes obvious that there is a repeated sequence of stacking. This sequence

A B C A is a stacking fault (and therefore partial dislocation at its boundary) and is produced if this stacking sequence is upset. This can be done in three ways. The first method is to slip a layer in the <112> direction which would produce a stacking sequence of A B C ***B C*** A B instead of A B C ***A B*** C A. The second method is to remove one layer, which would have the same effect as the previous method. The third would be to add another layer, which produces A B C ***B*** A B C A. In practice, partial dislocations are formed by the splitting of a full dislocation into two partials which, collectively have less energy or by the mass transport of vacancies or interstitial atoms.

The production of a partial dislocation by slip on a close packed plane produces a partial whose Burgers vector lies in the plane of the fault and is known as a Shockley partial. The adding or removing of part of a close packed plane produces partial dislocations whose Burgers vectors are normal to the fault plane, These are known as Frank partial dislocations and are always pure edge in character. The removal of part of a close packed plane produces a negative Frank partial and the addition of part of a plane producing a positive one. Since partial dislocations can only move in the plane of the fault, Shockley partials can only glide, whereas Frank partials can only move by climb. A dislocation that is unable to glide is known as a sessile dislocation, the opposite being known as glissile. Shockley partial dislocations have been seen experimentally in silicon, germanium and diamond (Cockayne, 1981 and Pirouz et al 1982). The stacking fault energies of these materials were found to be 54, 66 and 279mJm^{-2} for silicon, germanium and diamond respectively.

1.5 Motion of Dislocations

As a dislocation loop expands through the crystal, it inevitably encounters obstacles. The dislocation is either pinned at the obstacle or traverses it. Traversal is either by a conservative (glide) or non-conservative (climb) mechanism. The outcome of the interaction is that the mobility of the dislocation is affected. The degree to which the dislocation is slowed by obstacles is reflected in its stress/strain and work hardening characteristics.

Kinks, jogs and climb:

Looking closely at a straight section of a dislocation line it is possible to see parts of the line that are not atomically straight, *i.e.* there are small steps in the line of the order of a few atoms high. A step in the line that lies in the plane of the dislocation is known as a kink and does not impede the glide of the line. A jog, however, is a step in the line that is not in the glide plane. A jog in an edge dislocation has the same Burgers vector and therefore does not impede glide. A jog on a screw dislocation has edge character and therefore its Burgers vector is perpendicular to the direction of motion. For a jog in a screw dislocation to move with the dislocation, non-conservative motion or climb would be required. Figure 1.6 shows schematic diagrams of the motion of kinks in edge (A) and screw (B) dislocations and also jogs in edge (C) and screw (D) dislocations.

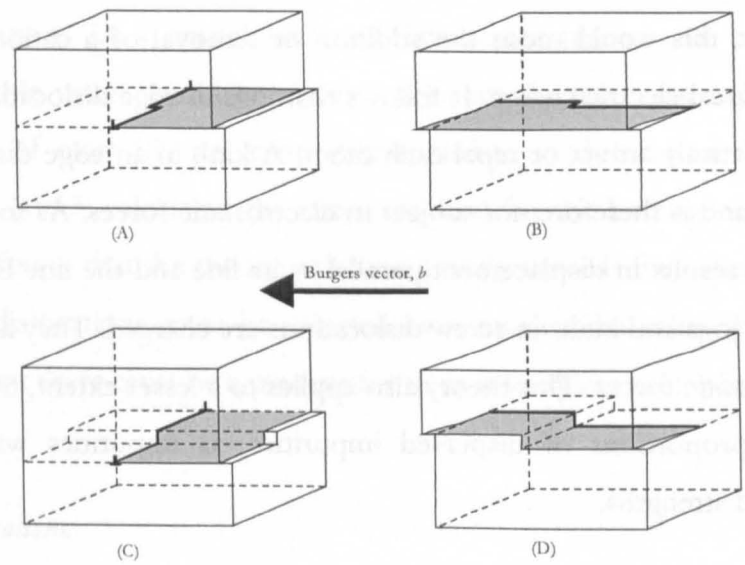

Figure 1.6. Diagram showing kinks (A and B) and jogs(C and D) in edge and screw dislocation lines respectively.

Climb occurs when an edge dislocation moves out of its glide plane. For this to occur, vacancies or interstitial atoms must diffuse to the line. By looking at a cross section of an edge dislocation, it is possible to visualise this (figure 1.7). For the end of the extra half plane to move up or down an atom must be either removed or added respectively. The edge dislocation moving up, *i.e.* removal of atoms is known as positive climb whereas moving down is known as negative climb. The movement of jogs in screw dislocations by the process of climb are, therefore, sources of, or sinks for, vacancies and interstitials. As climb requires the mass transport by diffusion of either interstitial atoms or vacancies, climb is a thermally activated process. As vacancies generally have lower activation energies than interstitials, it is assumed that most climb is carried out by the diffusion of vacancies.

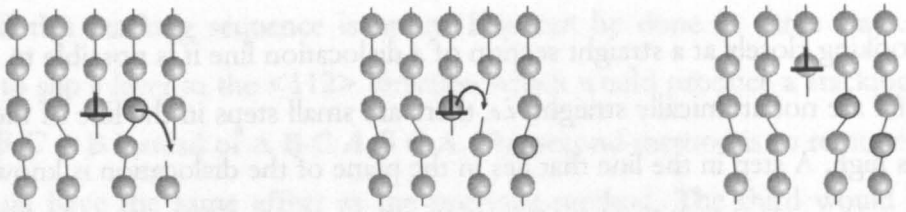

Figure 1.7. Diagram showing the climb mechanism of an edge dislocation.

In the case of ionic crystals, it is important to remember that the rearrangement of atoms that occurs during dislocation motion will be affected by the positive and negative charges on each atom. This can mean that dislocations have a charge associated with them that will affect their movement. In the case of an edge dislocation with burgers vector ½[110] gliding on {110}, for climb to occur, an atom must be added or removed. In ionic crystals, however, this would mean the addition or removal of a cation or anion, which would upset the local electric charge. It follows that jogs in edge dislocations carry a charge and will electrostaticaly attract or repel each other. A kink in an edge dislocation does not carry any charge and is therefore not subject to electrostatic forces. As motion of a ½[1$\bar{1}$0] screw dislocation results in displacement parallel to its line and the line is of single charge, the movement of jogs and kinks in screw dislocations are charged. They are both, therefore subject to electrostatic forces. This theory also applies to a lesser extent, to covalent crystals that have large proportions of dispersed impurities, as impurities will have different valences and bond strengths.

Cross Slip:

Slip is usually confined to certain planes, but screw dislocations are able to change from one slip plane to another. This happens when the magnitude of the resolved shear stress is higher in a plane other than the one in which the dislocation is gliding. For instance, figure 1.8 shows a screw dislocation moving in the [$\bar{1}$01] direction on the {111} plane is free to change to the {1$\bar{1}$1} plane whilst still slipping in the same direction. The slip plane in b.c.c. crystals is not as well defined as in f.c.c., crystals, therefore cross slip is more prevalent and dislocations tend to produce wavy slip.

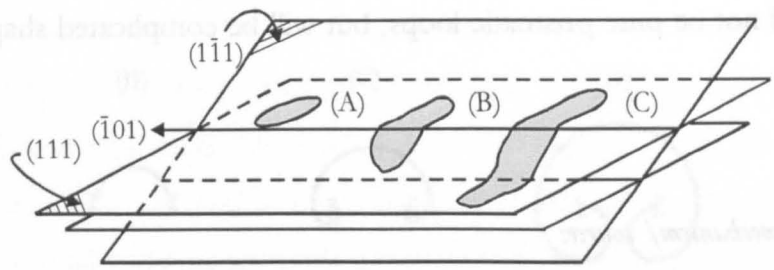

Figure 1.8. Diagram of cross slip in a f.c.c. crystal.

1.6 Initiation and Multiplication of Dislocations:

Once the theory of plastic deformation through the mechanism of dislocation had been accepted, there was another problem between the theory and experimental results to consider. Normally, annealed crystals have a grown in dislocation density of about $10^6 cm^{-2}$, When a crystal is deformed however, the dislocation density is increased. If all of the grown in dislocations in a crystal were on favourable planes and able to glide, the maximum attainable strain would be about 1 per cent. In fact, experimental results have produced strains of over 100 per cent, corresponding to dislocation densities of about $10^{12} cm^{-2}$. Cottrell (1953) calculated the stress required for the homogeneous nucleation of dislocations. He found that the theoretical stress greatly exceeds the experimental values. It is obvious that dislocations must be initiated by a mechanism other than homogeneous nucleation and that there must be a process for their subsequent multiplication.

Nucleation of dislocations:

The nucleation of dislocations must be due to a heterogeneous mechanism. Such a mechanism is likely to be due to local stress concentrations within the crystal lattice, caused by imperfections such as inclusions or dislocations.

Jones and Mitchell (1958) introduced stress concentrations in the form of spherical glass inclusions into annealed silver chloride crystals. The crystals were held at 370°C to remove any local strain caused by the inclusions and then cooled. Upon cooling, the difference in the coefficients of thermal expansion between the glass balls and the silver chloride was enough to initiate prismatic dislocations, which progressively moved away from the inclusion with each subsequent loop initiation. Although this was a simplistic case, it was sufficient to develop a model for a mechanism by which dislocations are produced around local stress concentrations. With real inclusions, which are invariably not perfect spheres, the associated stress field will not be simple and therefore the resultant

dislocations will not be pure prismatic loops, but will be complicated shapes and of mixed character.

The Frank-Read mechanism/ source:

A mechanism for the regeneration of dislocations was proposed by Frank and Read (1950). If a dislocation were pinned at one end then (figure 1.9A), under an applied shear stress, the dislocation could continue to glide with the pinned end and the lattice friction causing the line to bend (B). As the unpinned end of the dislocation moves, it will begin to rotate around the fixed end (C) and will continue to rotate indefinitely, under the applied shear stress, producing a spiral formation (D). For each complete revolution one unit of slip is produced and the dislocation remains pinned to produce more slip (figure 1.9). This method of regeneration is known as the Frank- Read mechanism and has been seen experimentally in silicon single crystals by Dash (1957).

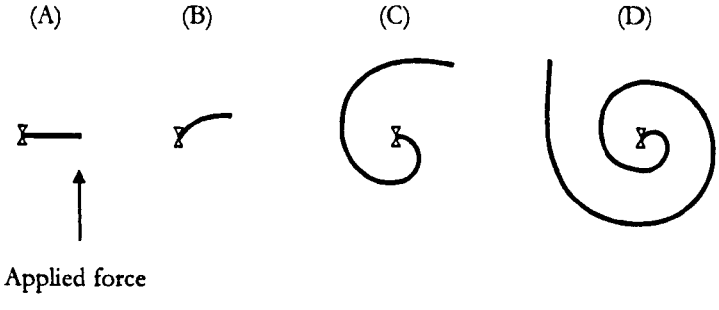

Figure 1.9. The Frank Read mechanism of dislocation multiplication.

The model of the mechanism was developed to produce the double ended Frank-Read mechanism or Frank- Read source (figure 1.10). If a dislocation were constrained at both ends and a suitable shear stress were applied (A), then the unrestrained dislocation segment would bend (B). A continuation of the applied stress would force the distorted dislocation to bend back on itself, producing two spirals, similar to two opposing Frank-Read mechanisms (C + D). At some point, the two spirals would have distorted so much that they would meet behind the original position (E). When the two ends of the spiral meet, the portions that have like character, but opposite sign, will annihilate to produce a complete dislocation loop and leaving the original section of pinned dislocation to restart the process. These two mechanisms rely on the glide process of the dislocation, however, similar mechanisms can be produced during climb of a dislocation that has one or both ends fixed. In the case where both ends are fixed the mechanism is called a Bardeen-Herring source (Bardeen and Herring, 1952).

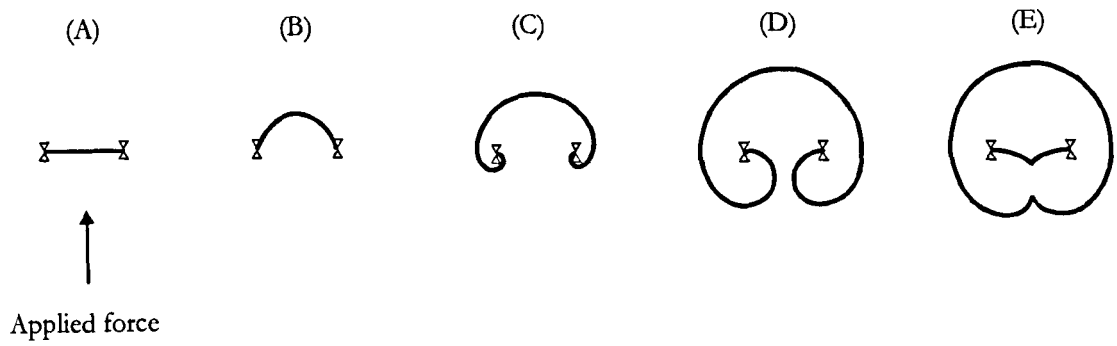

Figure 1.10. The Frank-Read Source.

Multiple cross slip:

It is possible for an expanding screw dislocation to change from one glide plane to another by the process of cross slip. It is possible that a cross-slipped dislocation loop could then cross slip back onto its original glide plane. This would produce three areas of slip connected by two jogs. The jogs connecting the slip planes are relatively immobile, which pins the dislocation loop. The pinning of the loop creates a situation similar to that of the Frank- Read source, *i.e.* the dislocations lying on the original glide planes are free to rotate around the pinned portions of the line. When cross slip is favourable, a dislocation loop may change planes many times, producing a long complicated dislocation loop containing many jogs and therefore many more dislocation sources. When this situation occurs, multiplication of dislocations and the subsequent widening of slip bands can be a much faster process than the simple Frank-Read source mechanism alone.

1.7 Dislocation Interactions

In a crystal that has mobile dislocations, it is inevitable that these dislocations will, at some point, either approach each other or intersect. The main emphasis of this chapter is to give an overview of the most common interactions in f.c.c. crystals, but some behaviour is given that is applicable to h.c.p. and b.c.c. crystals.

Before considering the intersection of dislocations, it is necessary to consider the forces between dislocations that do not intersect. The forces between dislocations are found by using the surface integration method (Cotterell, 1953). This supposes that a dislocation is added to crystal in which a dislocation already exists and is not subject to any additional external forces. The force between the two dislocations will then depend on the

strain energy in the whole crystal. The total strain energy can then be separated into three terms; the self-energies of each dislocation and the interaction energy between the two.
It can be seen that the forces between two parallel edge dislocations with parallel burgers vectors (b) depend, not only on how far apart they are in the x-direction, but also how many planes separate them in the y-direction. Two dislocations with the same sign will repel each other when x>y but will attract each other when x<y. The opposite situation occurs when the dislocations are of opposite sign to each other. When x=y and x=zero the force between them is in equilibrium, but the x=y position is unstable. In this way, parallel edge dislocations with parallel but opposite signs will tend to stack up on each other, whereas those of the same sign will tend to spread out. When the distance y=zero (*i.e.* the dislocations lie on the same atomic plane), edge dislocations with the same sign will repel each other, whereas those with opposite signs will be attracted to each other and annihilate. Due to the radial symmetry of the forces around screw dislocations, the interaction between them is more simple. Parallel screw dislocations of the same sign will repel each other whilst those of opposite sign will attract. There is no attractive or repulsive force between parallel edge and screw dislocations.

In cases where the Burgers vectors of the dislocations are not parallel, there is still a force acting between them, but the magnitude and direction of the forces would have to be calculated for each separate case.

Intersecting dislocations:

When dislocations of the same sign meet, if it is energetically favourable, they can combine to produce a new dislocation with new Burgers vector. The opposite can also happen and a single dislocation can reduce its energy by dividing into two separate dislocations or partials. The point at which dislocations join (or separate) is called a node. According to Frank's rule of conservation of the Burgers vector, the sum of the Burgers vectors entering a node is equal to the sum of the Burgers vectors leaving the node. From the equation for the self-energy of a dislocation line, it can be seen that the energy of a dislocation line is proportional to the square of its Burgers vector. Therefore, any dislocation with Burgers vector b_1 can dissociate into two dislocations with Burgers vector b_2 and b_3 providing $b_1^2 > b_2^2 + b_3^3$. The reverse is also true, several dislocations can join together if the resultant burgers vector has a smaller magnitude. This rule also includes interactions involving partial dislocations.

If two dislocations intersect, and it is not energetically favourable for them to combine, jogs may be formed. In the case where two perpendicular dislocations intersect one another, a jog will be formed in each dislocation, irrespective of the character of the dislocations, and the strength of which is equal in length and direction to the Burgers vector of the other dislocation. A jog will not be formed if the Burgers vector of the other dislocation lies in the plane of the dislocation.

In the case where two dislocations on different planes but with identical burgers vector intersect, *L* shaped dislocations may be formed. At the point where the dislocations intersect, a node will be formed. At this point, there are four separate dislocations joined by the node, rather than two intersecting dislocations. It is possible that one half of an original dislocation combines with half of the other dislocation and vice versa, forming two bent dislocations. This is possible as the Burgers vectors of both halves of the bend are conserved and the overall length of dislocation line is reduced. These bent dislocations are important, as under the correct conditions, the apex of the bend will act as a pin for one section to rotate about the other, forming a Frank-Read mechanism.

Pile-up:

When a dislocation meets a sessile obstacle it can either move around the obstacle or become sessile itself. If the source of the dislocation is regenerative then a series of dislocations will move towards the same obstacle on the same plane and also become sessile, in what is known as a pile–up. As all of the piled-up dislocations are of the same character and sign, they cannot combine. The elastic forces of each of the dislocations interact to cause the spacing between the dislocations to decrease towards the front. The applied stress that caused the dislocations to move in that direction is then concentrated on the lead dislocation and is proportional to the original stress multiplied by the number of dislocations in the queue. A back stress is applied that acts on the dislocation source that will aid in the formation of new dislocations. In this way, a large stress concentration can be produced at the barrier and may reach such a level that the critical resolved shear stress is exceeded. New dislocations are then formed or cracks initiated.

Thompson's Tetrahedron:

In 1953, Thompson devised a method for visualising the intersection of the four {111} planes in F.C.C. crystals (ignoring the positive/negative directions). He created a tetrahedron (ABCD) in an eighth of a unit cell with edge length a/2 (figure 1.11).

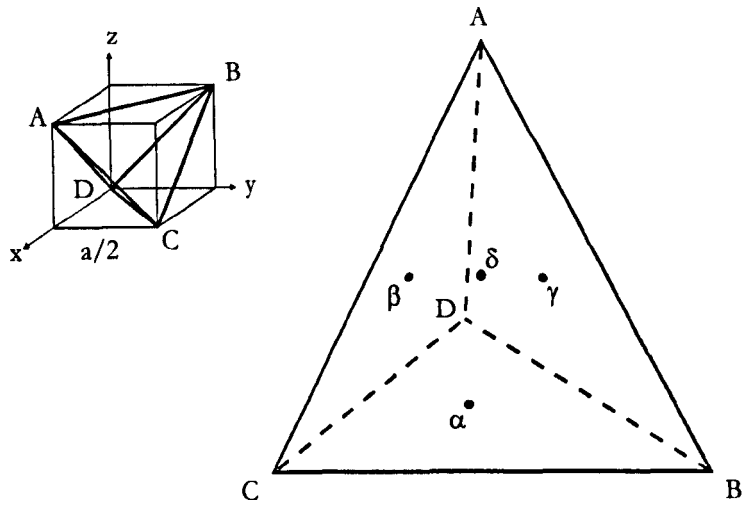

Figure 1.11. Thomson's Tetrahedron, describing the slip plane interactions in F.C.C. crystals.

The edges of the tetrahedron form the six possible intersections with <110> slip directions and the midpoints ($\alpha\beta\gamma\delta$) of the faces correspond to the a/6[112] Shockley partial dislocations. The Burgers vector of a dislocation can be described by using the letters corresponding to the end points of the dislocation, *i.e.* an a/2 [110] dislocation can be described as AB. The dissolution of AB into two Shockley partials can likewise be represented as:

$$AB = A\delta + \delta B$$

F.C.C. interactions

Within the f.c.c. structure, there are twenty four possible interactions between a given primary slip system and the remaining secondary slip systems. Using Thompson's notation, Hirth (1961) calculated the possible outcomes of these interactions. He considered the long and short-range interaction of extended dislocations and the edge or screw character. The outcome of the calculated interactions is shown in figure 1.12, which shows the Thompson tetrahedron opened at corner D. The primary slip system, BA(d) is in simple shear of magnitude $\sigma=1$, in addition, the resolved shear stress for each secondary slip system is given. The (+) or minus (-) indicates that the long-range forces are attractive

or repulsive respectively. For each case, the most likely interaction between the primary and secondary slip system is written next to the secondary slip system in question.

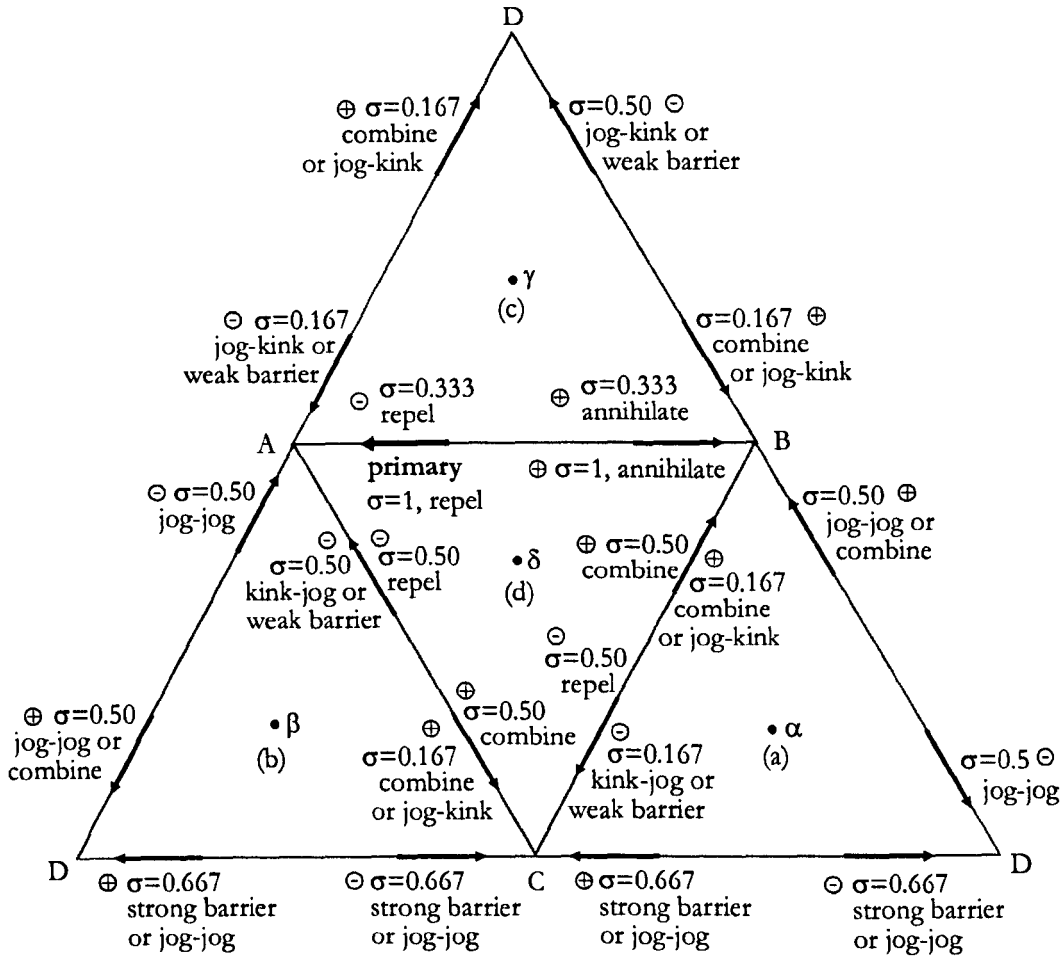

Figure 1.12. The most likely outcome of interactions in a FCC crystal, superimposed onto Thompson's tetrahedron (Hirth, 1961).

Calculation of the interactions showed that out of the 24 possible interactions only 12 result in barriers to dislocation motion. Of the possible interaction involving partial dislocations, it is noted that only intersecting systems along DC produce a Lomer-Cottrell style, strong barrier. Also that in many cases the partial dislocation have a long-range repulsion but short range attraction. This means that for the reaction to occur an energy barrier must be overcome, making it likely that they will only occur at points of high stress concentration such as pile-ups.

The Lomer-Cotterell lock/ barrier:

If two unit dislocations of the form a/2[1$\bar{1}$0], lying on intersecting {111} planes, are both parallel to the line of intersection, it is possible that they could combine to form a partial dislocation along the edge which is sessile. Using Thompson's notation, this could

happen if the unit dislocations DA(β) and BD(α) both dissociated into two Shockely partials:

$$DA = D\beta + \beta A$$
$$BD = B\alpha + \alpha D$$

It is energetically more favourable for two of the partials to combine to form a third partial. The new partial being sessile as the resultant partial dislocation is of pure edge character and its Burgers vector does not lie in either of the intersecting {111} planes:

$$\alpha D + D\beta = \alpha\beta$$

The sessile partials lie in the six directions represented by the edges of the Thompson tetrahedron and their Burgers vectors lie along the lines connecting the midpoints of the faces. The resultant partials are also a form of stair-rod dislocation. Stair-rod dislocations are formed when a dissociated dislocation cross slips to another glide plane or, as in this case, reacts with another dislocation and different plane.

Interaction between dislocations and impurities:

There are two separate cases to consider when investigating the effect of point defects on dislocation motion. The first case involves defects that are immobile whereas in the second they are mobile. In the case where a dislocation encounters an immovable object then there are two ways in which it can bypass it. The first is via thermal fluctuations and the second is via Orowan's "pinch-off" mechanism (figure 1.13). Orowan's method states than when a section of dislocation line is pinned by an immobile defect, then the sections of the line that are not pinned continue to advance. The extra line tension exerted on the sections means that they begin to curve around the obstacle (figure 1.13B). Eventually, they curve around so much that they come into contact with one another (figure 1.13C). The sections that contact each other annihilate, freeing the dislocation line from the obstacle, but leaving it surrounded by a section of the dislocation (figure 1.13D). The degree to which the defects hinder dislocation motion in this fashion is dependent on the size and number of the obstacles.

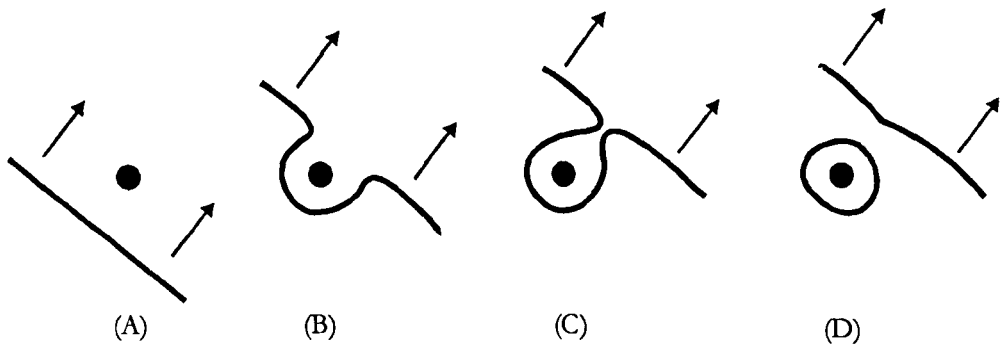

Figure 1.13. Orowan's "pinch-off" mechanism for the bypass of an immobile obstacle by a dislocation.

If the impurities within the crystal are mobile, then their diffusion through the lattice will be affected by the stresses exerted by dislocations. In the case where an edge dislocation approaches a large substitutional atom, the interactive force would be repulsive in the upper (compressive) region of the dislocation and attractive in lower (tensile) region. In the case where the substitutional atom is smaller than the atom that it replaced, the direction of the forces would be reversed. The same applies to vacancies and interstitial atoms, where they act like small and large impurities respectively. There would be no net interactive force between a substitutional atom and a screw dislocation. The net result of the attractive and repulsive forces is that an edge dislocation will attract impurities (or vacancies and interstitials). The nature of the impurities will determine the side of the dislocation that the are attracted to. Impurities that are attached to a dislocation in this manner are known as Cottrell atmospheres.

Cottrell atmospheres tend to render their parent dislocation immobile, to the extent that extra stress is required to extract the dislocation in question from its cloud. This leads to a hardening of the material, and is a reason cited for the observed yield drop seen in many materials. If the movement of the dislocation is slow enough and the diffusion rate of the impurities fast enough, then it is possible that the Cottrell cloud will "catch up" with its dislocation. This leads to a repeat of the process mentioned before and gives rise to the saw tooth shape caused by repeated yield drops in certain non-ferrous alloys. This phenomenon is known as the Portevin-Lechatelier effect (Friedel, 1964)

1.8 Summary

There are many factors involved when considering the plastic deformation of single crystals. It has been suggested that, on a macroscopic level, the onset of plastic behaviour and degree to which a material deforms is dependent on the experimental conditions, and also on the definitions imposed by the experimentalist.

The factors affecting the level of plastic deformation, such as work hardening and creep have been discussed, together with more microscopic factors such as pinning and cross slipping of dislocations.

Chapter 2

DIAMOND –REVIEW

2.1. Introduction

Although diamond has had a virtually mystical appeal throughout the ages, in reality, it is simply an allotrope of carbon, which places it in the same family as graphite and C_{60} ('Bucky balls'). There are, however, very good reasons as to why diamond has gained such prestige when graphite has not. The short bond length (0.154nm) and almost perfect tetrahedral sp^3 bonding make diamond the hardest material known to man. In conjunction with this, the clarity of the crystal and a high refractive index make it a must for the jewellery trade. The high hardness of diamond, together with the highest bulk modulus, thermal conductivity, tensile cleavage stress, extremely low coefficient of friction and chemical inertness, amongst other properties, make it almost as valuable a material in engineering applications as in the jewellery trade. The usefulness of diamond is tempered only by its brittleness, perceived rarity and high cost, although with the advent of synthesised diamond for engineering purposes, the cost is becoming more reasonable. In fact, diamond usage has increased dramatically over the last century, from being used solely for polishing and glass cutting, to its use today, as machine tools, wire drawing dies, radiation detectors, heat sinks and even as medical scalpels.

On a basic level diamond is simply a tetrahedrally bonded super-lattice of carbon, however, in reality diamond is more complex. Over the years, geologists and physicists have noticed distinct differences between diamonds. Other than by the colour (of which there are many), a rudimentary categorising of diamond has been devised, based on the defects they contain. There are two categories of diamond, types I and II, each with two sub-types. The initial division into two categories was made in 1934 by Robertson *et al* who observed differences in the ultra-violet and infrared absorption. Kaiser and Bond (1959) later determined that the differences were due to nitrogen in the crystal lattice, where type I diamonds contain appreciable amounts and type II virtually none. Type I diamond was then sub-divided into types Ia and Ib following observations by Smith (1959) of single

substitutional paramagnetic nitrogen (type Ib). Type Ia diamond was then further sub-divided into types IaA and IaB to accommodate observations by Sutherland (1954) and Clark *et al* (1956). It was determined that nitrogen can be found in pairs (A defect) or as a cluster of four (B defect). Custers (1952, 1954) suggested the subdivision of type II, following the discovery of electrically semi-conducting diamond that contained substitutional boron but no nitrogen (type IIb). A general summary of the diamond types and sub-types is given in table 2.1.

Type	Description
Ia	97% of natural diamond. Nitrogen concentration between 100-1000ppm nearly all of which is present as various types of aggregate. Electrically insulating. All colours.
IaA	Contain nitrogen almost exclusively as A centres.
IaA/B	Nitrogen present mainly in A and B centres also N3 centres. Usually, but not always, contain platelets in the cube planes, ranging in size between 10nm ~3μm.
IaB	Nitrogen present in B centres but not A centres.
Ib	0.1% of natural diamonds, most synthetics are of this type. Nitrogen present as dispersed substitutional paramagnetic atoms (C defects). Electrically insulating. Yellow to green in colour.
IIa	Relatively nitrogen free, rare in nature. Electrically insulating but enhanced thermal properties. Frequently brown in colour.
IIb	Boron as a substitutional impurity, extremely rare. Semi-conducting. Blue in colour.

Table 2.1. Description of the classification of diamond.

It is important to note that the diamond categories were devised with respect to the abundance and position of nitrogen in natural diamond. There is, therefore, no category to distinguish between natural and synthetic diamond even though they may exhibit different properties. This is made all the more confusing when the various diamond synthesis methods such as high pressure, high temperature (HPHT), chemical vapour deposition (CVD) or shock synthesis are taken into account. Previously, the distinction between

natural and synthetic diamond was not an issue, as synthetic diamond was generally of poor quality, small size and synthesis costs high. Recently, however, with the production of large, gem quality, synthetic diamonds at an ever decreasing cost, there have been moves to improve the classification to protect the gem trade from fakes (Sunagawa, 1995 and Welbourn *et al*, 1996). In addition, the different mechanical properties exhibited by the different types could be reflected in an improved categorisation system, to aid in diamond selection for industrial purposes. The main differences between natural and synthetic diamonds are due to the different growth conditions. As such, it would be necessary to further subdivide synthetic diamonds into those produced by the HPHT method and those produced by vapour deposition techniques as the diamond genesis in each case is vastly different. For the purpose of simplicity, the various vapour deposition techniques will be called CVD, although it is known that there are many different techniques for producing diamond from gaseous plasmas.

Natural diamonds were produced deep within the earth's crust and spent an inordinate amount of time (measured in Giga Anna) going through very complex growth cycles. As such, they have an impurity content consisting mainly of nitrogen and silicates, reflecting their original growth environment. The ever-changing growth conditions produce a very complex growth pattern although in general, natural diamonds exhibit an octahedral form. It is not unusual for a natural diamond classified as type IaA to have regions of different habits that conform to different classifications, *i.e.* they are of mixed habit.

HPHT diamonds on the other hand are produced in reaction cells at a pressure of 5-6 GPa and at temperatures of 1550-1600°C in a relatively short space of time (measured in hours rather than millennia). As such, HPHT diamonds generally exhibit very simple growth patterns and contain metallic inclusions from the reaction products (see pp 39-41). In general HPHT diamonds are cubic in form although the morphology is dependent on the synthesis conditions and the choice of solvent catalyst (Strong *et al*, 1971, Sungawa, 1984, Kanda *et al* 1989). As the HPHT method of growing diamonds is better understood and improved, the inclusions and crystal habit are being altered and controlled, such that it should be able to produce diamond with any required format. When such a time arrives, the only real difference between natural and synthetic diamond will be that synthetic diamonds will be more perfect than those found in nature.

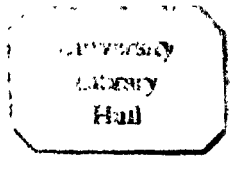

2.2 Impurities

Diamond is perceived to be a very strong, very pure crystalline material, although it is not uncommon for diamond to contain chemical inclusions and/or high levels of impurities. Indeed, these foreign atoms can readily be seen in some of the world's most famous diamonds. Invariably impurity atoms in diamond cause the crystal to absorb certain wavelengths of light, changing its colour. Famous diamonds such as the Hope, Orlov, Tiffany, and the Dresden green are all examples of diamonds that have sufficient levels of impurity to totally change the colour. The fact that the impurity atoms absorb discrete wavelengths of light means that the colour of a diamond is a very good indicator as to the impurity that lies within its crystal structure. However, care must be taken, as the colour of the diamond seen by the eye may be a mix of several different colours emanating from within the crystal. As a general guide, nitrogen absorbs blue/green light, making the diamond a yellow colour (the Tiffany diamond) and boron absorbs yellow/red light making the diamond blue (the Hope diamond). It is possible to have diamonds with virtually any colour and it is often possible to change the colour of a stone by bombarding it with radiation or via heat treatments. It is important to note that not all colours exhibited in diamond are due to impurity atoms, some colours are due to defects such as vacancies and dislocations, others are due to a combination of impurity and defect. Other colours, such as pink and brown are, as yet unexplained, although they are linked with plastic deformation. It is also important to note that the absence of any colour within the stone is not a guarantee that there are no impurity atoms present.

There are two main groupings of impurity atoms in diamond. The first group consists of H, N, O and S. These elements are relatively common in both natural and synthetic diamonds and have concentrations of up to 1000ppm. The second group contains B, Mg, Al, Si, S, Ca, Ag, Ba, and the transition metals. These are usually found in concentrations of 0.1ppm to 100ppm (Bibby, 1982). The nature and concentration of impurities depends heavily on the history of the diamonds themselves. It is not uncommon to find that diamonds from the same kimberlite pipe or alluvial deposit have very similar impurity contents. In this way, it is possible to determine where a particular natural stone originated. This is can also be applied to synthetic diamonds, where impurity contents are strictly monitored during the synthesis process. In fact, impurity elements are crucial to the synthesis of diamond as they dictate the growth rate and habit of the final product. However, there is always a residual concentration of impurities left inside the crystal and certain companies prefer to use different impurities. Therefore the type, nature and

population of impurities are indicators not only to the growth history of the stone but also the manufacturer.

Nitrogen:

By far the most significant impurity in diamond is nitrogen, as it is the most abundant and the marker for the current classification of diamond types. Nitrogen also dictates the properties of diamond such as the thermal, electrical and, as will be shown, the mechanical properties. The three main forms that nitrogen takes up in the lattice are the single substitutional (Charette, 1961 and Dyer *et al*, 1965), the A and the B defect. Each defect has a characteristic infrared absorption spectrum from which the concentration of each can be found. Figure 2.1 shows typical infrared absorption spectra taken from diamonds containing **A**, **B** and **C** defects, labelled a, b and c respectively

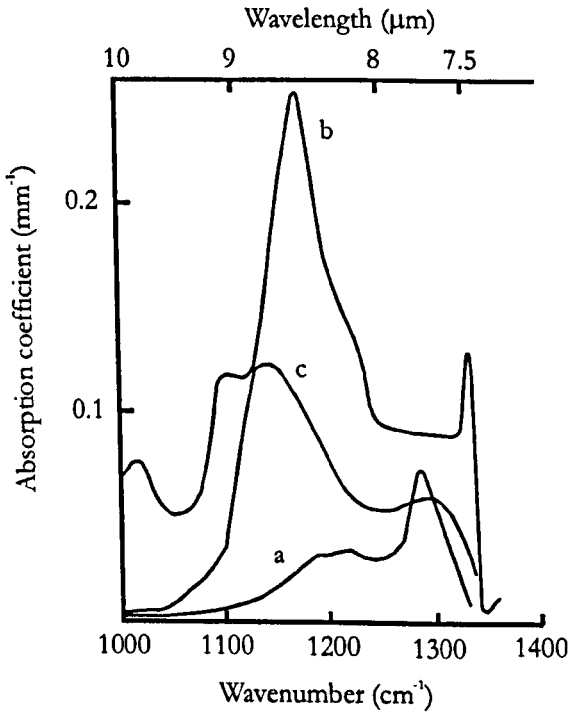

Figure 2.1. Graph showing the characteristic absorption peaks created by nitrogen defects within the diamond lattice. (a) **A** centre, (b) **B** centre (c) **C** centre.

Over the years there has been much deliberation as to the correct absorption coefficient to use when calculating nitrogen defect concentrations from the heights of the absorption peaks. The coefficient of absorption for the single substitutional nitrogen defect at 1130 cm^{-1} was determined by Sobolev (1969) and later confirmed by Chrenko *et al* (1971). The **A** centre coefficient at 1282 cm^{-1} was established by Kaiser and Bond (1959) and Lightowlers and Dean (1964) and the **B** centre, also at 1282 cm^{-1}, by Sobolev *et al*

(1972) and Burgemeister (1980). The final values as calculated by Collins (1980) and Woods *et al* (1990a,b) are shown in table 2.2.

Nitrogen type	Peak Position (cm^{-1})	Concentration (ppm/cm^{-1})
A centre	1282	17.5
B centre	1282	103.8
Single	1130	22

Table 2.2. The coefficients used to calculate nitrogen concentrations from IR absorption spectra.

The single substitutional nitrogen atom is observed in most HPHT samples but only rarely in natural samples, although it is commonly seen in the coats of coated stones (Faulkner *et al*, 1965). The nitrogen is preferentially incorporated into different growth sectors in HPHT diamonds, with {111} sectors having about twice as much nitrogen as {001} sectors and {011} virtually none at all (Strong and Chrenko, 1971 and Burns *et al*, 1990). There is some evidence though, that nitrogen take-up by growth sectors is dependent on the synthesis temperature (Satoh *et al*, 1990). Careful observation of a single growth sector reveals that the nitrogen content within it is not constant. It can be seen that the nitrogen concentration varies as the synthesis capsule temperature varies. The nitrogen take-up concentration is so sensitive that the small fluctuations in temperature that are part of the normal control programme of the equipment are enough to produce a banded nitrogen concentration structure within individual growth sectors. Figure 2.2 shows a cathodoluminescence (CL) micrograph of an HPHT sample in which the synthesis process has been interrupted and then returned to its original parameters. The dark line in the sample coincides with the point at which the interruption was made and FTIR measurements showed that it was higher in nitrogen content (Burns and Davies, 1992). The nitrogen banding due to the synthesis cycle can also be seen, as the intensity of the green luminescence is related to the concentration of H3 defects which is related to the overall nitrogen concentration (Woods and Lang, 1975).

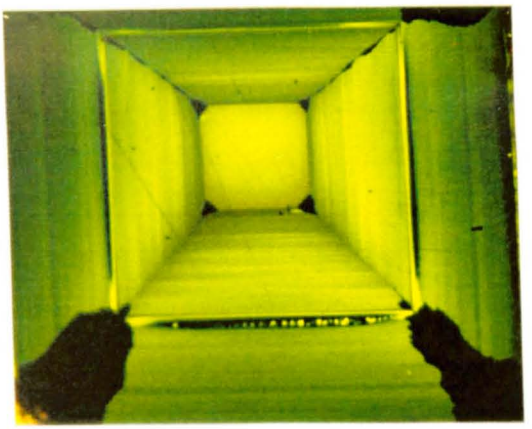

Figure 2.2. Cathodoluminescence micrograph of the {001} face of a synthetic HPHT diamond, showing the dominance of the cubic growth sectors (green), the variation of nitrogen uptake (related to green intensity) and the box formation deliberately introduced by briefly altering the growth cycle (Burns et al, 1999).

It is possible to aggregate single substitutional nitrogen into **A** centres by subjecting the crystal to about 5GPa of pressure and a temperature above 1700°C (Davies *et al*, 1976, Chrenko and Strong, 1977 and Satoh *et al* 1990). The aggregation rate of single substitutional nitrogen to **A** centres also depends on the growth sector, with the {111} sectors having a higher aggregation rate than {100} sectors. The aggregation rate is enhanced by the presence of vacancies, produced by 2 MeV electrons. Following irradiation, a lower temperature is needed for aggregation and the rate is increased (Collins, 1980).

The **A** centre, which is the most common nitrogen centre in natural diamonds, is comprised of nearest neighbour pairs of substitutional nitrogen atoms lying on a {111} plane (Davies, 1976). As with single substitutional nitrogen, it is possible to aggregate **A** centres into **B** centres. This aggregation is thought to happen via the diffusion of **A** centres rather than the dissolution of **A** centres into single nitrogen atoms and subsequent diffusion (Evans, 1982).

The **B** centre is thought to consist of four substitutional nitrogen atoms, tetrahedraly arranged around a vacancy (van Wyk and Loubser, 1980). IR absorption spectra showing **B** centre absorption are usually accompanied by another absorption peak known as the **B'** peak, found to correspond to platelets (Sobolev *et al*, 1968). Platelets are microscopic planar defects, seen in electron microscopy, which are oriented along {001} planes. Following annealing experiments, Evans and Phaal (1962) suggested that platelets are nitrogen containing. However, despite a number of imaginative models and serious experimental observation, the nature of the platelets is still unclear. Descriptions of the nitrogen and other impurity complexes with their zero phonon line emission frequencies are given in table 2.3.

Name	Description	Absorption peak (cm^{-1})
N centre	Single substitutional, paramagnetic nitrogen atom	1130, 1344
A Centre	Two adjacent substitutional nitrogen atoms	1282
B centre	Four adjacent substitutional nitrogen atoms around a vacancy	1282
B' centre	Platelet	1365
	Carbon interstitial	1531
C centre	Nitrogen interstitial	1450
	Single, uncompensated substitutional boron atom	2802
	Carbon-hydrogen bond	3107, 1405

Table. 2.3. Defect centre descriptions and absorption peak positions.

Hydrogen, boron and other impurities:

Not excluding the elements found in inclusions, the other main impurities in diamonds are hydrogen, oxygen, boron and solvent/metal catalysts. Hydrogen and oxygen have been found in the lattice with concentrations up to 1000ppm (Hudson and Tsong, 1977). There is some evidence that hydrogen is bonded within the crystal (Chrenko *et al*, 1967 and Runciman and Carter, 1971), probably as a carbon hydrogen bond, although there is some conjecture that it may be a nitrogen hydrogen bond or a methene group. In general, it is not easy to detect either oxygen or hydrogen, but there are many ongoing experiments to understand these impurities better (Sellschop, 1992). Absorption features connected with hydrogen have not been found in HPHT synthetic diamond, but have been observed in CVD (Bi *et al*, 1990).

Although there has not been a lot of investigation into the effect of hydrogen on the properties of diamond, a considerable amount of work has been done on metals and on the diamond cubic structured semiconductors such as silicon and germanium. It is widely accepted that nascent hydrogen embrittles metals, either through phase transformations, hydrogen enhanced plasticity or by the weakening of grain boundaries (Myers *et al*, 1992).

The mechanism of hydrogen enhanced local plasticity or HELP (Beachem, 1972) of metals has led to an understanding of the lowering of the yield stress and ultimately premature fracture via the process of increased dislocation interaction (Birnbaum, *et al*, 1974 and Lynch, 1986). More relevantly, hydrogen has been found to affect the properties of single crystal silicon. It has been shown that hydrogen can compensate both n-type semi-conducting dopants (Pankove *et al*, 1983, 1984) and p-type (Bergman *et al*, 1988). It also affects the mechanical properties of silicon. Corbett *et al* (1989) showed that hydrogen causes embrittlement at low temperatures, whilst Zhang and Haasen (1989) have shown that it affects the brittle-ductile transition. It has also been seen that hydrogen aids dislocation motion at elevated temperatures (Kisielowski-Kemmerich *et al*, 1990). Considering that diamond behaves in a similar way to most other materials in its class, there is no reason to believe that it will be different in its response to hydrogen. If this is the case, then hydrogen may be one of the most important property changing impurities found in diamond. Greater understanding of the role of this element will be fundamental to controlling the mechanical properties of diamond.

Another important impurity element in diamond is boron. This is because, when uncompensated by nitrogen, boron makes diamond a p-type semi-conductor. Only small quantities of boron are needed to produce semi-conducting diamond. Studies by Lightowlers and Collins (1976) and Sellschop *et al* (1977) have indicated that concentrations of only 0.02ppm are sufficient to produce effects and concentrations above 0.5ppm are sufficient to cause a visible blue colouration (Chrenko, 1973). The fact that substitutional nitrogen compensates the effect of boron means that semi-conducting diamond must be virtually impurity free. As with nitrogen, boron is incorporated into HPHT diamond inhomogeneously, *i.e.* the boron concentration in each growth sector is dependent on the nitrogen concentration within that growth sector (Kanda *et al* 1989). A schematic representation of the uncompensated boron uptake in different growth sectors can be seen in figure 2.3, where N_A represents the concentration of boron acceptors and N_D represents the concentration of nitrogen donors. Therefore N_A-N_D is the concentration of uncompensated boron, provided that $N_A > N_D$ and is the point at which the diamond will become semi-conducting.

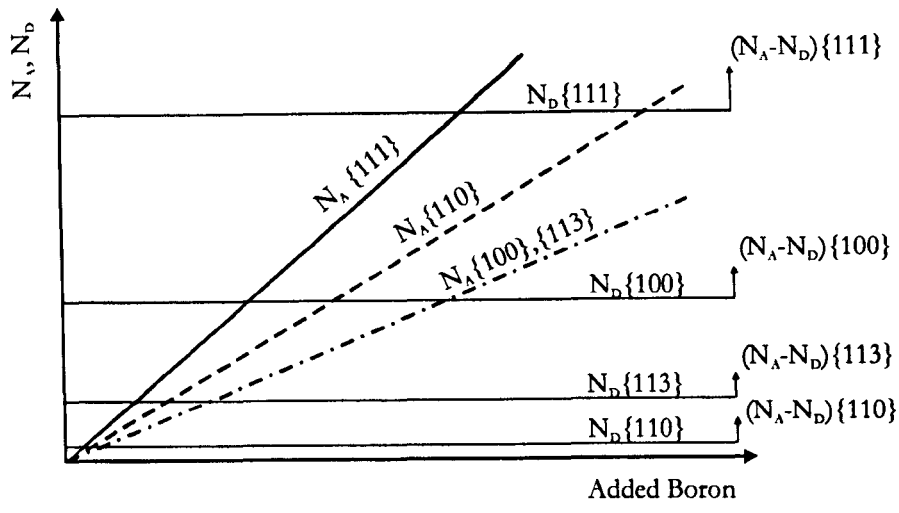

Figure 2.3. The Kanda diagram showing the preferential boron-nitrogen concentration in different growth sectors.

Metal /solvent catalysts such as the group VIII transition metals, are commonly used to catalyse the growth of diamond via the reconstitution method. Work by Loubser and van Rynefeld (1966) and Collins and Spear (1982, 1983) has shown that of all of the possible solvent catalysts, it is only nickel that is incorporated into the lattice as a single substitutional impurity. Collins *et al* (1990) subsequently showed that nickel is only incorporated into octahedral growth sectors.

Inclusions:

Natural diamonds often contain impurities that reflect their origin. Rather than as dispersed singular impurities, these impurities tend to aggregate into microscopic inclusions. These can be either included within the crystal from " birth" or be forced into the diamond via fractures. From a geological viewpoint the first type are very important as they provide a microscopic snapshot of the conditions of synthesis. Inclusions in natural diamond are also a good indication as to the country of origin of the diamond.

Synthetic HPHT diamonds also contain varying amounts of inclusions depending on the quality of the product. They usually comprise graphite or amorphous carbon that has not transformed or combinations of carbon and solvent/ metal catalyst that were trapped. For aesthetic and mechanical reasons, steps are taken to minimise the number and size of these inclusions and as the HPHT technique is developed, they are becoming less numerous.

Nanoscopic (1-10nm) sized octahedral features have been seen in some natural diamonds. Study of these features revealed that they were relatively empty, so the term voidite was coined (Stephenson, 1978 and Barry *et al*, 1987). The content of the voidites is

still under discussion but it is thought that they contain nitrogen in some format, maybe as ammonia (Hirsch *et al*, 1986).

2.3 Defects

There are several categories into which defects can be placed, such as point, line, volume or optical. The most basic of defects is the point defect and most basic point defect is the neutral vacancy. In diamond, the neutral vacancy is known as the GR1 centre, whereas a vacancy with a negative associated charge is known as a ND1 centre. Vacancies are formed during the crystal solidification process by lattice vibration causing displacement of carbon atoms (*i.e.* vacancy plus interstitial) or by the movement and interaction of dislocations. In comparison to the **C** centre, the neutral vacancy is highly mobile. The migration energy for the GR1 is 1.7-1.9ev (Bernholc *et al*, 1988) and is mobile at temperatures above 800°C (Collins, 1980). In contrast, the single substitutional nitrogen defect is relatively stable, having an energy of diffusion of 2.6ev-5ev (Chrenko *et al*, 1977 and Evans and Qi, 1982) and is only mobile at temperatures above 1600°C. Using a semi-empirical method, Mainwood (1994) was able to show that vacancies were likely to aid nitrogen migration. She calculated that the energy of migration of nitrogen atoms via substitutional sites was 6.3ev whilst the activation energy was lowered to 4.5ev for vacancy assisted migration.

There are many other defects observed in diamond, most attributed to nitrogen vacancy interactions, which can be produced by a combination of radiation damage and annealing or by plastic deformation. There is evidence that some of the more complex defects are incorporated into the lattice at the time of growth, e.g. the H3 (N-V-N) defect in HPHT diamond (Dodge, 1986). When a defect either emits or absorbs incident radiation it is known as an optical defect. The optical centre associated with a nitrogen vacancy pair (N-V centre) is of particular interest to this work as it is associated with plastic deformation (Brookes, E.J. et al, 1993). The trapping of a vacancy by a substitutional nitrogen atom can produce two distinct zero phonon lines (ZPL), one at 1.945ev and the other at 2.945ev (575nm centre). The 1.945ev centre has a neutral charge state whilst the 575nm centre has a negative one. Both are also associated with radiation damage and subsequent annealing (Davies, 1976). A list of the most abundant optical defects, together with their descriptions and ZPL absorption peak values is listed in table 2.4.

Name	Description	Zero phonon line	
		(eV)	(nm)
N3	Three nitrogen atoms around a vacancy	2.985	415.2
GR1	Neutral vacancy	1.673	740.9
ND1	Negative vacancy	3.150	393.5
H3	**A** centre plus a vacancy	2.463	503.2
H2	Negatively charged H3	1.257	986.1
1.945	**C** centre plus a vacancy	1.945	637.3
575	Neutral **C** centre plus a vacancy	2.156	574.9

Table. 2.4. Defect centres with luminescence zero phonon line positions.

The most basic line defect is the dislocation. Although diamond is considered to be an almost perfectly brittle material (*i.e.* no dislocation mobility at room temperature) dislocations are observed in diamonds. In general, diamond exhibits the same number of grown in dislocations as any other covalently bonded crystal with the exception of natural type IIa diamonds. Natural type IIa diamonds tend to have a dense, polygonized dislocation structure. The reason for this is unknown, but it is thought that either the lack of nitrogen as an impurity makes the crystal more easily deformed or that the growth conditions were different. Dislocations introduced via deformation processes are described in greater detail later.

2.4 Luminescence

Most diamonds, when irradiated with UV light, lasers, x-rays or electrons luminesce. When they luminesce because of bombardment by light or x-rays, it is known as photoluminescence and when it is due to electrons it is known as cathodoluminescence. The emitted radiation can be of any wavelength longer than the exciting radiation and is due to the absorption and re-emission from the diamond itself and from some defects. This phenomenon is used extensively in the recovery of diamond from rock in mines where X rays are used as the exciting radiation. By recording the emission spectra, the structure (Raman), state or defect content (PL) of a diamond can be evaluated. Luminescence of diamond has also been observed when polishing diamond under certain conditions. The effect of tribo-luminescence on the polishing rate of diamond and on the final product itself is still under investigation (Chapman, 1999).

Photoluminescence:

Photoluminescence (PL) studies are relatively simple, as all that is needed is a light source and a collector, although most studies have to be carried out at very low temperatures. PL techniques have the advantage in that the exciting radiation produces a spectrum of scattered transmitted light that can be used for Raman investigation. Raman (1928) noticed that frequency-shifted lines in the scattered, transmitted light spectra of a transparent object were independent of the exciting radiation. This meant that the frequency shift was a characteristic of the material under observation. Further experimentation established the relationship between the Raman spectrum of a substance and its vibrational and rotational frequencies. However, it is only with the advent of suitable instrumentation (the laser and CCD camera) that the Raman scattering technique has been realised as a tool for investigating the structure of materials. Raman lines that are shifted to longer wavelengths are known as Stokes lines and those shifted to shorter wavelengths are known as anti-Stokes lines. The energy difference represented by the shift in frequency is related to the frequency of the vibrational state. The position and sharpness of the Raman line is related to the degree of crystallinity of the scattering medium. Therefore, the exact position of the Raman spectrum lines can be used as an indication of magnitude and orientation of residual stress within the lattice whilst the line widths are an indication of the degree of perfection of the crystal structure. In diamond, the Raman line at 1332cm^{-1} wavenumbers is used for investigation purposes. The nature of the exciting radiation in PL means that the beam can be focused at any point within the bulk of the crystal to gain spectra, without too much loss. Figure 2.4 shows a PL spectrum taken from a HPHT sample, the Raman, H3 and 1.945ev centre peaks are indicated along with the expected position of the 575nm centre peak.

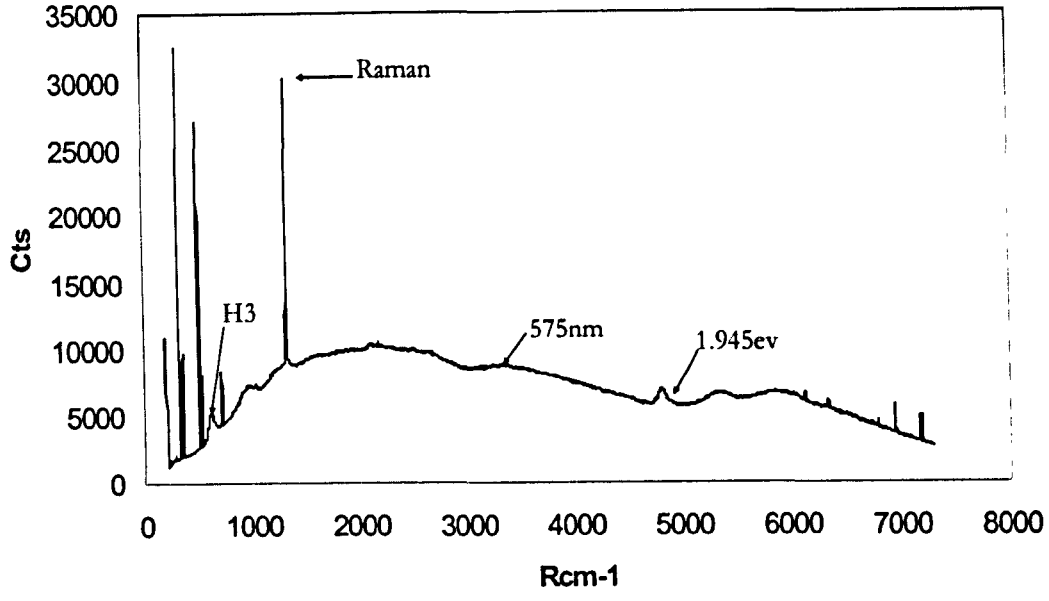

Figure 2.4. PL emission spectrum showing the principal Raman line and the H3, 575nm and 1.945ev centre absorption peaks (514.5nm Ar ion laser)

Cathodoluminescence:

The emission of light due to incident electron irradiation is known as cathodoluminescence (CL) and is most commonly utilised in the phosphor coatings on the back of television and VDU screens. The energy produced is due to the recombination of electron-hole pairs that are created when the material is bombarded with the electrons. This phenomenon is generally seen in materials that have discrete band gaps, such as diamond. For diamond and many other ceramics, the band gap structure means that band gap transitions produce photon emission with wavelengths in the visible range. The presence of dislocations or impurity atoms in the lattice can introduce localised defect states into the band gap structure causing the wavelengths of the produced photons to change. If the photon emission is due to a fundamental band gap transition, then it is known as an intrinsic emission. Conversely, if the photon emission is due to electron transitions that are only possible in the presence of impurity atoms, dislocations etc, then it is known as extrinsic. The low penetrative ability of electrons means that CL is only a surface phenomenon. It is still however, a very useful technique as it can be used to excite large areas and can be incorporated into a scanning electron microscope (SEM). As with PL, great care must be taken with CL when making quantitative measurements of defect concentrations. The intensity of the emitted light is affected by the energy of the incident electrons and is a competitive process, *i.e.*, the measured intensity due to a specific defect

can be affected by other defects in the vicinity of the emitting centre being measured. For this reason, CL is used, mainly as a qualitative rather than quantitative tool.

CL has been a very useful tool in the investigation of the growth history of diamond. This is because the different impurity make-up of each growth sector emits very different colours. In synthetic HPHT diamonds, for instance, the cubic growth sector luminesces bright green, {011} steely blue, {113} light blue and the octahedral growth sector does not luminesce (Woods and Lang, 1975). CL is also dependent on temperature (Burns *et al*, 1990). At temperatures of about 90K the {110} growth sectors change from a steely blue colour to not luminescing at all. This effect can be seen in figure 2.5, where two CL images of the same {110} slice of a HPHT diamond have been taken at different temperatures but otherwise exact experimental conditions. The green colour associated with the cubic growth sectors is attributed to the H3 defect and is polarised due to the preferential orientation of H3 centres as they are incorporated during growth (Dodge, 1986).

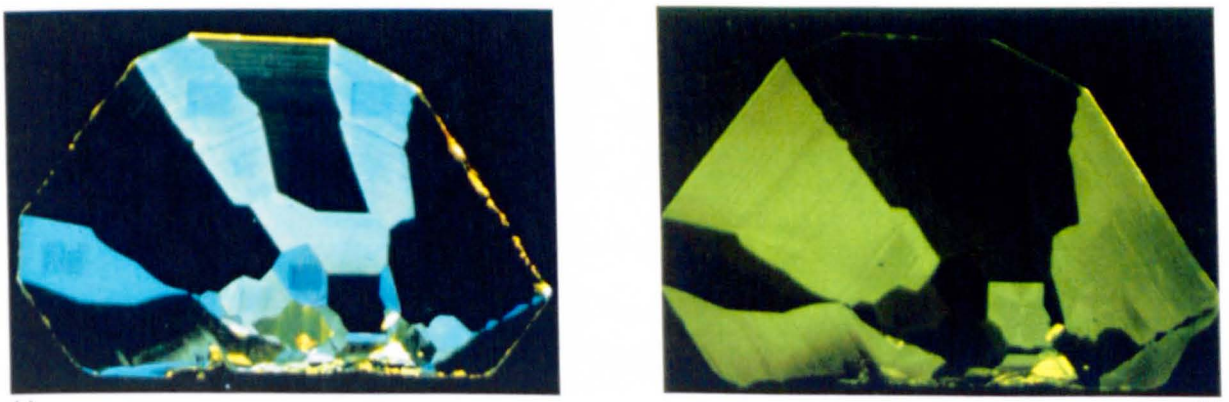

(a) (b)

Figure 2.5. Cathodoluminescence topograph of a {110} sliced HPHT synthetic diamond viewed at different temperatures (a) 290K and (b) 90K (taken from Burns, 1990).

2.5 Synthetic Diamond (HPHT)

The HPHT synthesis of diamond was developed following the calculation of the diamond – graphite equilibrium line Berman and Simon (1955). Figure 2.4 shows the Simon-Berman equilibrium line, where graphite is stable below it and diamond above. Superimposed onto the diagram is the melting line of nickel and carbon. The shaded region indicates the diamond growth regime. The production of large synthetic single crystals is via the reconstitution technique (Burns and Davies, 1992). This method involves dissolving a carbon source (usually graphite or diamond powder and allowing it to precipitate out under conditions where diamond is the most stable carbon allotrope. Reconstitution is

facilitated by using a temperature gradient inside the capsule and by providing the precipitating diamond with a nucleation site, in the form of a seed crystal. For the production of large synthetic crystals, diamond powder is the preferred carbon source, as it does not produce a volume change in the capsule upon conversion. In addition, solvent/metal catalysts are used to aid the melting and subsequent re-crystallisation of diamond by lowering the conditions needed for graphite to diamond conversion. The HPHT equipment is usually referred to as the belt apparatus (Hall, 1970). Although it is clear that the apparatus currently used is based on the belt apparatus, it is almost certain that the companies involved in producing large synthetic crystals have developed it, but not published, for commercial reasons. In general, the solvent/metal catalysts are complexes of iron-cobalt-nickel or manganese-nickel. The exact solvent metal catalyst used is dependent on the final result required and the synthesis conditions and is a commercial secret. For this work, no attempt was made to classify the samples by identification of the solvent metal catalyst used as it was felt that it would not affect the results.

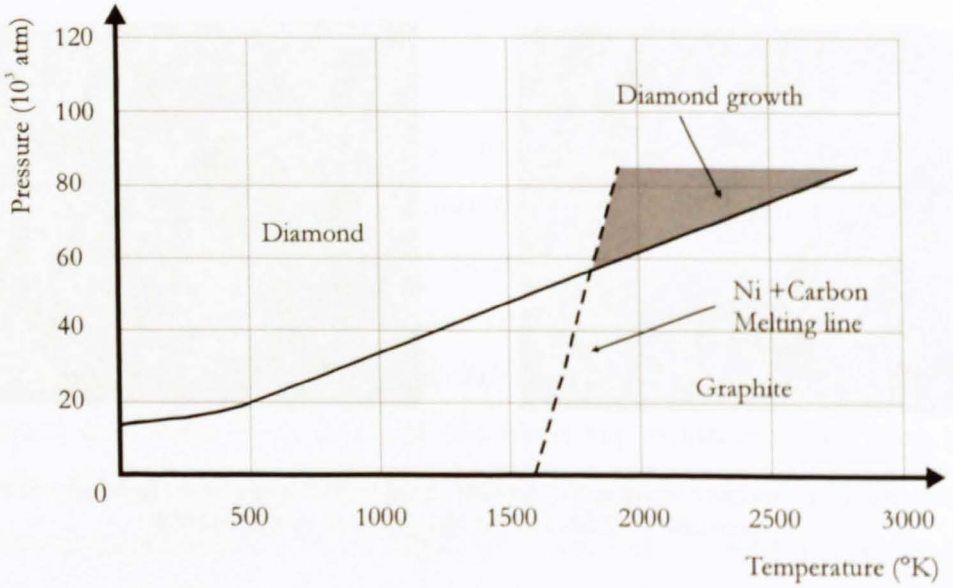

Figure 2.6. The Simon Berman line of diamond – graphite equilibrium.

The morphology of synthetic (HPHT) diamond is similar to natural diamond in that it is dependent on the conditions of growth, but tends to be cubo-octahedral in habit rather than octo-dodecahedral. The exact reason for this is still under discussion but the cubic nature of HPHT diamonds make them particularly useful for monolithic industrial purposes, as they require little finishing. The relationship between the cubic {001} growth and octahedral {111} growth depends on the solvent metal catalyst, the synthesis temperature and the nitrogen content (figure 2.7). In general, the higher the nitrogen content, the more dominant the cubic growth. As the seed crystal grows within the capsule

it offers five {001} faces on which to grow (the sixth is attached to the seed pad). In between each of these {001} sectors there is an interconnecting sector, usually of {111} or {110} habit but {113} sectors have been reported. No two sectors of the same habit touch; there is always a layer with different habit in between, although it is sometimes very small. The three dimensional nature of the growth, coupled with the competitive growth of the {001} and {111} sectors, means that the growth sectoring of a stone can be very complicated. As the stone grows away from the seed the sectoring becomes simpler as certain sectors are overgrown and annihilated. Once removed from the reaction cell, the diamonds are cleaned and the seeds removed. If enough of the reconstituted diamond is removed with the seed, the result is a crystal that consists, almost exclusively, of {111} and {001} sectors. If the synthesis conditions are favourable, it is possible to produce stones that are almost exclusively {001} growth sectors.

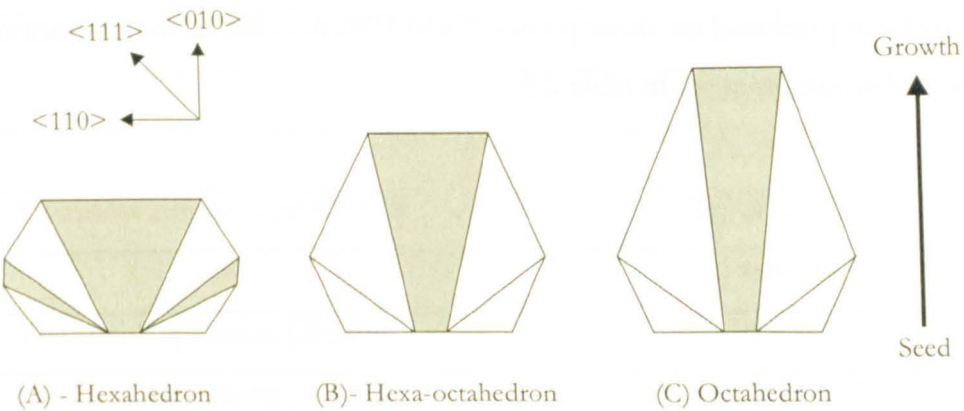

Figure 2.7. Showing the synthesis temperature dependence of growth sectors in synthetic diamond for a pressure of 5.5GPa. Where (A) represents a synthesis temperature of 1350°C, (B) 1370°C and (C) 1400°C. Diagrams show {001} growth sectors (shaded) and {111} sectors (unshaded) for a {110} cross section.

2.6 Mechanical Properties

The main reason why diamond has such exceptional mechanical properties is the C-C bonding. There are many materials that have C-C bonds within their structure, but it is the tetrahedral formation of the C-C bonds in diamond that allows it to exhibit the C-C bond strength in all directions. For example, graphite also has C-C bonds, but it has three C-C bonds in a trigonal planar formation with the extra valency electron forming a van der Waals bond. The trigonal planar bonds form sheets of two dimensional, hexagonaly bonded carbon atoms with the van der Waals bonds providing the bonds between successive sheets. Although a single sheet of graphite may exhibit very high strength properties, the fact that the sheets are free to glide over one another makes graphite, macroscopically speaking, a soft material. In diamond, however, all four valence electrons

form covalent bonds. The small size of the carbon atoms means that C-C bond has virtually the perfect tetrahedral bond angle, also that the bond is very short (0.155nm). This means that carbon can form a tetrahedral arrangement with virtually full theoretical strength, enhanced by the length of the bonds. This arrangement produces a crystal in which the bonds are very stiff and difficult to break, which in turn, means that the elastic modulus is very high and dislocation movement very difficult. The same effect, but to a lesser extent (as they are larger atoms), can be seen in the crystalline forms of the elements that are in the same period group as carbon, such as silicon and germanium.

The extreme stiffness and hardness produced in diamond, however, means that this atomic structure is very brittle. The energy to produce a crack is equal to the energy needed to create the two new surfaces, *i.e.* there is little or no energy lost to plastic behaviour. The crystal periodicity of diamond means that fracture in diamond is anisotropic, with cleavage occurring predominantly on the {111} plane, although under the suitable conditions, cleavage has been produced on other planes (Field 1992a). A list of the relevant mechanical properties of diamond is given in table 2.5.

Property	Symbol	Value
Density	ρ	3520 Kgm^{-3}
Refractive Index	η	2.417
Young's Modulus	E	1141 GPa
Shear Modulus	G	507 GPa
Bulk Modulus	K	442GPa
Tensile Strength	σ	300$Kgmm^{-2}$
Compressive Strength	S	8.84 GPa
Poisson's Ratio (Isotropic)	ν	0.07
{111} Cleavage Energy	γ	5.5 JM^{-2}
Stress Intensity Factor	K_{IC}	3.4-5 $MNm^{-3/2}$
BDTT		(IIa) 1100°C
		(Ia) 950°C
		(Ib) 770°C
Thermal Conductivity (293K)		(IIa) 2000-2200
		(Ia) 600-1000
Thermal Expansion (293K)		$0.8x10^{-6}$
Electrical Resistivity		(IIa-Ia) $>10^{14}$
		(IIb) 0.1-10

Table. 2.5. Properties of diamond (Field, 1992b)

Hardness testing:

The concept of the hardness of a material was first used by Mohs who ranked various substances based on which could scratch which. Mohs devised a scale of 1 to 10 and gave each mineral a number. Any mineral with a higher number was able to scratch a mineral with a lower number. The scale is not linear as the gap between the number nine material (corundum) and the number ten material (diamond) is much greater than the gap between the number nine material and the first one (talc). The scale does, however, take into account many of the available materials of the time and was a useful guide to relative hardness.

The concept of hardness as a material property is a difficult proposition, as the hardness of a material depends on the type of test used and the conditions under which it

was done. For example, it has since been shown that, given the right experimental conditions, materials on the Mohs scale are capable of scratching each other, irrespective of their ranking. The concept of hardness is really the concept of the ability of a material to withstand plastic deformation by whatever means and as such, is probably not a true material property. The difficulty of defining such a mixed property with precision has led to standardising of techniques for measuring hardness.

The main techniques used today are based on forcing a shaped indenter into a flat surface of the specimen, under a known normal load. The hardness is a function of size of the depression that is created. There are several popular shapes of indenter in use, each having advantages and disadvantages. The Brinell and Rockwell tests both use hardened balls whereas the Vickers, Knoop and Berkovich methods use polished, pyramidal shaped diamonds. Here, discussion is restricted to the use of the diamond indenter methods, as these are the only ones capable of measuring the hardness of diamond itself. Another consideration, when performing hardness tests, is that there is a constant relationship between the area of the indentation and the load. For an indentation to be geometrically similar, irrespective of its depth, the indenter must have a high ratio between the load and the indentation radius, with the perfect ratio being infinity. This is achieved by an ideal cone. As such, sharp tipped indenters, such as those used in diamond indenters have a high ratio, whereas ball shaped indenters have a low one.

The Vickers, Knoop, and Berkovich methods utilise a diamond that is polished to a sharp point, such that there is geometric similarity in the indentations. The Vickers method uses a square based pyramidal diamond with faces polished at an included angle of 136°. The Knoop indenter also uses a square based pyramidal indenter but with one diagonal seven times longer than the other. The angle between the faces on the long diagonal is 172°30′ and 130° for the short diagonal. The Berkovich indenter on the other hand is a triangular based pyramidal indenter with a 65° angle between each facet and its axis. The Knoop indenter is favoured over the Vickers indenter in situations where cracking is likely or where surface properties are required. This is because the geometry of the Knoop indenter reduces the likelihood of cracking and also penetrates less deeply into the bulk of the sample. The Berkovich indenter is preferred for nano indentations, as its geometry produces a single sharp point rather that a chisel edge making it easier to manufacture.

Other than geometric similarity, there are a great number of factors that can affect the calculated value of hardness. From the graph of hardness versus load for the {001} plane of diamond shown in figure 2.8, it can clearly be seen that the hardness value increases as the load decreases. This phenomenon is known as the indentation size effect (ISE) and several explanations have been forwarded. Khruschov and Berkovich (1951)

hypothesised that sample preparation techniques, such as polishing, leave a residual hardened layer. As the load is reduced, the proportion of the indentation lying within this zone will be increased thereby increasing the measured hardness. Burnand (1974) hypothesised that it was due to the nature of the slip associated with the deformed zone. He calculated that if the distances between the slip bands were smaller for lower loads, then this would produce more strain and therefore work hardening. It was found that the ISE is most significant below loads of 20N and that it has a greater effect as the intrinsic hardness of the specimen increases (Brookes, 1979). Another reason for the ISE may be that as the load is reduced the sampled specimen area is correspondingly reduced. As this happens it is more likely that the sampled material is defect free and as such will require increasing values of stress to initiate deformation (Brookes, 1984). A quantitative model produced by Bull *et al* (1989) showed that the ISE was due to the recovery of the elastic component of deformation within the deformed zone, which decreased the size of the measured indention.

The load is not the only factor that can affect the measured hardness. The type or indenter used also plays a part in the final result, although this effect is not as strong as in the ISE. The geometry of the indenter can often give different results, as the sides of the indenter create shear stresses that, when resolved, act in particular directions.

Room temperature hardness of diamond:

Although indentation hardness experiments have been carried out on diamond since just after the Second World War, surprisingly little data is available. This is mainly because a suitable indenter material is not available for indenting diamond. What data there is, however, is contradictory, with values of between 60- 300GPa being quoted for the {001} plane. Figure 2.8 shows a summary of hardness data for the {001} plane of natural diamond obtained using different loads. For simplicity, it is assumed that the hardness values are independent of the type of indenter used or its orientation. As can be seen from the graph, all of the data so far collected of the indentation hardness of diamond was made at loads below the recognised level where the ISE becomes critical. Whatever the reason for the indentation size effect, it is clear that care must be taken when choosing the indentation load and when comparing different sets of data.

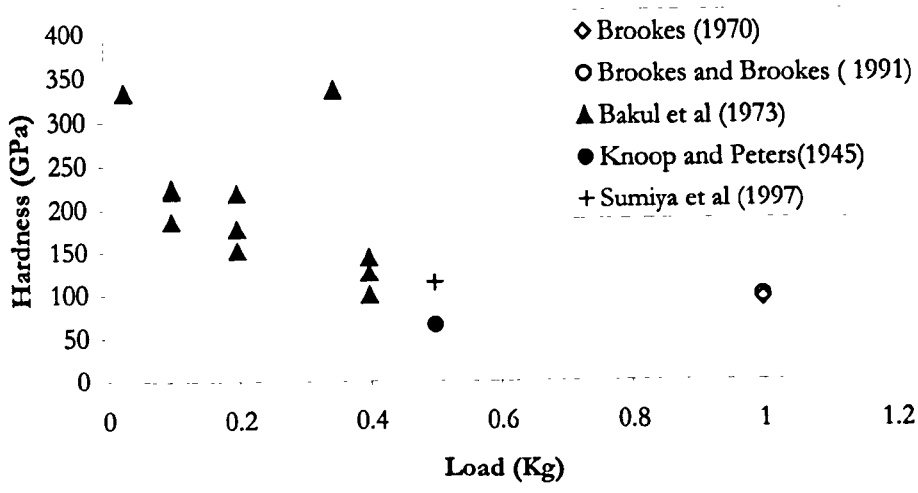

Figure 2.8. Graph of hardness versus load for the {001} plane of natural diamond.

The indentation hardness anisotropy of diamond was first reported by Semenova *et al* (1969) where different crystallographic planes were indented. It was found that {111} planes were significantly harder than {001} planes. During this work the specific orientation of the indenter on the surface was not recorded and it was later determined that it is of considerable significance. In 1971 Brookes carried out a detailed investigation into the anisotropy of crystals and determined that it was intrinsic to all crystals and due to the different active slip systems and their orientation to the facets of the indenter. Later Brookes (1979) reported that the <100> and <110> directions on the {001} plane exhibited significant hardness anisotropy in type Ia diamond, with the <110> direction being harder.

Hardness of diamond at elevated temperatures:

It has been shown by several authors (Loladze *et al,* 1967, Brookes, 1979, Evans and Sykes, 1974, Trefilov et al 1975 and Novikov *et al,* 1991 and 1994) that the hardness of diamond decreases uniformly with increasing temperature. At some point (~1500°C) the rate decrease in hardness starts to level out, as shown in figure 2.9 (Borisenko *et al,* 1973). The reason for the initial linear decrease in hardness is due to the increasing amount of dislocation activity. It is thought that the increase in dislocation activity is due to the increased temperature aiding the dislocations to overcome the Peierls barrier, to create laminar flow. The ease of dislocation movement aids the lattice to flow thereby creating a larger indentation and conversely, a lower hardness is measured. The point at which plastic deformation becomes significant is usually one half to two thirds of the melting point and is an indication as to the brittle ductile transition temperature. Although there is some

scatter amongst results, significant plastic deformation is only seen at temperatures above 750°C. At higher temperatures, however, the relationship between hardness and temperature ceases to be linear and the rate of decrease in hardness is reduced. This is due to the work hardening effect of the dislocations interacting with one another to slow down the dislocation movement. Although the measured hardness of diamond is reduced by an order of magnitude by raising the temperature from room temperature to 1500°C, the rate of softening is not greater than that observed for other materials. The hardness of diamond is still expected to be the highest of all materials at any temperature (Brookes, 1992).

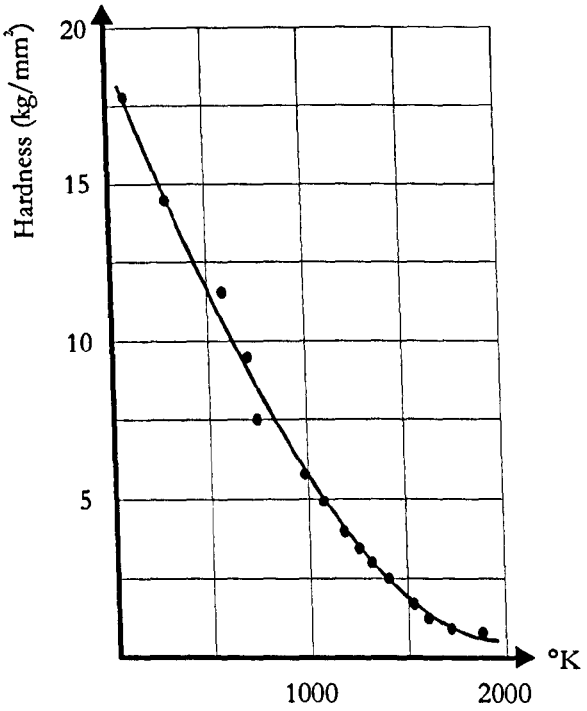

Figure 2.9. Graph showing the hardness of diamond versus temperature (Borisenko *et al*, 1973)

The effect of nitrogen content:

The true nature of the effect of nitrogen content on the mechanical properties of diamond has yet to be determined, despite a wealth of information. It is clear from work carried out so far that nitrogen content does have an effect, but that effect has yet to be agreed upon. For instance, Bokii and Kirova (1975) and later Bokii *et al* (1979) determined that the compressive strength of small synthetic diamonds was decreased by doping with nitrogen. Whilst Field (1992) found that although there was some evidence of a drop in strength with increasing platelet concentration, there was no definite correlation between strength and nitrogen concentration. Also, during abrasion resistance testing, Chrenko and Strong (1975) noted that there was a decrease by approximately a factor of 10 when the nitrogen content of synthetic type Ib diamond was raised from 0.1ppm to 200ppm, whilst

Wilks and Wilks (1982) stated that there was no discernible difference between good quality diamonds containing different levels of nitrogen when subjected to abrasion tests.

Hardness measurements of diamond have been carried out by several research groups, with a view to determining the effect of nitrogen content. Brookes (1979) showed that nitrogen-containing diamond was significantly softer than those containing little or no nitrogen but large dislocation networks (IIa). Novikov and Dub (1992) stated that the fracture toughness of types Ia and Ib diamonds, as measured from Vickers indentations was similar. Sumiya *et al* (1997) and Miyoshi (1998) have stated that the hardness of natural type Ia and synthetic type Ib diamond is decreased as nitrogen content is increased, but with type Ia diamond being harder than the type Ib. They also stated that there was considerable hardness anisotropy, with {001} <100> being the hard direction, but that the anisotropy is reversed in type IIa samples.

The apparent contradiction in the results between the various groups may be due to the inhomogeneous nature of the samples that were tested. It is likely that it is not just the simple case of nitrogen concentration, but the fact that nitrogen type, position and experimental temperature could affect results. This is probably exacerbated by the presence of dislocation networks and the stress/ strain conditions. However, with large, good quality synthetic diamond routinely being produced, a better understanding of the effect of impurity elements in terms of their modification of mechanical properties is now possible.

2.7 Plastic Deformation

Before discussing the plastic deformation of diamond, it is prudent to describe the structure of diamond in greater detail. Diamond is made up from carbon, which has a valency of four. In the case of diamond, each carbon atom is bonded to another carbon atom (assuming no impurities) in a tetrahedral formation (figure 2.10). The distance between the atoms 0.155nm with a bond angle of 109.5°. When viewing the diamond lattice in the traditional unit cell form, it can be seen that diamond produces two interpenetrating F.C.C. cubes offset from on another by1/4 [111] (figure 2.11).

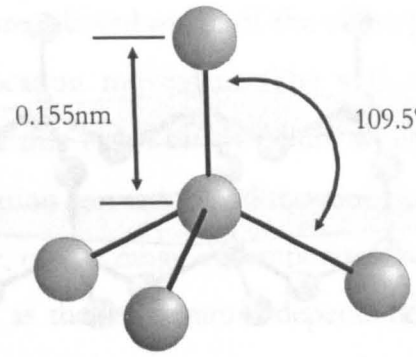

Figure 2.10. Tetrahedral arrangement of diamond.

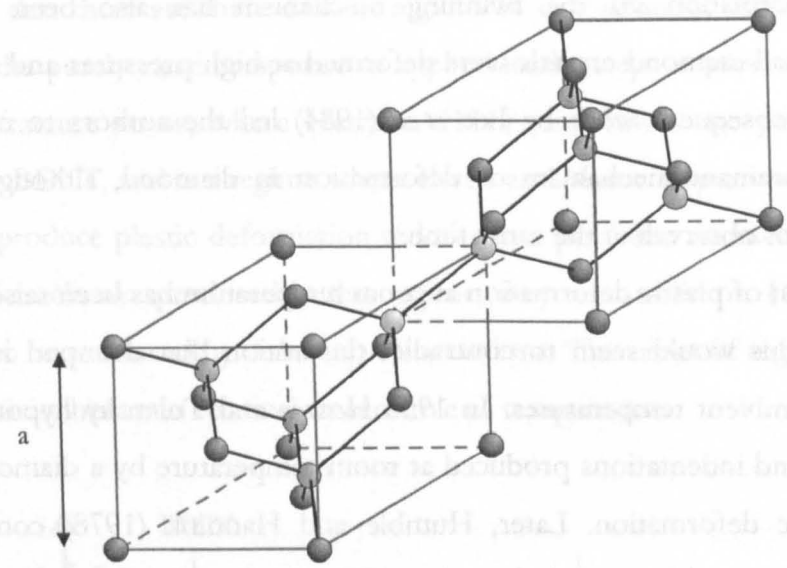

Figure 2.11. Arrangement of the diamond cubic unit cells.

The F.C.C. structure of diamond means that the slip system is {111}<110>, *i.e.* the closest packed planes and the shortest lattice vector. A dislocation of unit magnitude is $a/2\sqrt{2}$, where **a** is length of the edge of the unit cell. There are three types of dislocation observed in diamond, those that have the burgers vector parallel and perpendicular to the dislocation line (screw and edge respectively) and those with the burgers vector at 60° to the dislocation line. The dislocations in F.C.C. crystals are able to dissociate into partial dislocations with lattice vector a/6 <112>. The diamond cubic structure means that it is necessary to distinguish between alternate {111} planes, because the stacking sequence of the {111} planes produces two different atom densities in the dislocation direction. The alternate planes are known as the glide and shuffle planes. Dislocation activity is generally confined to the glide rather than the shuffle plane as it has the higher atom density (figure 2.12).

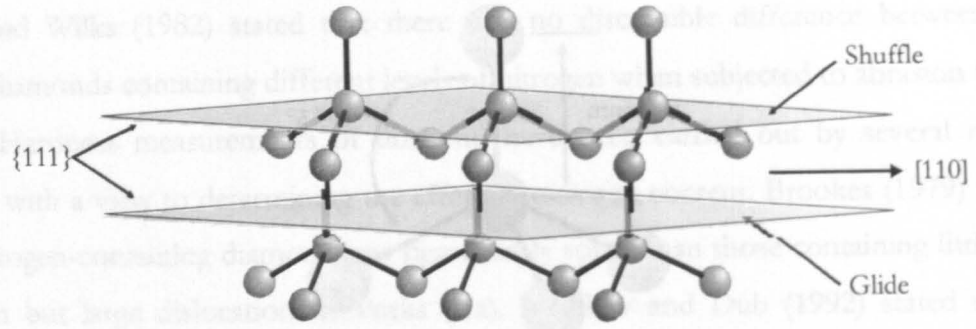

Figure 2.12. The diamond cubic structure showing the glide and shuffle planes.

Plastic deformation via the twinning mechanism has also been observed in diamond where small diamond crystals were deformed at high pressures and temperatures (DeVries, 1975). Subsequent work by Lee *et al* (1984) led the authors to conclude that twinning is the dominant mechanism of deformation in diamond, although twins and dislocations were not observed at the same time.

The question of plastic deformation at room temperature has been raised by several authors, although this would seem to contradict the notion that diamond is a perfectly brittle material at ambient temperatures. In 1955 Howes and Tolansky hypothesised that the raised area around indentations produced at room temperature by a diamond ball, was produced by plastic deformation. Later, Humble and Hannink (1978) confirmed that dislocations were produced beneath indentations (Vickers) by using transmission electron microscopy. The theory of room temperature plasticity is used to explain hardness anisotropy in diamond (Brookes, 1970).

The observation of the plastic deformation in diamond at elevated temperature is less controversial and now a widely accepted fact. Work carried out by Evans and Sykes (1974) on the mutual indentation of crossed diamond wedges, showed that diamond was fully plastic above temperatures of 1850°C. Work on the high temperature fracture toughness, as calculated from Vickers indentations, led Novikov *et al* (1993) to state that the brittle –ductile transition temperature of type Ia diamond was closer to 1350°C. The development of the soft impressor technique to produce plastic deformation in diamond in a manner that inhibits crack growth, has shown that the brittle-ductile transition temperature (BDTT) for type Ia diamond is in fact closer to 950°C (Brookes, 1979 and Brookes, E.J. 1992). Note that this figure is well below the conventional point for the onset of plastic deformation of 0.5Tm (Tm = homologous temperature). The disparity in the results may be due to the difference in the definition of plastic deformation used by each of the authors. Another possible explanation stems from the fact that the critical resolved shear stress for diamond is higher than the stress necessary to cause cleavage fracture. Therefore, in many of the previous investigations, a brittle response was observed before a

plastic one. The brittle fracture relieved much of the stress produced that would otherwise have been relieved by dislocation movement. The soft impressor technique, however, inhibits stress concentrations that cause brittle failure whilst allowing shear stresses to be set up that encourage dislocation formation and movement *i.e.* plastic deformation. Use of the soft impressor technique, over a range of temperatures, has led to identification of the BDTT for diamond as well as the temperature dependence of the critical resolved shear stress. Brookes, E.J. (1992) developed a schematic diagram to represent the effect of temperature and pressure on the deformation of diamond (figure 2.13). It can be seen from this diagram that there are three distinct regions of deformation, or regimes. Regime I is denoted by the purely elastic response to applied load except at pressures high enough to exceed the fracture stress, where Hertzian {111} ring cracks are produced. Regime II begins at the BDTT, and is a regime where elastic and plastic responses are evident but the pressure to produce plastic deformation reduces in a parabolic manner as the temperature increases. If cracks are produced in this regime, they tend to lie on {110} planes and are considered to be produced by dislocation interactions. The onset of regime III is where the level of plasticity becomes relatively insensitive to temperature.

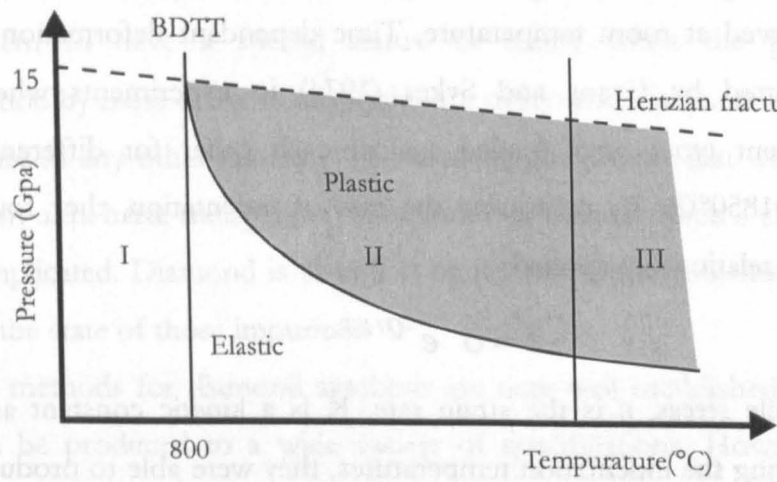

Figure 2.13. Schematic diagram showing the brittle-ductile transition of diamond.

The effect of nitrogen content:

As with the effect of nitrogen on the indentation hardness of diamond, the results of the effect of nitrogen on the plastic properties of diamond seems to be contradictory. Evans and Wild (1965) reported that when subjected to three-point bend tests, type IaB diamond required higher stresses for deformation than type IIa. Mao and Bell (1978) also noticed that deformation of high-pressure diamond anvils was a minimum when the diamond contained high level of nitrogen and platelets. Conversely Evans and Sykes (1974)

reported that under mutual indentation testing type IIa diamond became fully plastic at a lower temperature than type Ia (1700° and 1750°C respectively). Brookes E.J. (1992) used the soft impressor technique to estimate the brittle-ductile transition of types Ia, Ib and IIa diamond. In that work it was reported that whilst the form of the elastic- plastic transition was the same for all types of diamond, the temperature for the onset of plasticity (BDTT) was different for each type. The BDTT was found to be 770°, 950°, and 1100°C for types Ib, Ia and IIa respectively. In that work it was also shown that an increase in the nitrogen concentration of type Ia diamonds reduced the critical resolved shear stress.

It is clear that the type of nitrogen present, as well as its concentration, plays an important role in the plasticity of diamond. It is also clear that great care should be taken not to mistake the effect of dislocation networks and platelet concentrations for that of dispersed nitrogen concentrations.

Creep:

Knoop indentation creep experiments carried out by Harrison (1973) revealed that although significant indentation creep was observed at temperatures of 1100°C and above, no creep was observed at room temperature. Time dependant deformation or creep of diamond was reported by Evans and Sykes (1974) in experiments where diamond octahedra of different types were loaded against each other for different times and temperatures (1500-1850°C). By measuring the rate of indentation, they found that the following Arrhenius relationship applied:

$$\dot{\varepsilon} = \sigma \; e^{-Q/KT}$$

where σ is the tensile stress, ε is the strain rate, K is a kinetic constant and T is the temperature. By varying the indentation temperatures, they were able to produce values of activation energy (Q) of 10.7ev ($31RT_m$) and 14ev ($40RT_m$) for types II and I diamond respectively.

More recently, the soft impressor technique has been used to investigate the impression creep properties of single crystal (Brookes E.J., 1992) and polycrystalline diamond (Harris, 1997). Again, using the soft impressor technique it was possible to show that extensive deformation of diamond is possible at lower temperatures than previously thought. In the work by Brookes, E.J. (1992) it was shown that diamond creeps at temperatures just above the brittle–ductile transition temperature. This was achieved by loading a cubic boron nitride (cBN) cone against the {001} surface of different types of diamond. In each case several impressions were made, each with different dwell times (300,

1000, 2000 and 3000s) at a constant temperature. The resultant impression volume was then calculated using optical interferometry and assuming that the impression volume approximated to a truncated cone. The contact area increased, due to creep of the impressor material. The depth of the impression continued to increase, due to creep of the diamond and as a result, the volume of the material displaced from the impression also increased with contact time. The rate of change of volume for a given temperature was measured for natural diamond types IIa, Ia and synthetic HPHT type Ib. The experiments were repeated for temperatures in the range 800-1400°C. Graphs of volume rate change versus reciprocal temperature were plotted and activation energies (Q) taken from the slopes of those lines. The activation energies (Q) calculated were 2.92eV ($8.48RT_m$), 2.89eV ($8.38RT_m$) and 1.2eV ($3.5RT_m$) for types IIa, Ia and Ib respectively.

2.8 Summary

The notion forwarded by people such as Pliny the elder and Jean Baptist Tavernier and perpetuated by the jewellery trade, that diamond is the most perfect of materials and has the ability to resist any force, is a fallacy. Although the ultra high properties may make diamond seem to have a special status, in reality when the problems posed to experimentation by these extreme properties are overcome, diamond is subject to the same laws of nature as any other material. This chapter has shown that whilst on a basic level diamond is an ultra hard, transparent super lattice of carbon, when a closer look is taken, it is more complicated. Diamond is classified by the impurities substituted into its structure and also by the state of those impurities.

The methods for diamond synthesis are now well established and diamond single crystals can be produced to a wide variety of specifications. However, the mechanical properties, particularly at elevated temperatures are not as clearly understood and there is considerable scope for future work. This chapter has looked at diamond with respect to its most basic defect structure, *i.e.* what the defects are and how they are identified. The measurement of hardness is outlined and the effect of nitrogen.

The work in this thesis will show that using the soft impressor technique together with studies of luminescence will give information on the state of the carbon lattice and the defect interaction after controlled levels of plastic deformation have been introduced. Continued experimentation in this field may lead to a better understanding of the mechanical limits of diamond, which will in turn will aid with designing diamonds for industrial rather than cosmetic use.

Chapter 3

EXPERIMENTAL APPROACH

3.1 Introduction

The traditional method for measuring the properties of materials such as hardness, toughness and strength is to load the specimen surface with a rigid, diamond or semi-rigid spherical indenter and measure the size of the indentation produced. The problem with these methods is that they produce large stress concentrations that encourage crack formation, which often masks more subtle reactions, such as the onset of plasticity. It was shown in 1972, by Brookes and Green, that it was possible to multiply and move fresh dislocations in single crystal magnesium oxide as a result of the pressure developed by a conical cone of copper loaded against the surface. This work not only showed that soft materials can induce significant deformation in harder materials, but that they can produce as much deformation as rigid indenters at stresses significantly lower than the cleavage stress. This effect is shown in figure 3.1, where two indentations have been made under exactly the same conditions, one using a Vickers indenter and the other using a soft impressor at a temperature of 1300°C. It is clear that in both instances significant plastic deformation has occurred, however the soft impressor has avoided cracking altogether.

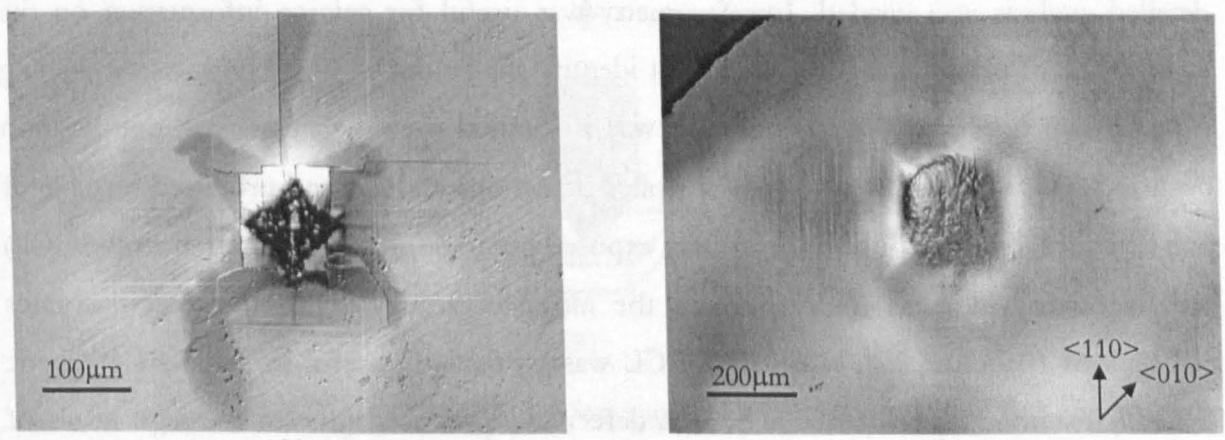

Figure 3.1. Optical micrographs of (a) a Vickers indentation and (b) a soft impression made in diamond, at 1300°C under a load of 115N for dwell time of 300s.

Following this discovery, the *soft impressor technique* was developed and is now used to produce a range of levels of deformation in many different materials. The beauty of the soft impressor technique is its subtlety. A rigid indenter can only produce a limited, discrete range of contact pressures, dependent on the load used. That pressure is often accompanied by large stress concentrations, unavoidable due to the geometry of the indenter. The soft impressor technique on the other hand can produce a virtually infinite range of pressures whilst avoiding any large stress concentrations, the only limitation being the choice of materials with which to fabricate the cone. Using this technique is it possible to determine the pressure to produce a few dislocations or many thousands and has led to the studies of extensive plastic deformation of diamond (Brookes, 1992). As shown in the work by the research group in the department of Engineering Design and Manufacture (EDM) at the University of Hull, the soft impressor technique is not restricted to static loading scenarios. By reciprocating, or rotating the specimen whilst loaded, friction experiments can be made. By cycling the applied load to the impressor, fatigue data can be gathered and by varying the time that the specimen is under load, the time dependent plastic flow or creep characteristics can be determined. The specially designed equipment (figure 3.4) also allows the testing environment to be flooded with any chosen atmosphere, thereby allowing all of these experiments to be made under inert, corrosive, lubricated conditions etc.

Many techniques have been used in this study to identify the quantity and structure of the slip for these experiments, each having varying levels of success. Optical microscopy was very useful for gaining an overall view of the deformation, but it was limited when a detailed analysis was needed. Interferometry was useful for gaining information on the topography of impressions, but could not identify slip or dislocations. Dislocation etching exposed slip lines and dislocations, but was of limited use when extensive deformation occurred. This was because the etch pits piled up on one another and produced a tangle of pits that gave a picture rather like an over exposed photograph. Cathodoluminescence (CL) on the other hand was useful because the nitrogen-vacancy (575nm) defect decorates dislocations (Brookes, E.J. *et al*, 1993). CL was particularly useful in standard synthetic (HTHP) diamond, as a lot of the 575nm defect was produced (due to the high levels of nitrogen) and luminesced bright red, whilst the {001} growth sector luminesced bright green due to the grown-in H3 defect. The overall result was a micrograph displaying bright red dislocations on a bright green background, which provided a very good contrast. Like standard optical microscopy techniques, however, CL does not reveal dislocations with

impunity or in any great detail. Although none of these techniques was perfect, they could all be used in conjunction with one another to gain the desired information. For the sake of simplicity and brevity, in this report only the technique or techniques that best described the desired result were displayed. It can be assumed that all the different techniques were applied as part of the investigative process.

The soft impressor technique:

The soft impressor technique uses a conical cone with included angle 120°, which replaces the usual pyramidal diamond indenter. The fact that the cone is fabricated from a material that is softer than the specimen means that upon loading against the surface the cone deforms (figure 3.2). The cone continues to flatten until the normal applied load is supported quasi-hydrostatically. The degree to which the cone flattens is dependent on the hardness of the cone material and independent of the specimen material. The mean pressure (P_m) supplied to the specimen is then calculated by determining the area over which the cone has flattened out (the contact area) and dividing it into the applied load used, *i.e.* $P_m = L/A$, where L is the applied load (N) and A is the contact area between the cone and the specimen (m^2). The fact that the cone is unconstrained and free to flow means that any stress concentrations at the interface and periphery of contact are minimised. This reduces the instances of brittle failure.

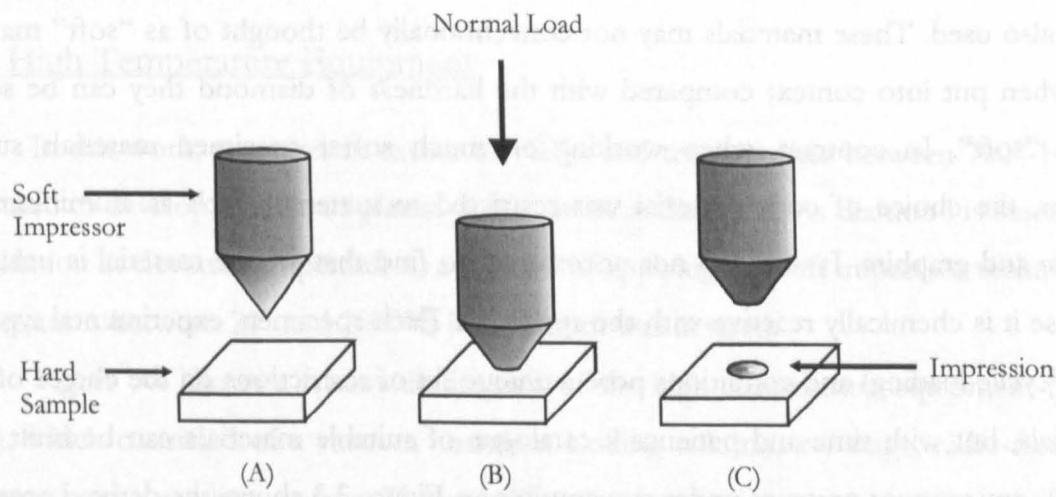

Figure 3.2. The Soft impressor technique

When a large depression is formed in the specimen there may be a small component whereby the sides of the depression restrict the cone from flattening further. There may also be some instances where the friction between the cone material and the

specimen is sufficient to inhibit the flattening out of the cone. In both cases, this does not effect the outcome of the experiment as the pressure produced by the cone is measured for each experiment. Owing to the obvious difference between the soft cones and rigid indenters, it was felt that the term indenter was inappropriate. Therefore, the term impressor was coined.

Impressor materials:

For experiments on diamond and other super-hard materials, it was necessary to increase the temperature of impression to gain any permanent deformation other than brittle fracture. This was accomplished in much the same manner as with conventional high temperature indentation techniques. However, care had to be taken when choosing a suitable cone material, as not only would the cone flatten out more at elevated temperatures, but also in some cases the cone material was unstable at the required temperature.

The choice of impressor material is fundamental to the soft impressor technique. To produce a range of pressures for a given load, temperature and time, different impressor materials must be carefully chosen, each material having a progressively higher hardness (at the chosen experimental temperature). To achieve sufficient pressures to deform diamond the cone material must be extremely hard. For this reason, the cone materials predominantly used in this work were reaction sintered cubic boron nitride (cBN), silicon nitride (Si_3N_4) and hot pressed titanium di-boride (TiB_2), although others were also used. These materials may not conventionally be thought of as "soft" materials, but when put into context compared with the hardness of diamond they can be seen as being "soft". In contrast, when working on much softer specimen materials such as copper, the choice of cone material was restricted to materials such as aluminium (Al), bronze and graphite. It was also not uncommon to find that a cone material is unsuitable because it is chemically reactive with the specimen. Each specimen, experimental type (e.g. static/cyclic loading) and conditions pose a unique set of restrictions on the choice of cone materials, but with time and patience a catalogue of suitable materials can be built up to provide any amount pressure under any conditions. Figure 3.3 shows the derived pressure/ temperature relationship for the range of materials that were used in this work, to produce plastic deformation in diamond. Each line indicates the expected pressure that the cone material will produce over the temperature range. An estimation of the resultant pressure can only be made, as the properties of the cone materials used are subject to the manufacturing route, can be inhomogeneous and do not necessarily flow as expected. This

diagram does however produce a good indication as to the most likely pressure that will be produced, which in turn allows the cone material to be more intuitively chosen. For the purposes of this work it was not thought appropriate to describe in any detail the structure and properties of these materials other than the pressure they impart at a given temperature and load. This is because the pressure supplied is the only property of the cone material that is important in this study.

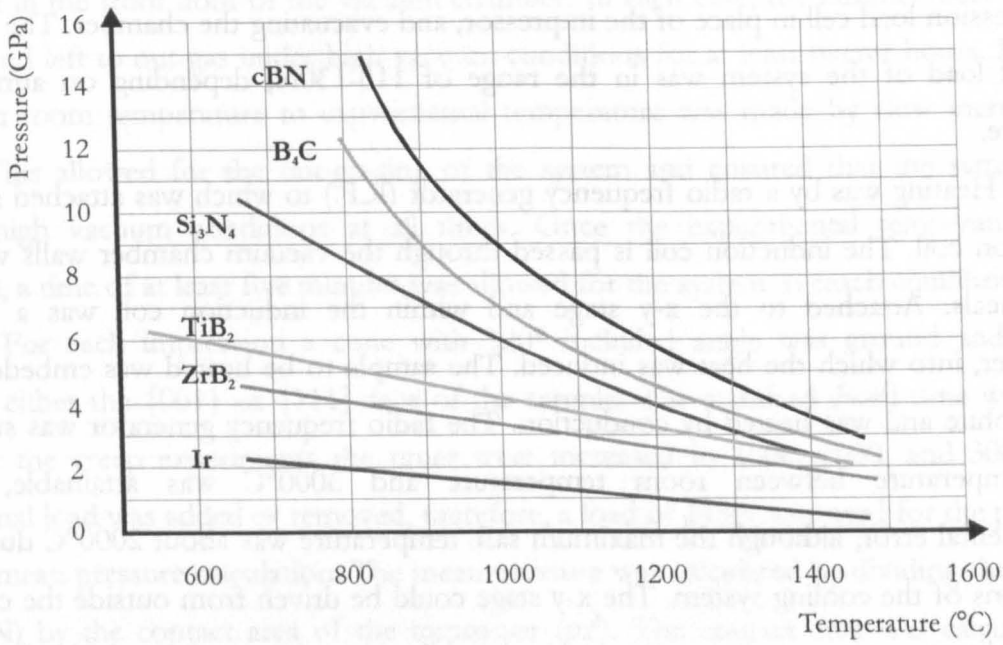

Figure 3.3. Graph showing the expected pressure produced by an impressor material for a range of temperatures, under a load of 115N.

3.2 High Temperature Equipment

In this work, pressures in excess of 1GPa, and temperatures between 700°-1400°C were used to develop a range of plastic deformation in diamond. As diamond is susceptible to oxidation at elevated temperatures, a method of applying the soft impressor technique at temperatures between 20° and 2000°C in a vacuum was devised.

Figure 3.4 shows a schematic diagram of the high temperature equipment (not to scale), which consisted of a vacuum chamber, loading column, x-y stage, radio-frequency generator and a cooling system. The vacuum chamber was a square box, approximately 40cm^3, fabricated from austenitic stainless steel. Access to the chamber was via the front face, which was a hinged door. This was sealed by using "O" rings and vacuum grease. Visual contact of work in progress was made via a porthole in the front door. The vacuum attainable was 10^{-6}mb and was provided by a diffusion / rotary pump backed system.

The loading column ran through the top of the vacuum chamber and was free to slide along its axis. The vacuum was maintained by a Wilson seal. The load was applied via the mass of the column plus the force produced by the difference in pressures between atmospheric and the vacuum. The load supplied by the column and pressure difference combined could be increased or decreased by adding known masses to an external pulley system. The impressor was attached to a pyrophillite holder which was in turn attached to the loading column. Calibration of the load was achieved by attaching a Kistler compression load cell in place of the impressor, and evacuating the chamber. The standard applied load of the system was in the range of 115-130N, depending on atmospheric pressure.

Heating was by a radio frequency generator (R.F.) to which was attached a copper induction coil. The induction coil is passed through the vacuum chamber walls via glass-metal seals. Attached to the x-y stage and within the induction coil was a graphite suscepter, into which the heat was induced. The sample to be heated was embedded into the graphite and was heated by conduction. The radio frequency generator was such that any temperature between room temperature and 3000°C was attainable, within experimental error, although the maximum safe temperature was about 2000°C due to the limitations of the cooling system. The x-y stage could be driven from outside the chamber in the x direction via a stepper motor and in the y direction via a small hand wheel.

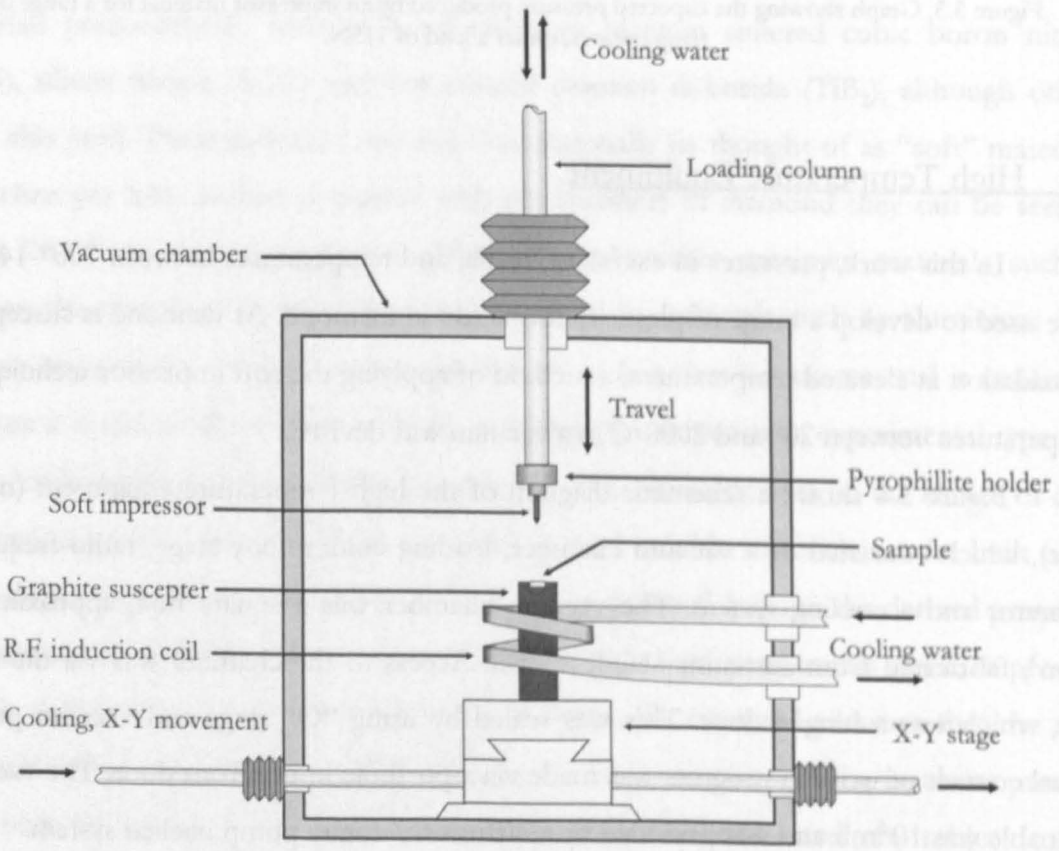

Figure 3.4. Diagram of the high temperature, high vacuum equipment.

3.3 Methodology

The samples were first embedded into a graphite susceptor, to facilitate heat conduction and ensure that the sample remained in the position that it was placed during set-up. The synthetic diamond samples were paramagnetic and had a tendency to levitate in the magnetic field produced by the induction coil. The experimental temperature was determined by using a disappearing filament optical pyrometer, viewed through the porthole in the front door of the vacuum chamber. In each case, the samples were aligned by eye and left to out-gas under high vacuum conditions for at least twelve hours. Heating up from room temperature to experimental temperature was made by slow incremental steps. This allowed for the out-gassing of the system and ensured that the sample was under high vacuum conditions at all times. Once the experimental temperature was reached, a time of at least five minutes was allowed for the system to reach equilibrium.

For each impression a cone with 120° included angle was ground and loaded against either the {001} or {111} face of the sample. The standard dwell time was 300s, but for the creep experiments the times were increased to 1000, 2000, and 3000s. No additional load was added or removed, therefore, a load of 115N was used for the purposes of the mean pressure calculation. The mean pressure was calculated by dividing the applied load (N) by the contact area of the impressor (m^2). The contact area was calculated by measuring the diameter of the contact region using a Nikon Optiphot II microscope and a Filar eyepiece micrometer. For each impression, four measurements of the diameter were recorded and an average calculated. The flattened tip of the impressor was also measured in the same manner to evaluate experimental error. In the case where the contact area on the specimen was indeterminable, the flattened cone tip area alone was used.

The placing of the impressions on each sample was considered carefully. Care was taken to place the impression as far away as possible from the edges, the centre (where there tends to be a region of residual stress, caused by growth) and when multiple impressions were placed in a sample, from each other. Cathodoluminescence micrographs were used to identify the growth history of the stone prior to making the impressions. For synthetic stones, only regions of {001} growth were impressed, as these were the most predominant growth sectors. In most cases, only the growth face was impressed, as this face tended to exhibit large single character, growth sectors. This meant that it was possible to be confident that the deformed zone of the impression beneath the surface did not intersect a different growth sector.

3.4 Specimen Description/Preparation

The synthetic diamond specimens used in this work were either {001} or {111} grown. In each case, the morphology was dominated by cubic growth sectors with minor octahedral growth sectors running out towards the corners. A schematic diagram of a typical synthetic Ib stone is shown in figure 3.5. As can be seen, the {001} oriented stones tended to be square with {100} edges and small {111} cleavage planes at the corners although some samples did have {110} edges. The {111} oriented stones tended to be either triangular or hexagonal with {111} edges. The size was usually 2mm square and about 1mm thick, although some larger sized diamonds were used. The standard De Beers product samples were as polished on near parallel {001} planes. The Diamond Trading Company (Maidenhead) polished non-standard stones near to the desired face. In some cases windows on perpendicular {100} faces were polished so that it was possible to view induced deformation from the side. Polishing lines lying in the same {100} direction could clearly be seen on the polished {001} faces. The polishing lines on the near {111} faces were much more random in direction. The growth sectors for each sample were identified by using cathodoluminescence spectroscopy. The nitrogen content of each stone was measured using Fourier transform infrared spectroscopy (FTIR). The concentration for the standard samples was found to be an average of 550ppm in the {001} sectors. Other samples were used with specifically higher or lower nitrogen concentrations, nitrogen levels of these samples are indicated at the relevant point.

Each new diamond sample received was first heated to 280°C in a solution of $NaNO_3$ + H_2SO_4 then boiled in HCl +HNO_3. This ensured that all contaminants and graphite were removed. Subsequently the samples were cleaned using alcohol and an ultrasonic bath.

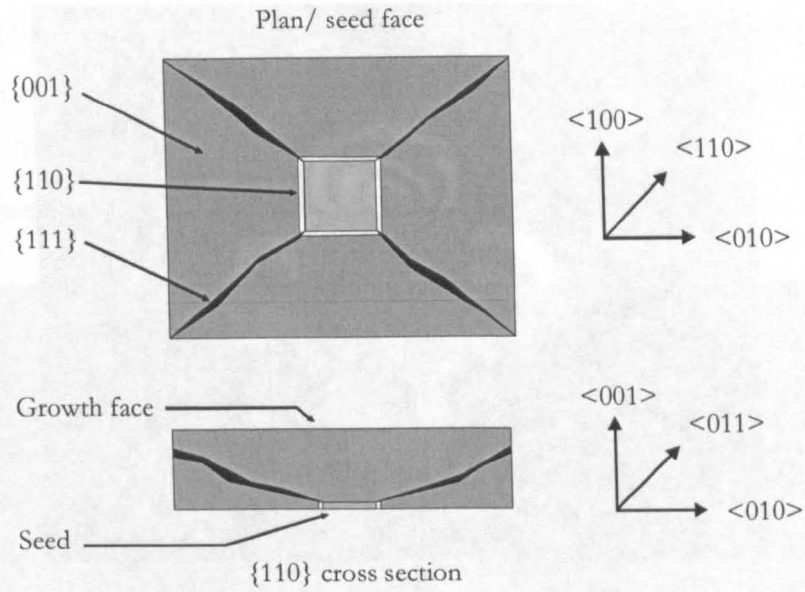

Figure 3.5. Schematic diagram of the growth sector morphology of the synthetic diamond samples used in this work.

3.5 Microscopy

Optical:

All optical micrographs were taken using a Nikon microscope fitted with differential interference contrast filters (DIC), for better depth resolution when observing in reflected light mode. Optical interferometry, using a dedicated Nikon microscope, fitted with Mirau lenses and an X-Y-Z stage. The interferometry technique involves the splitting of the beam of light travelling through the objective by a semi-silvered mirror in the Mirau lens. When the two beams of light are recombined, they are out of phase with one another. Any change in the specimen height causes constructive and destructive interference between the beams (fringes). Height measurement can be calculated, as the distance between consecutive fringes is a quarter of the wavelength of the light used. For these experiments, the distance between consecutive fringes was 136.5nm. The depths of the impressions and the height of the pile-up were evaluated for each case by counting the number of fringes. The volume of the impressions was calculated by assuming that the impression volume was a truncated cone. Figure 3.6 shows an example interferogram of an impression produced by a Si_3N_4 impressor at a temperature of 1400°C. It can be seen that the impression is 17 black fringes deep, which corresponds to a depth of 4.25μm.

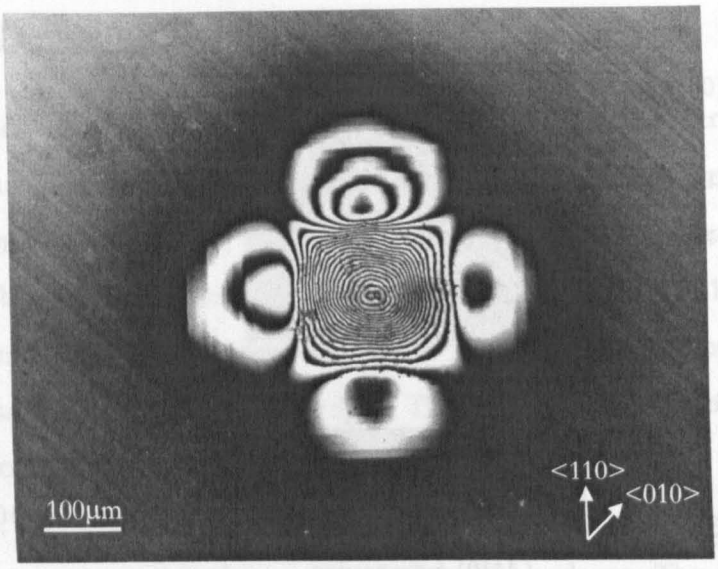

Figure 3.6. Example interferrogram of an impression.

Atomic Force Microscopy (AFM):

Atomic force microscopy (AFM) was carried out on the piled-up areas in the rosettes, outside of the contact area. The aim of these experiments was to gain an insight into how the pile-up is formed and what affect the concentration of nitrogen has. In AFM, a diamond stylus is attached, via a Si_3N_4 tripod, to three piezo-electric crystals, which record the movement of the tip in three dimensions. The tip is scanned across the specimen whilst in contact or extremely close to the specimen. For this set of experiments, a Digital Instruments Dimension 3100 microscope was used which was run in contact mode. It is possible to obtain atomic resolution using this microscopy technique, however, the resolution obtainable for these experiments was about 10nm. This was because the surface roughness of the specimens due to the polishing lines and the slip steps near the impressions were too high. For each impression investigated images were taken just outside of the contact area, within the rosette pile-up region. In each case the image was levelled using the automatic levelling software built into the programming. In addition to the images taken, a step height analysis was made for characteristic slip steps within the rosette formation. In order to produce the analysis a line was scanned by the AFM and a profile of the slip steps produced. Again, for this analysis, a region had to be chosen against which the rest of the profile could be levelled. The step-height analysis software then allowed the user to choose two points about which the vertical height could be measured. The AFM technique was not accurate enough to determine the correct angle that a step makes to the surface, therefore, it was assumed for the step height analysis that slip steps were perpendicular to the surface of the specimen. Figure 3.7 shows an example AFM image of

a rosette arm. The computer software produces two images. Image (a) is a plan view where the contrast represents height (quantified by the Z range) and (b) is a three dimensional representation. The parallel lines running from corner to corner are {110} slip lines whereas those just off vertical are polishing lines.

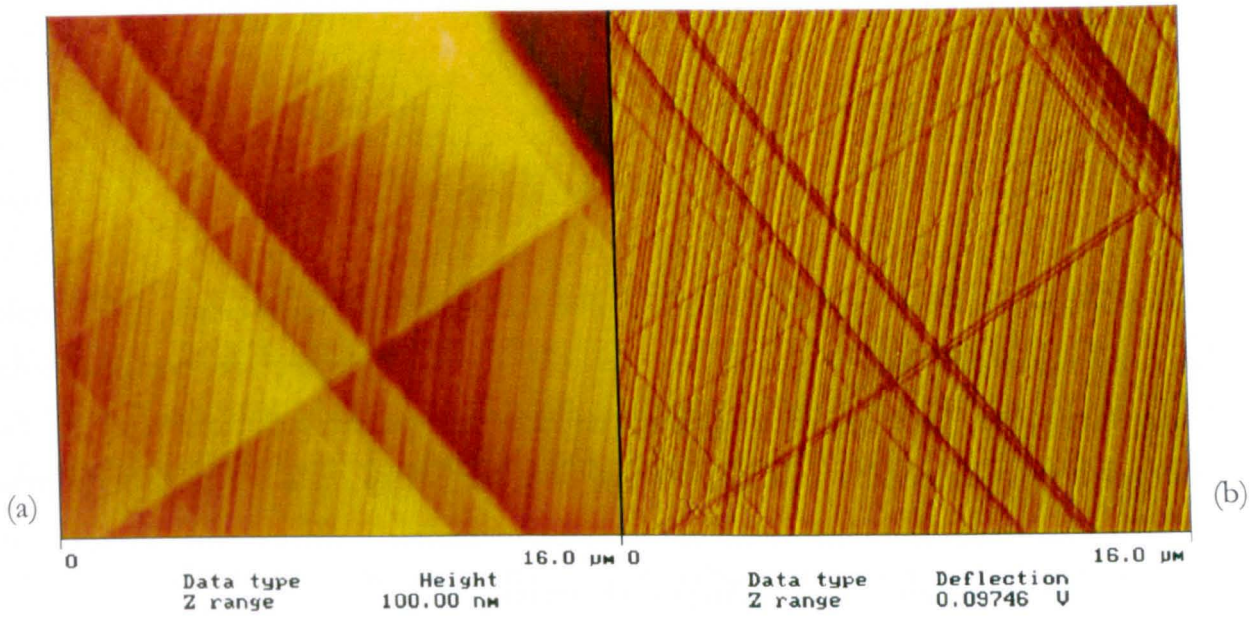

Figure 3.7. An example AFM image of a rosette arm.

3.6 Spectroscopy

Nitrogen measurement (FTIR):

The measurement of the nitrogen concentration of the diamonds was made by using the Fourier Transform Infrared (FTIR) technique. This involves passing an infrared beam of light through the sample and collecting the resultant absorption spectra. The nitrogen concentration of single substitutional nitrogen is proportional to the height of the absorption peak at 1130 wavenumbers. The relationship used was that quoted by Collins (1980) which was 22ppm/ cm^{-1}. The height of the peak was background corrected and normalised against a standard, to account for differences in the thickness of the sample. The equipment used for these measurements was a Nicolet Magna IR750 spectrometer with a spot size of 100µm. The nitrogen content was initially measured for each sample in several different areas, but always within a {001} growth sector. The average nitrogen content corresponding to particular impressions was also measured. This was achieved by measuring the content of an area just next to the contact area of the impression, as the deformed nature of the impression scattered too much of the infrared beam to gain accurate data.

Cathodoluminescence:

Cathodoluminescence (CL) experiments were carried out by placing the sample in a partial vacuum and washing it with electron particles. The electrons were accelerated from an electron gun with a beam current of 1 - 2mA (18kV) and diverted to wash over the diamond by using a standard bar magnet. The CL of the diamond was intense enough to be viewed via a porthole in the vacuum chamber. Optical micrographs were taken of the sample by using a stereo microscope and SLR camera loaded with P1600 Fujichrome slide film. The distance between the sample and the objective focal length of the microscope meant that the maximum attainable magnification was x64. Figure 3.8 shows two example CL images (a) is a whole synthetic HPHT sample of approximate size 2x2mm. The sample has been impressed four times, as can be seen by the signature red/orange 575nm luminescence. (b) is an image of an impression rosette, formed in a cube growth sector of a synthetic HPHT diamond. It can be seen that both the contact area and the rosette arms luminesced orange/red corresponding to 575nm centres, whereas the background luminesced bright green, corresponding to H3 centres.

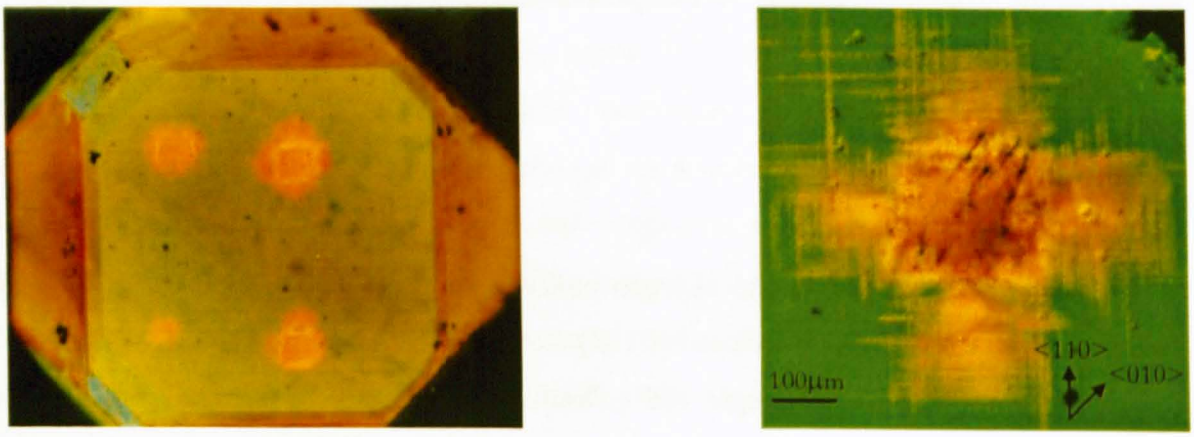

(a) (b)

Figure 3.8. Example CL images of impressions.

Photoluminescence, Raman:

Photoluminescence (PL) spectra were recorded using an Ar ion laser, 514.5nm line, single spectrometer mode using a 600lines/mm grating and a holographic notch filter to filter out the laser line. For H3 luminescence, the 488nm laser line was used. All spectral measurements were taken at a temperature of 10K ($He_{(Aq)}$) to minimise electron-phonon broadening of the ZPL's, using an Oxford Instruments microscope cryostat, cooled with liquid helium. The laser spot diameter was 20µm. The data was normalised

by removing the background intensity, not by comparing with intensity of the Raman peak. As a reference, additional spectra were taken from points on the specimens that were known to be deformation free.

The position and full width at half maximum (FWHM) of the Raman line was taken from the PL data collected using the 514nm line. The peak position and FWHM were calculated by using the Lorenzian curve fit function within the Origin 5 software. The peak position was converted into residual stress by using the relationship: $\sigma = \Delta\nu/1.9$. Where σ is the residual stress (GPa) and $\Delta\nu$ is the shift (Rcm^{-1}) of the Raman line at $1332cm^{-1}$. The Raman peak position and FWHM in the unstrained state was calculated by taking a spectrum from a natural IIa sample, known to be strain free. The position of the as recorded peak positions were calibrated against a mercury line whose position was assumed to be at $1122.468cm^{-1}$. It was assumed that a shift to a lower value indicated tensile forces and higher shift indicated compressive ones.

PL spectra were recorded around impressions made in samples containing different levels of nitrogen concentration. For each experiment a grid of spectra were taken at intervals of 100μm centred on the impression in question. The area of the grid was determined in each case such that the perceived area of plastic deformation around the impression was covered (determined by using interferrograms). As the deformed area of the 850ppm N sample was very small (by comparison) the grid spacing was lowered to 50μm. The PL results were represented as three-dimensional maps with colour representing the change in intensity for the PL peaks and shift and FWHM for the Raman line.

3.7 Etching

The diamond samples were etched in molten KNO_3 in a nickel crucible at 750°C for intervals of 5 minutes. The crucible was heated in a standard muffle furnace. The molten KNO_3 solution was allowed to solidify slowly before being dissolved in boiling water so that the sample could be reclaimed. Several attempts were made to etch diamond by using a vaporised oxygen and water mix at temperatures in excess of 750°C (De Theije *et al*, 1999b). Although these experiments succeeded in etching the diamond, the quality of the resultant etched surface was highly dependent on surface contamination of the specimen. For this reason a decision was made to etch using the KNO_3 method rather than O_2 method. Figure 3.9 shows two DIC micrographs of the same impression rosette, (a) is before etching and (b) after. It can be seen that although slip can be seen before etching,

the etching process reveals a great deal more dislocation activity than is suggested by the pre-etched optical image.

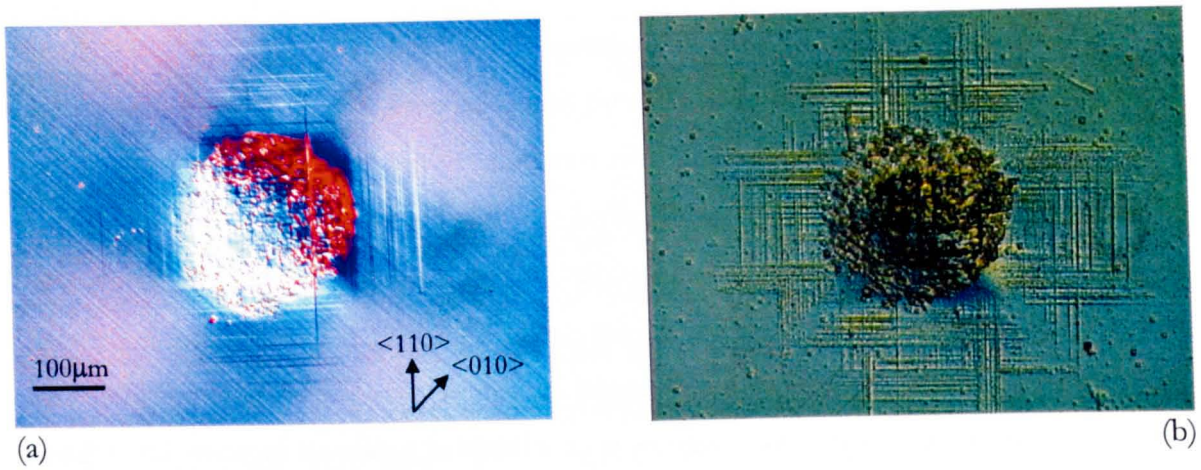

Figure 3.9 Example impression rosette (a) pre-etch (b) etched

3.8 Experimental Errors

Unfortunately, no experimental procedure can be free from errors. However errors do not pose a serious risk to the overall result providing that they are either quantified and factored into the final figures or are considered when making a final conclusion as to the meaning of the results. In every experimental procedure there are systematic errors. The fact that the results given in this thesis are of a comparatory nature rather than fundamental mean that systematic errors do not affect the final conclusions. It is important however to be aware of any errors so that their effect can be minimised and so that comparisons between these results and those of other authors can be made. A description of the most significant of these errors is given below:

- **Temperature:** The temperature was measured using a disappearing filament optical pyrometer. An accuracy of 2.5% at 1000°C has reported (Brookes, E.J, 1992), taking into account the effect of having a transparent medium between the sample and pyrometer.

- **Normal load:** The normal load provided by the loading column was determined by replacing the impressor material with a Kistler quartz linear load transducer. The accuracy of this quoted by the manufacturers was ±0.4%. When the fact that the final

delivered load is dependent on atmospheric pressure is taken into account the overall accuracy for the normal load is ±5N.

- **Contact area:** The contact area was measured directly using a microscope with a micrometer eyepiece attachment, calibrated by a graticule slide. Using this method an accuracy of ±0.3μm can be gained. The measurement of the contact area depends largely on the operator's decision as to the contact boundary. An accuracy of ±6% can be used to compensate for this (Ross, 1984). This accuracy also applies to any measurements made using a optical micrometer.

- **Nitrogen:** The nitrogen content of each sample was measured using transmitted FTIR. Using this technique an accuracy of ±10ppm can be gained. In addition to this the nitrogen content within a sample, or growth sector is not homogeneous. To minimise errors due to this FTIR measurements were taken from as close to each impression as was possible. The rough surface caused by the impression scattered the transmitted light too much to get an accurate reading from the centre of the impression. The error caused by inhomogeneity within a single growth sector can be assumed to be ±10ppm. In this thesis when making a comparison based on nitrogen content, the samples were chosen such that these errors were not significant.

- **Photoluminescence/Raman:** The repeatability of the equipment used was $1cm^{-1}$. However, the spectral measurements were taken using a 600 lines/mm grating, in conjunction with a CCD camera which produce a combined minimum spectral resolution of $2.2cm^{-1}$. Consideration of the accuracy of FWHM measurements shows that the bandbass resolution of this system was not ideal for measuring peak widths, *i.e.* the peak shape would not have been perfectly Lorenzian, but would have a small Gaussian component. However, the error due to instrumental broadening in this case is a systematic error, therefore, although the figures are not perfectly accurate the overall trend was not affected.

Chapter 4

DEFORMATION AND MODELLING

4.1 Introduction

With diamond increasingly used for industrial rather than cosmetic reasons, it is of greater importance that its properties are more fully understood. This is not only so that it can be used to greatest effect, but also so that we can understand its limitations. The attraction of diamond as an industrial material is concentrated around its ultimate hardness but it is also attractive for other properties. For example, the extremely high thermal conductivity of diamond makes it a perfect material to be used for thermal management or in high temperature cutting operations. These properties, coupled with the fact that diamond is virtually totally transparent to all wavelengths of light, makes it ideal for use as optical windows, especially for high powered lasers. One of the main uses for diamond, however, is in the manufacturing industry. Diamond, whether single crystal, polycrystalline compact, or abrasive grit, is now routinely used for many non-ferrous manufacturing operations such as grinding, sawing, turning, forming dies etc. As the current trend in manufacturing leans more towards cutting operations that are quick and pollution free, the use of coolant is becoming more undesirable. This inevitably means that the cutting tool responsible has to work at ever increasing temperatures without any loss in performance. Diamond with its already exceptional tooling capabilities, is increasingly at the forefront of new tooling technology, as its thermal properties match its mechanical ones.

The application of diamond to these uses makes it necessary to investigate the reaction of diamond when exposed to high temperatures and forces and what that reaction means for the integrity of diamond components. For these reasons, the soft impressor technique has been used to develop a range of pressures at various temperatures and the resultant levels of deformation studied.

This study mainly used single crystal synthetic type Ib diamond. The samples were provided by De Beers Industrial Diamond Pty, from their synthetic single crystal range, *i.e.* material normally used for wire-drawing dies. Type Ib diamond was chosen instead of natural or specially synthesised specimens for two reasons. The first reason was that

synthetic diamonds are mass-produced and are, therefore, virtually identical in habit, impurity content and size; this makes it easier to compare results between different individual samples. In contrast, natural stones tend to have a mixed habit, various impurity contents, size and morphology. Although it would be possible to find an experimental population of natural stones, this is time consuming and the results could never match the identical nature of a synthetic population. The second reason for choosing to work with standard synthetic stones was that the mechanical properties of this type of diamond are potentially of greatest interest to the industrial community. Although natural diamond is used for industrial purposes, the large majority that is used is synthetic. Therefore, it seemed prudent to maximise relevance by investigating the properties of diamond by using the same type as would be used in industry. A clearer understanding of plastic deformation of diamond and the conditions that produced it, will aid geologists in better understanding the history of natural diamond. It could also shed some light on the controversy regarding pink and brown coloured stones.

4.2 Modelling Single Point Contacts

Earlier work by Brookes, E.J. (1992) used the soft impressor technique to establish a brittle-ductile transition temperature (BDTT) for different types of diamond (Ia, Ib, and IIa) and, to evaluate the critical resolved shear stress (CRSS) for those diamonds at temperatures above the BDTT. The experimental work reported in this thesis has extended the original schematic diagram, by investigating the deformation of carefully selected diamonds at temperatures and pressures above the critical resolved shear stress under conditions of point loading. Particular notice was taken of the change between localised slip around the contact area of the impressor and the formation of extended slip and rosettes. An upper limit for plastic deformation of diamond without stress relief cracking was determined.

Models:

There have been a number of models for anisotropy in the indentation hardness of crystals (Daniels and Dunn, 1949, Pospiech and Gryziecki, 1970 and Brookes et al 1971). These were based on the calculation of an effective resolved shear stress beneath an indenter using the Schmid-Boas resolved shear stress equation, modified by various constraint terms.

Generally, there is a good fit between the resolved shear stress curves created by the models and the experimental results for the majority of crystals. However, in developing these models, a number of assumptions have been made. The effects of friction at the contact interface; elastic recovery and densification have been ignored. Also, equal weighting was given for all slip systems and contributions due to secondary slip systems, such as twinning, were not taken into account.

Whilst models of the indentation process provide a qualitative explanation of hardness anisotropy, they do not explain the observed ratios of mean contact pressure to yield strength or why there is significant variation between materials with the same crystal structure, bonding and slip systems. Nevertheless, the most suitable model at present is due to Roberts (1988) who modelled the whole of the slip pattern over an area 2**a** (where **a** is the contact radius) for both adjacent to and beneath different point contacts. Earlier models assumed that the slip systems immediately adjacent to the facets of the indenter controlled the hardness anisotropy. Roberts on the other hand, used extended stress fields produced by a circular contact in an elastically isotropic material (after Love, 1929), to predict the likely slip patterns and the stresses on them. This allowed complete three-dimensional patterns of the relevant slip planes to be visualised together with the resolved shear stresses on them.

For diamond cubic materials, contour maps of the maximum resolved shear stress on the (010) and (110) planes (sectioned through the diameter of the contact) have been generated, reflecting the most stressed slip system at each point as a result of impressing the {001} plane (figures 4.1 and 4.2). The contours are expressed as a percentage of the contact pressure and are overlaid by a slip system convention indicating the particular system onto which the highest shear stress resolved. The devised convention is that the positive sense of the slip plane is upwards with respect to the impressed surface and its direction into the bulk. A negative sense of the resolved shear stress is represented by a bar over the number.

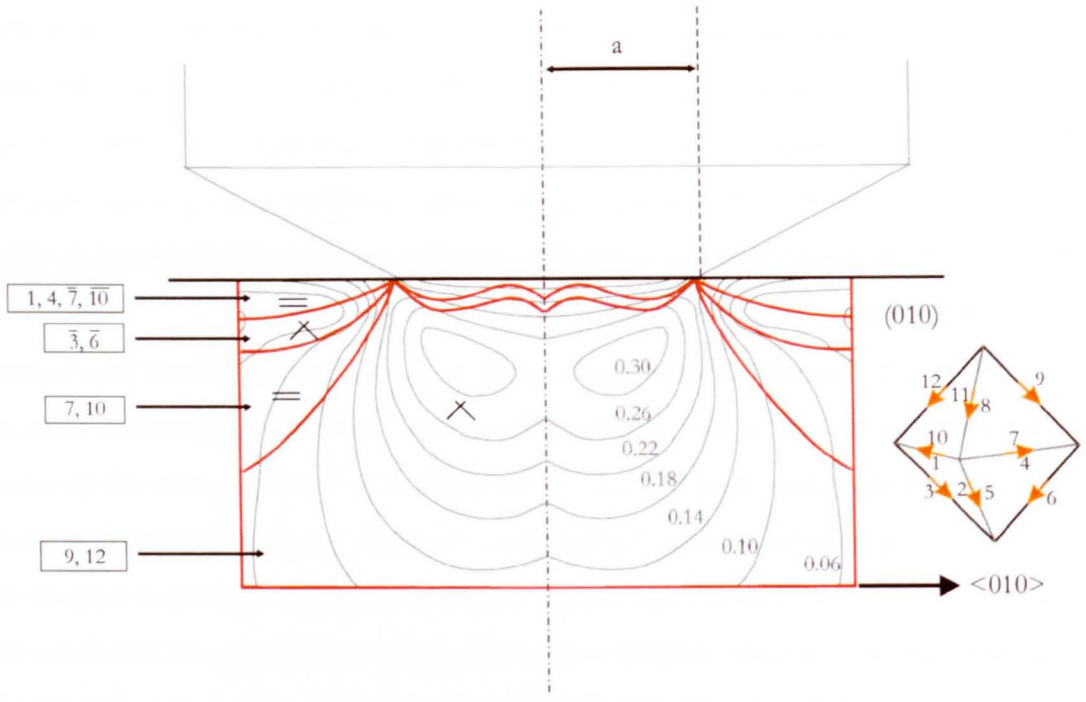

Figure 4.1. The resolved shear stress contours developed beneath a circular contact on the diamond slip system on the (010) plane. The figures represent percentages of the applied contact pressure.

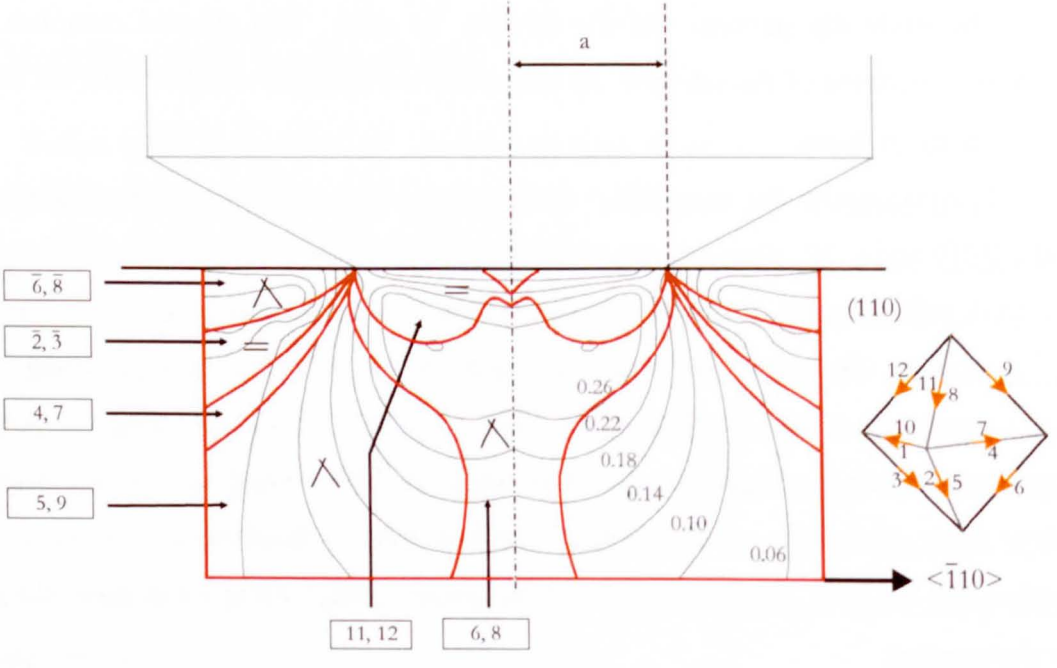

Figure 4.2. The resolved shear stress contours developed beneath a circular contact on the diamond slip system on the (110) plane. The figures represent percentages of the applied contact pressure.

It can be seen from the model that the RSS values immediately below the surface are relatively low. However, there are two positions of the maximum RSS values at approximately 0.5**a** below the surface, where **a** is the radius of contact. When projected into three dimensions, this produces an area of maximum resolved shear stress roughly toroidal in shape. Table 4.1 shows position and value of the maximum resolved shear stress for the two low index planes.

	Position		
Plane	X	Z	Max. RSS
(010)	0.58a	0.54a	$0.316P_m$
(110)	0.52a	0.5a	$0.3P_m$

Table 4.1. Showing the position and maximum value of the resolved shear stress, where (a) is the radius of contact and P_m is the applied pressure.

When his model was initially calculated, Roberts defined a surface area of 2a below the contact surface. However, the depth modelled does not extend to cover the whole of the deformed zone developed as result of these experimental conditions. In an attempt to estimate the depth of deformation, Greenwood (1998) reasoned that it was proportional to the applied load, and independent of the contact area or resultant pressure. Using this theory, he calculated that the maximum depth of the deformed zone was about 240μm, based on an applied load of 115N.

Observed deformation:

Adapting the Schmid-Boas resolved shear stress criteria to model deformation associated with indentation and impression techniques has been successful in predicting the nature of anisotropy in indentation hardness and identifying the slip systems (Brookes *et al*, 1971). It has not, however, been able to tell us what has happened once the load has been applied and the contact pressure developed. Ideally the stress field model should be elastic:plastic, including the stresses from effects generated at the surface plus stresses from other defects inevitably present within the plastic zone. It is clear from the Roberts model that even at low loads and only taking into account the highest shear stress values, the number of operating slip systems is extensive. This is the case at low temperatures, just above the brittle-ductile transition temperature, but at temperatures, approaching 0.5Tm, it is conceivable that the number of operable slip systems is dramatically increased. From the moment that the first slip plane is activated, the proposed shear stress contours will change. By the time that significant dislocation activity has occurred, the shear stress contours will be much more complicated and by the time a rosette structure has formed, it is presumed that this type of model would not reflect reality at all. However, despite the oversimplification of the modelling, some insight can be gained into the types of slip initiated during deformation.

The slip in single crystals is inhomogeneous and is restricted to certain planes and directions. The shear stress to nucleate and move dislocations on those particular slip systems is specific to each material, and is known as the critical shear stress. In this work, a pressure was applied to the crystal at an angle to the active slip systems. The shear stress to initiate the slip is a component of the applied pressure and is known as the critical resolved shear stress (CRSS). As can be seen from the Roberts model, the maximum shear stress, resolved onto the inclined {111} planes, is a certain distance below the surface and is toroidal in shape. Here, the shape of the volume was relatively unimportant, but its location was. The fact that the maximum value is below the surface meant that slip was most likely to start at that point but then move towards the surface. As an estimate, it was decided that the critical resolved shear stress was achieved when the first slip step was observed on the surface. The magnitude of the CRSS was dependent on the temperature at which the pressure was applied. Therefore, the amount of deformation could be controlled by varying the amount of pressure applied at a certain temperature. By doing this, it was possible to produce a description of the phases that the deformation went through before ultimately producing a crack. The description of the deformation "story" is given below assuming that the temperature and loading conditions are raised with each consecutive number (Brookes, E.J. 1992).

(1). When the applied pressure was sufficiently high (below the BDTT), a series of Herzian ring cracks formed on intersecting {111} planes (Howes and Tolanski, 1955).

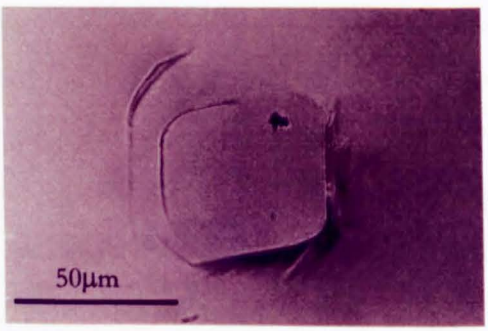

(2). The first slip steps reached the surface within the contact area of the soft impressor (due to its position when initiated and the slip plane geometry).

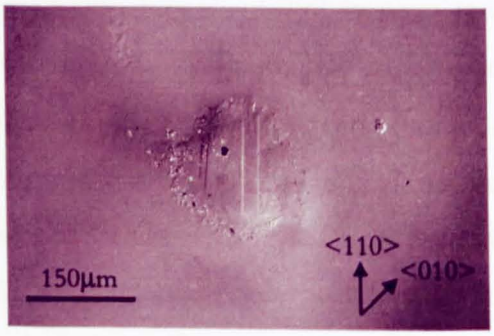

(3). Subsequent deformation emanated from or near that initial point on any of the favourable {111} <110> slip systems.

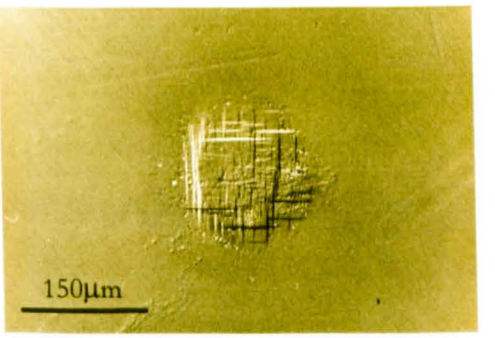

(4). The slip extended beyond the compressive/tensile boundary at the edge of the contact area.

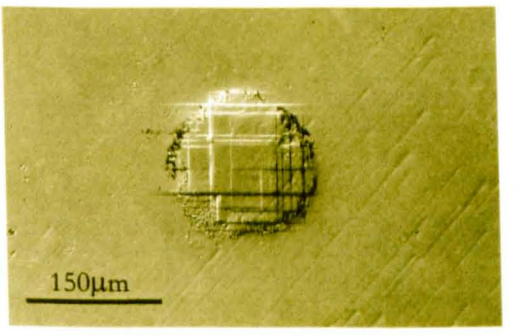

(5). The residual stress in the lattice after the load was removed was sufficient to cause relaxation. This produced picture frame slip (Brookes and Ross, 1987 and Hirsch *et al*, 1985a).

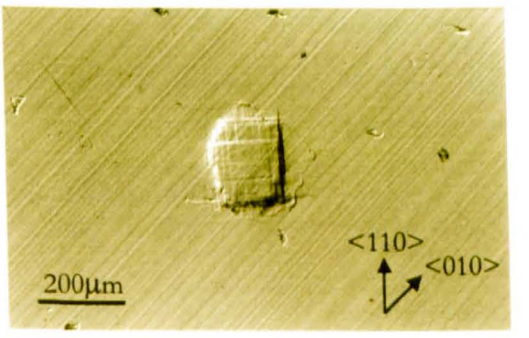

(6). Slip was produced in <110> directions cruciform in shape, emanating from the contact area to produce a rosette.

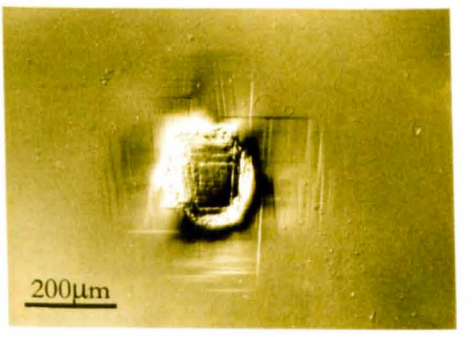

(7). Predominantly {110} cracks were formed, due to increased dislocation interaction.

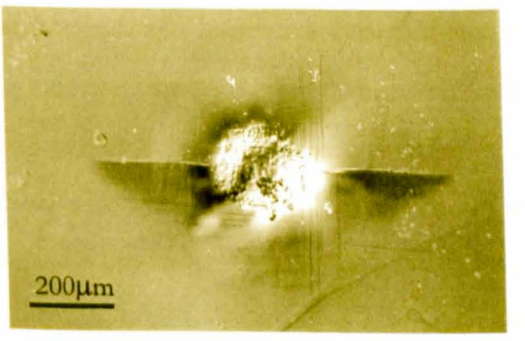

Figure 4.3 Descriptions and accompanying representative micrographs of the different levels of deformation observed on the {001} plane of diamond when loaded at different pressure and temperature, using the soft impressor technique.

Figure 4.4 is a schematic diagram of the brittle-ductile transition of diamond. Overlaid are diagrams representing the levels of deformation as shown above that expected at the particular temperatures and pressures. The deformation "story" can clearly be seen to depend on the temperature and pressure. The exact positions of the transitions between the different deformation forms are also dependent on the diamond type (Brookes, 1992) the length of dwell time (this chapter) and impurity concentration (chapter 5).

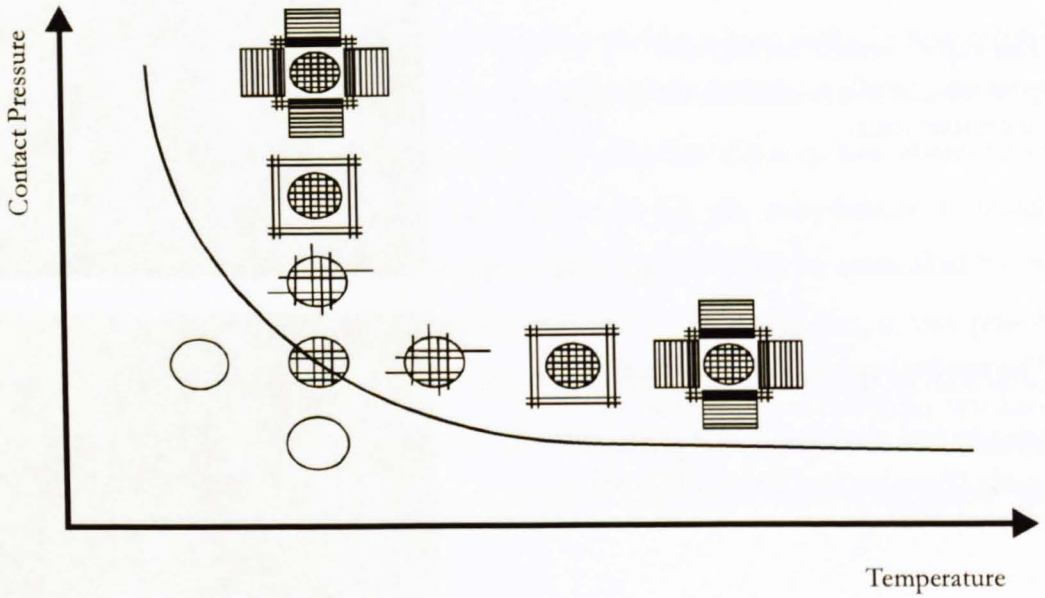

Figure 4.4. Schematic of the brittle-ductile transition of diamond with the expected deformation profiles overlaid.

The mechanism of deformation:

For a better understanding of the deformation produced by soft impressors, it was necessary to gain an insight into the mechanism by which dislocation activity produces an identifiable plastic strain. Elastic behaviour to fully plastic deformation and ultimately to strain-induced cracking has been observed experimentally, however, the mechanism by which this occurs is not understood. Only when this mechanism is better understood, can the limiting factors of plastically deforming diamond be established. The deformation process can be split up into three parts; the first being the initiation and multiplication of dislocations. The second is the mechanism by which they fill the highly stressed volume beneath the impressor. The third part of the process involves the mechanism by which further dislocation initiation and subsequent movement manifests itself as the visible rosette formation with accompanying pile-up.

The onset of plastic deformation:

When subjected to a stress, the crystal will slip on the plane most favourably oriented to allow dislocations to move. As a result of measurements on real crystals, Schmid's law states that slip occurs in a crystal when the applied shear stress τ reaches the critical resolved shear stress, τ_c for that material. That is, for a given material, dislocations are created and begin to move at a fixed level of resolved shear stress, but restricted to certain planes and directions. In diamond, the applied stress is resolved onto {111} planes in the <110> directions. The critical resolved shear stress is the resolved stress required to create and move a dislocation onto the surface. Therefore, it is possible to envisage a picture whereby a dislocation is initiated at a discrete point under the contact area, and expands under the applied stress until it reaches the surface. A simplistic description of this is given in (figure 4.5) where the contact area has been cross-sectioned and the dislocations are represented as solid lines. It can be seen that the dislocations are created at a discrete point and move under the applied load both onto the surface and into the bulk.

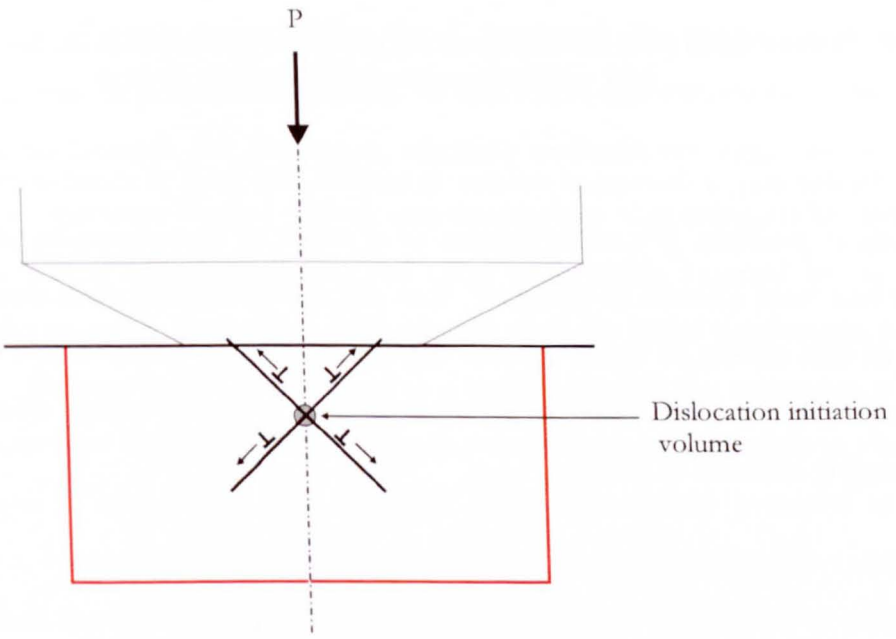

Figure 4.5. Cross sectional diagram of the point at which the critical resolved shear stress is reached.

The deformed volume:

The point of highest shear stress has been identified and from that the subsequent dislocation activity determined. Increasing the pressure by a small amount will increase the volume in which the resolved shear stress (RSS) is sufficient to initiate dislocations. This leads to further dislocation production, each one able to expand on their respective slip

planes under the applied shear stress. A dislocation that expands into the bulk of the material, rather than towards the surface, will continue to expand until the resolved shear stress acting on it is insufficient to cause further expansion. Figure 4.6 shows the Roberts model (110 cross section), the dark shading indicates the area in which the RSS is high enough to initiate dislocations. The lighter shading indicates the limit of the area in which the RSS is sufficient to cause dislocation loop expansion.

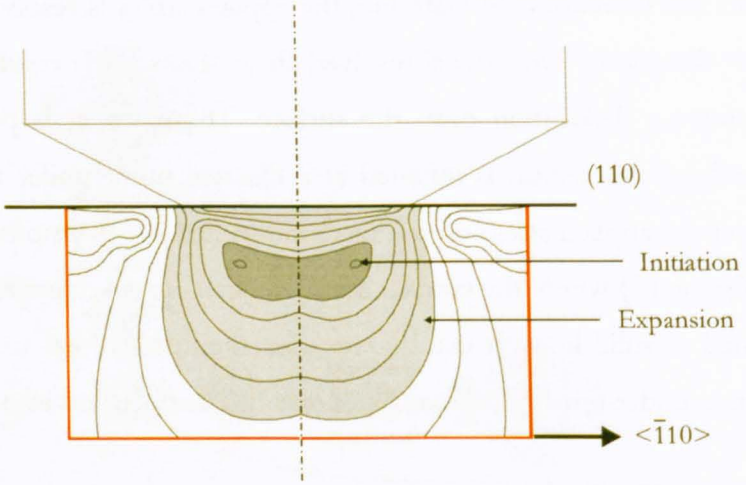

Figure 4.6. Roberts model (110) showing the area of dislocation initiation (dark shading) and the subsequent limit of dislocation loop expansion (light shading).

In this way, a dislocated volume is created, the level of strain is increased and work hardening is possible. If a cross section were taken of an impression where a significant volume had been allowed to dislocate, then the resultant dislocation structure might look similar to that shown in figure 4.7. As the slip system of diamond creates two points of maximum RSS, the dislocation structure is that of two overlapping structures, each one being roughly identical in shape.

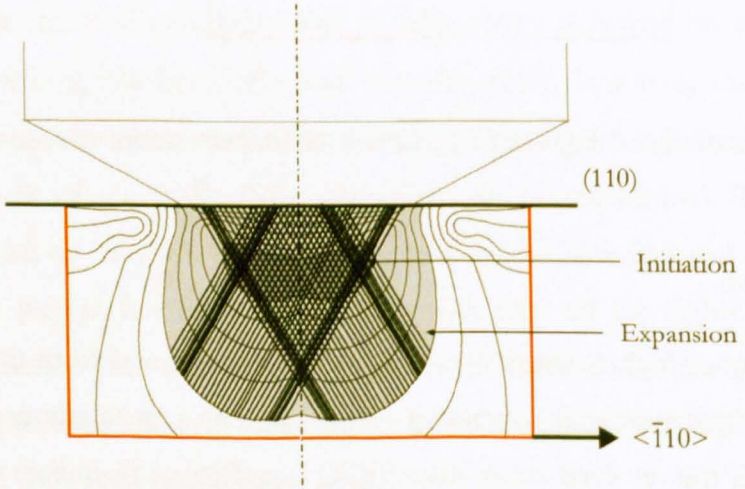

Figure 4.7. Roberts model (110) showing the likely resultant dislocation structure of an impression, before the onset of reversed plasticity.

In reality, the picture is somewhat more complicated, but the principle remains. The initiated dislocations are not confined to those slip systems that intersect the surface or those that are perpendicular to the (110) plane; slip on all of the {111}<110> slip systems is possible. With dislocations produced in two volumes and able to expand in any direction (defined by the slip system), it is likely that individual dislocations will be divergent and interact. Once that the first dislocation is produced, the ideal shear stress distribution, as shown in the Roberts model, is altered. As more dislocations are produced, the volume in which dislocation initiation is possible is increased, as the stress field of each dislocation will distort the elastic stress field. When all these factors are taken into account, it can be seen that the dislocation structure beneath an impression becomes increasingly chaotic. The basic, elastic stress field calculations, however, remain valid when considering the whole of the deformed region, as the extent of the deformed volume is similar to that predicted.

At a sufficiently high level of applied stress, the level of strain within the dislocated volume resulted in reversed plasticity. The consequence of this was some pile-up. This occurred at levels of strain lower than 0.8%, *i.e.* lower than that associated with pyramidal indenter. At levels of strain approaching those produced by conventional hardness measurement a full rosette pattern was formed. At that stress dislocations could be initiated over a large volume beneath the impressor, resulting in strain sufficient to produce an impression with a significant depth (>2μm), and dislocations that emerged far away from the contact area. These factors, including the extra dislocations initiated by the reverse plasticity, created a scenario many times more chaotic than the initial mechanism described above. Again, the Roberts model can be used as a tool to identify the regions in which the rosette dislocations were created. When looking at this model it was possible to identify the active slip systems in each region and therefore those slip systems involved in the full rosette formation. However, when it was taken into account that those slip systems were not exclusive, then the model suggests that dislocations could be created at virtually any point beneath the impressor and expand in any of the <110> directions. However, observation of the pile up produced at the dislocation rosettes using AFM and etching techniques (figures 4.11 and 4.13) suggested that the strain mechanism was highly ordered. This implies that although the Roberts model predicts that virtually all of the slip systems are operable, the deformation process, as seen from the surface, only utilised a small number in discrete areas.

In general, rosettes were formed at certain higher pressures and temperatures. The critical resolved shear stress at temperatures above 1300°C (*i.e.* when it is relatively temperature independent) is between 0.32-1.3GPa (Brookes, E.J. 1992). From the map shown in figure 4.18, it is clear that at temperatures of 1300°C and above rosettes could be formed at contact pressures as low as 1.5GPa. Using the model of the deformation process, it can be shown that the resultant resolved shear stresses, at contact pressures of 0.32-1.3GPa, were sufficient to initiate dislocations from inside the contact area but not outside. Therefore, the dislocations form and start to move beneath the contact area. The geometry of the slip plane with respect to the surface means that the dislocations emerge outside the contact area. A cross section of an impression at the point where rosette formation just begins is shown in figure 4.8. This model of the dislocation structure was supported by micrographs taken of the deformed volume of impressions via a window polished into the side of specimens. Figure 4.9 shows a micrograph of an impression produced by E.J. Brookes (1992), where an image has been produced of the deformed volume of a rosette impression by polishing a (110) window on the side of the sample and viewing through the bulk of the crystal. It can be seen that the strain field produced by the dislocations resembled the dislocation structure model shown in figure 4.8

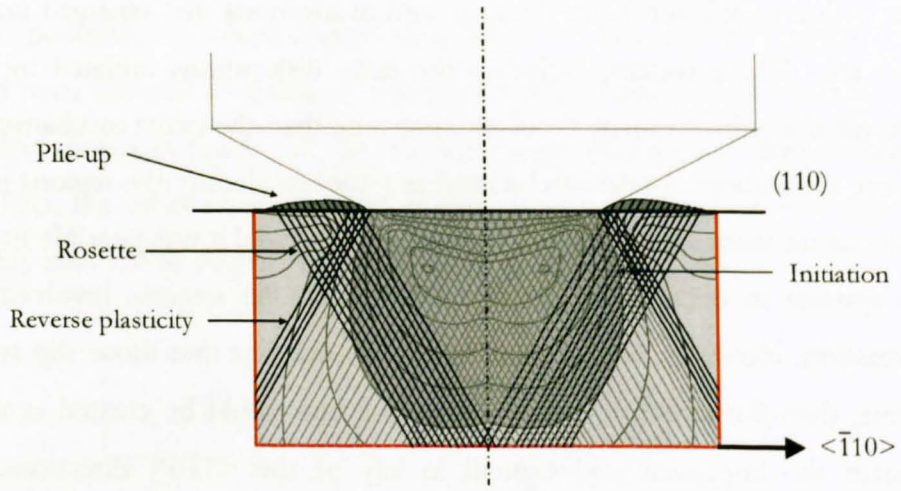

Figure 4.8. Roberts model showing the likely resultant dislocation structure of an impression just after the onset of rosette formation.

Figure 4.9. Micrograph of the deformed volume of an impression with a rosette formation, taken through a window polished on a (110) perpendicular to the impressed surface.

Pile-up:

When looking at interferograms of impressions with rosettes (figure 4.10a), it was clear that the dislocations emerging at the surface caused the surface to rise (pile-up). However, when looking at C.L. topographs of rosettes (where the dislocations were decorated by 575nm luminescence, figure 4.10b), it was clear that the dislocations were produced in discrete lines, not over an area, as was suggested by the interferrograms. Indeed, it seemed impossible to produce a smooth, three-dimensional, curved volume by using discrete dislocations. (NB Figures 4.9a and b are not of the same impression.)

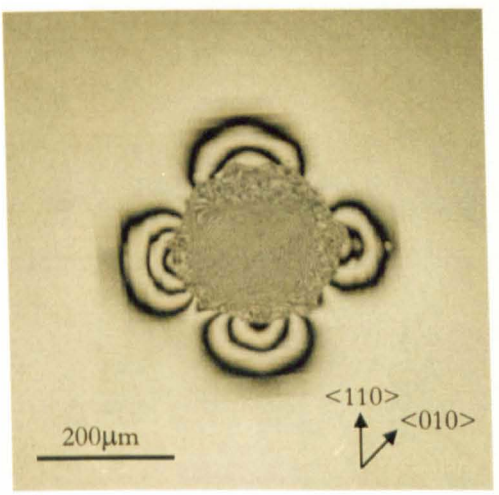

(a)

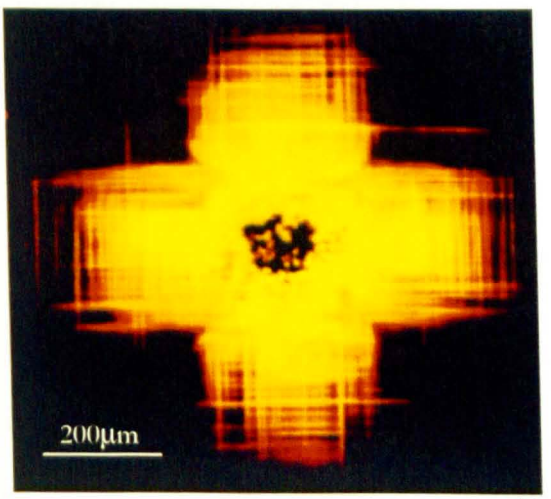

(b)

Figure 4.10. (a) Interferogram and (b) CL topograph of rosette impressions made on the (001) surface of synthetic diamonds.

To determine that the pile-up was actually atomically smooth and created by discrete dislocation lines, atomic force microscopy (AFM) was used to image small sections of the rosette arms. Figure 4.11 shows an AFM micrograph of a small section of the rosette arm of the impression shown in figure4.10a. Figure 4.11 consists of two images, (a) is a two-dimensional topographic map (elevation scale indicated above), whilst (b) is a three-dimensional representation produced by the computer software. The parallel lines from the

bottom left hand corner to the top right are slip lines, whereas those that are near vertical are polishing lines (figure 4.11). A height range is given, but it reflects only the height change within the frame. The actual height of the pile-up, in relation to the rest of the sample was about 1-2μm. It can be seen from the images that the slip lines are very discrete in nature with large distances (~5μm) between consecutive lines. It is obvious that the model of the rosette with equal length, parallel slip lines, does not apply to reality. The slip within the piled-up region was inhomogeneous in nature, the slip lines started and finished at any point within the rosette. In some cases, the slip lines were longer than the diameter of the contact region, such that it was possible for slip lines from the neighbouring arms of the rosette to interact. It can also be seen that the slip lines are curved, with the centre of the line higher than the ends. The curvature was not produced by small dislocation steps but was continuous, rather like bending a ruler. The area between consecutive slip lines was also curved rather than planar, *i.e.* the image of the smooth pile-up mound that is seen when looking at interferograms is closer to reality than the traditional ziggurat image of individual, stepped, dislocations (figure 4.12).

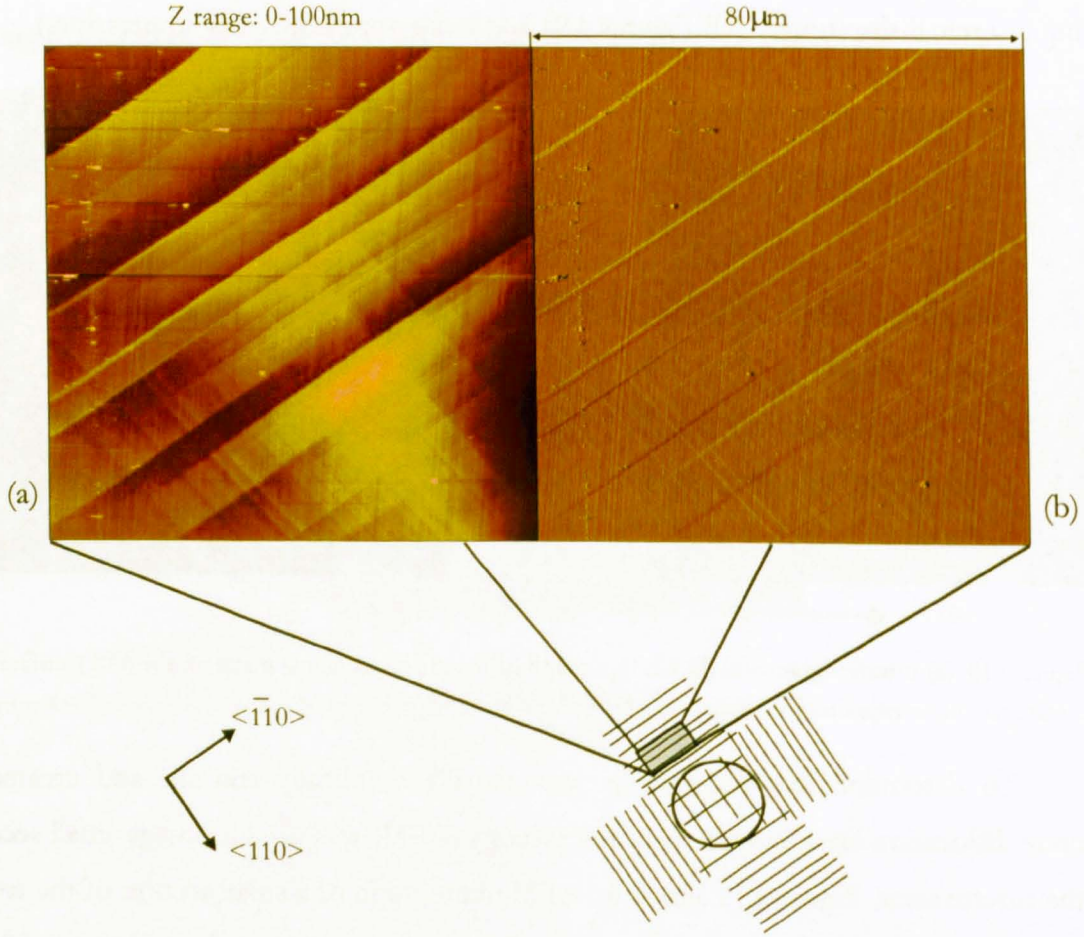

Figure 4.11. AFM micrograph of a section of the rosette pile up of the impression shown in figure 4.9(a).

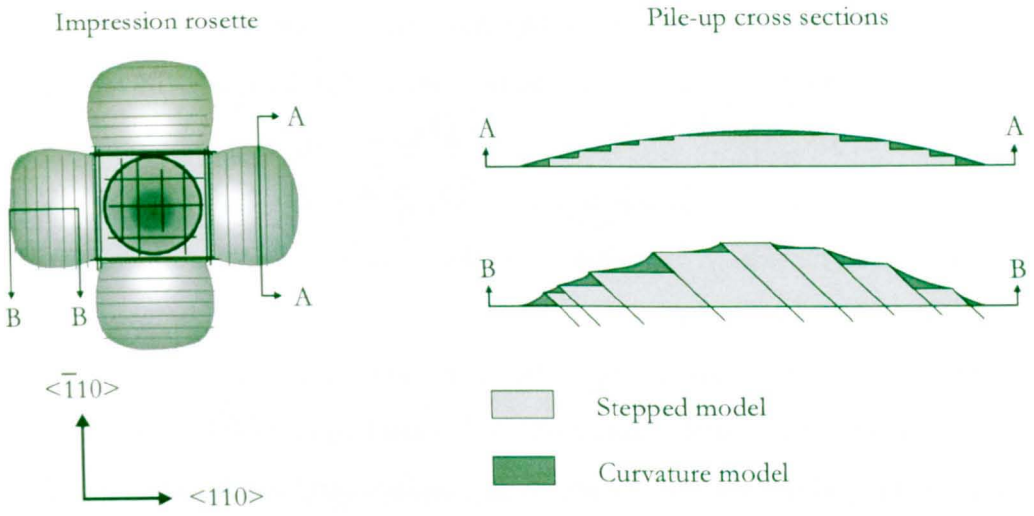

Figure 4.12. Cross sectional diagrams of the rosette pile-up.

It is possible to see slip lines that are perpendicular to those that are conventionally displayed when drawing rosette schematics (*i.e.* parallel to the side of the impression on which they are found). The slip lines that run perpendicular to the side of the impression from which they emerge were known as 90° slip lines, whereas the conventional ones were known as parallel slip lines. The 90° slip lines tended to be fewer in number and more closely spaced than the parallel ones. Step height analyses have shown that these 90° slip lines were lower than the parallel ones (4nm and 18nm respectively). There was no evidence to suggest that the 90° slip lines travelled all the way through the impression; rather is seems that they started and finished outside of the contact area on all four arms of the rosette. The slip line structure of the rosette can be seen in Figure 4.13 where an impression rosette has been etched to reveal the emergent dislocations. It can be seen that the 90° slip lines extended farther than the last parallel slip lines, also they tended to be strongest towards the edge of the contact area.

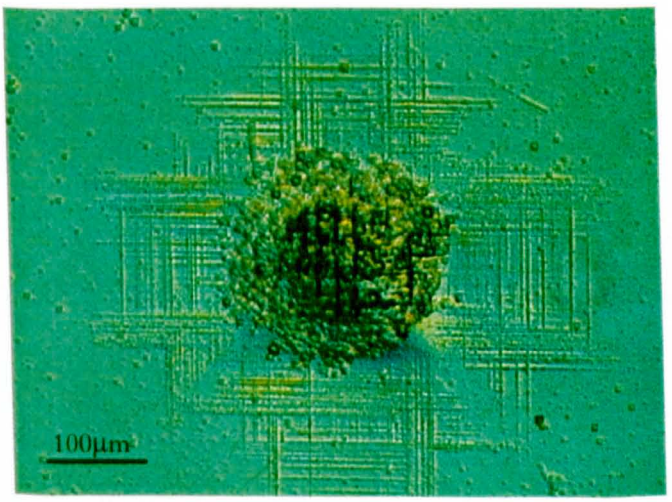

Figure 4.13. Micrograph of a rosette formation, etched to reveal the emergent dislocations.

As was shown by the onset of slip models, it is likely that the dislocations that produced the slip lines in the rosette were initiated underneath the contact area and travelled to the surface along a slip plane. The AFM micrograph in figure 4.11 shows that the slip lines were atomically straight. Therefore, it can be assumed that the dislocation loop that produced the slip step remained on the plane on which it was initiated (*i.e.* there is no cross slip, or kinking of the loop).

The step height of an average slip step was found to be 18nm, which is the equivalent about 117 atoms high (based on C-C bond length of 0.154nm). The step height produced by a single dislocation emerging at the surface can be calculated as follows:

- A step on the {001} surface of diamond must involve two stable atomic layers.
- The height between consecutive stable layers (n) is ¼ **a** (where **a** is the unit cell length =0.345nm)
- Therefore, the minimum achievable step height is 0.0892nm.
- An emergent dislocation has a burgers vector of ½<110>.
- A step height based solely on the burgers vector of the dislocation would be ½ the diagonal of the unit cell (=0.252nm).
- As the step must be terminated by stable atomic layers, *i.e.* multiples of (n), the height of a stable step is increased from the length of the burgers vector (0.252nm) to the height of at least three stable steps (0.268nm) (De Theije, 1999).

The steps produced by the dislocations in the impression rosette, however, are in the order of 18nm high. As dislocations cannot be of strength greater than the burgers vector, it must be assumed that the slip step was formed by about 62 single dislocations, all piled up on top of each other. Furthermore, the discrete nature of the slip steps suggests that all of the dislocations were created at the same point, *i.e.* a Frank-Read style source or mechanism. The proposed mechanism for the creation of the steps is shown schematically in figure 4. 14, where it is assumed that the steps are manifestations of the screw section of a dislocation loop that has intersected the surface. When a segment of the dislocation reaches the surface, it cannot expand upwards, but is able to continue to expand outwards.

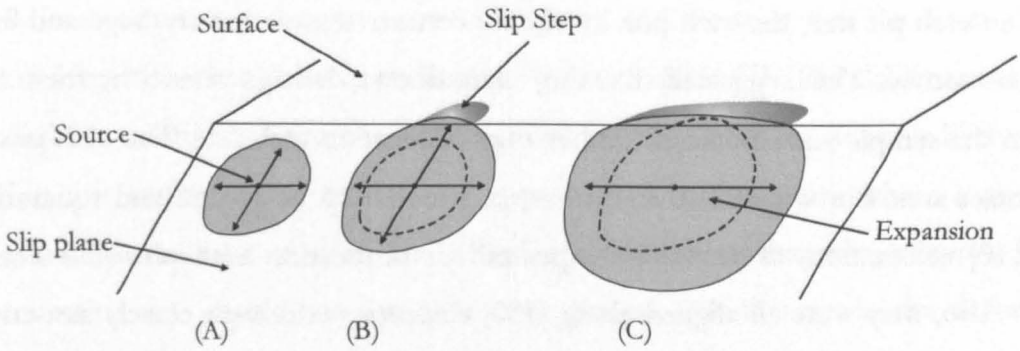

Figure 4.14. Diagram showing the creation of a slip step.

Figure 4.15 shows how the continued production of dislocations, by a mechanism such as the Frank-Read source would increase the slip step height. However, at the centre point of the slip step there will be a greater number of subsequent dislocations that have reached the surface than at the ends. This disparity in numbers of dislocations intersecting the surface is reflected in the curvature of the slip steps. The continued outward expansion of the dislocations would continue until the resolved shear stress on the loops is insufficient for further expansion. The cruciform nature of the slip step pattern is thought to be due to the anisotropic nature of the stress field *i.e.* the resolved shear stresses in the <100> directions inhibit the expansion of the slip steps, hence confining them to the <110> sides of the impression. The slip steps that do expand further are possibly able to because of the back stress created by the piled-up dislocations at the edge of the step.

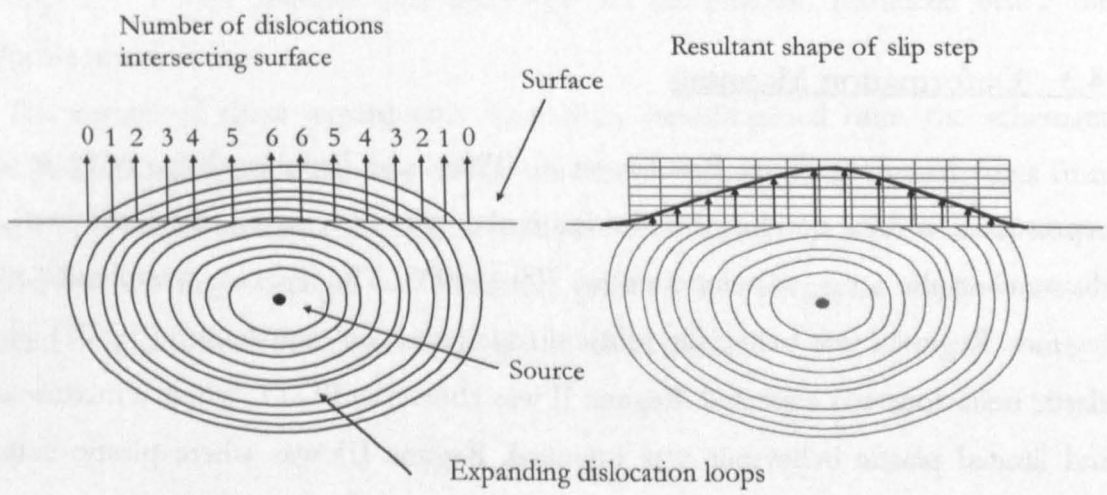

Figure 4.15 Mechanism for creation of a curved slip step via a Frank-read source.

A closer look at the etched impression rosette in figure 4.13 revealed that the slip lines were, indeed, comprised of many dislocations. The micrographs shown in figure 4.16 are higher magnification images of the etched, impression shown in figure 4.13. The contact area is towards the bottom right hand corner and can be easily distinguished by the

change in etch pit size, the etch pits inside the contact area were very large and tended to be flat bottomed. This suggested that they were due to damage caused by friction effects between the sample and impressor, rather than dislocation etch pits. The etch pits outside the contact area, but within the rosette arms, were sharp bottomed and square in shape with [110] orientation, as would be expected for dislocation etch pits (De Theije *et al*, 1999a). Also, they were all aligned along [110] directions and were closely associated with the observed slip lines. The fact that the etch pits (which are manifestations of edge dislocations intersecting the surface) lay along the slip lines suggested that the slip line itself was caused by the screw section of the dislocation loop.

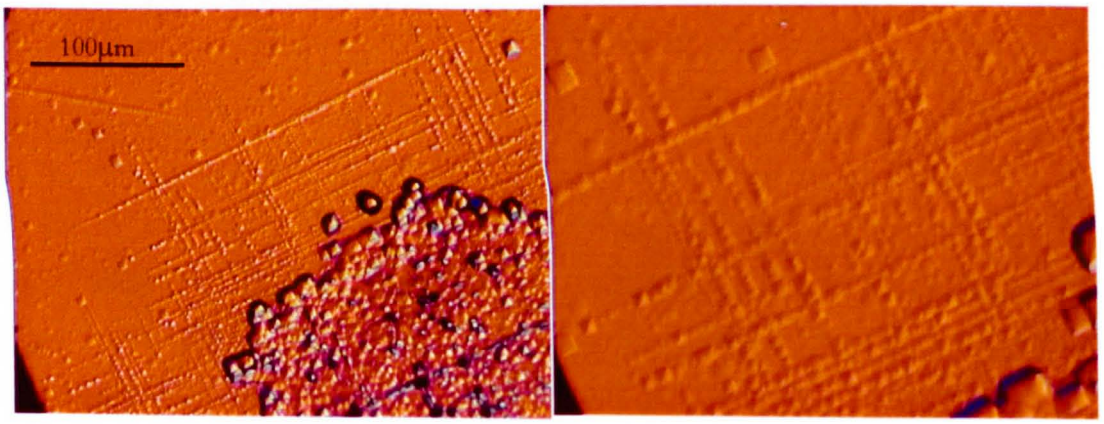

Figure 4.16. Higher magnification micrographs of an etched rosette formation, produced by a Si3N4 impressor, at 1400°C, under a load of 115N for a dwell time of 300s.

4.3 Deformation Mapping

In recent work by Brookes et al (1990) and Brookes, E.J. (1992) a schematic representation was developed to indicate the critical resolved shear stress (CRSS) of diamond in the range of temperatures, 700-1400°C. The diagram was divided into three regimes. Regime I was below the brittle-ductile transition temperature (BDTT) where only elastic behaviour was expected. Regime II was above the BDTT, where a mixture of elastic and limited plastic behaviour was expected. Regime III was where plastic deformation becomes dominant. Also depicted on this diagram was a line above which the pressure was sufficient to create cracks. Below the BDTT (Regime I) Hertzian fracture was expected, at high pressures and above it cracks were produced as a consequence of dislocation interaction. The CRSS and the BDTT were investigated thoroughly in those works, however, the division between regimes II and III and the upper cracking limit were not. It was the aim of this work to indicate, with more accuracy, these divisions.

Before considering the generation of figures and maps, it was necessary define a point of deformation change between Regime II and Regime III. The deformation profile of diamond is a continuous process, therefore the regime II-III boundary is likely to be a speculative one, unlike in the case of the upper, cracking boundary where a significant event occurs. For the sake of reference, a level of deformation that was definitely Regime III and one that was nearly but not quite was chosen. For this work, the deformation profile that was definitely regime III was rosette slip (figure 4.3 (6)). The deformation level that was nearly regime III but not quite was picture frame slip (figure 4.3 (5)).

Results:

A series of impressions were made on the {001} surface of several standard synthetic type Ib diamonds (~500ppm N). Varying levels of deformation were obtained by using different soft impressor cone materials (therefore changing the applied pressure) and by changing the temperature at which the impressions were made. The series of impressions were chosen to give a broad range of deformation profiles over the temperature range 770°C (BDTT) to 1400°C. For each case, the contact pressure was calculated and the temperature recorded. The various techniques, as mentioned above, were then applied in an attempt to identify the level of deformation produced. For the sake of simplicity, the deformation profiles 1+7, 2+3 and 4+5 as depicted in figure 4.3 were merged together. It was assumed that there was no deformation produced below the brittle-ductile transition line.

The results of these experiments were then superimposed onto the schematic diagram. The line indicating the brittle-ductile transition was calculated by using data from Brookes, E.J. (1992). The upper dotted line was also taken from that work and represents the theoretical cleavage strength of diamond, inferred by using the dependence on temperature of the of the Young's modulus and shear modulus.

Key

Catagory	Symbol	Description
A	○	(1) Hertzian fracture; (7) Dislocation induced Facture
B	■	(2) CRSS/BDT; (3) Slip inside contact area
C	△	(4) Slip outside contact area; (5) Reverse plasticity
D	▲	(6) Rosette

Figure 4.17. Key: Categories of observed deformation profiles.

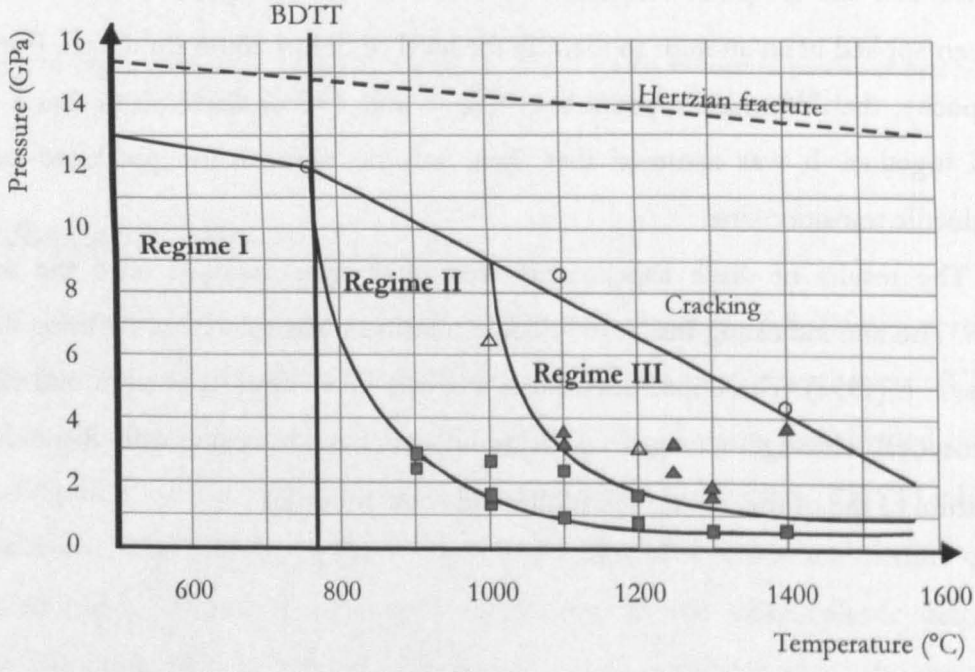

Figure 4.18 Revised schematic diagram of the temperature/pressure dependence of plasticity for the (001) plane in synthetic Ib diamond

It can be seen from the map shown in figure 4.18 that the results followed the predicted position of the BDT (Brookes, E.J, 1992). It also shows that the slope of the upper cracking limitation was greater than previously reported. The most significant observation to be made from this map, however, was the form of the Regime II/III

boundary. In previous work, this boundary has been represented as a vertical straight line, like that of the BDTT. From looking at the schematic diagram of the expected deformation profiles (figure 4.4), it was clear that the boundary would not be a vertical line but would slant inwards. Due to lack of sufficient data, however, the slope of the line could not be devised but was depicted as vertical. The additional data points produced in this study have allowed this boundary to be depicted in more detail. Firstly, it can be seen that the boundary is indeed, slanted inwards, however, the results suggest that the line is not straight. The form of the boundary is a curve that most likely mimics that of the lower BDT boundary. It was assumed, when producing this line, that at higher temperatures (>1300°C) there would always be a transition between elastic and totally plastic behaviour, *i.e.* that area of Regime II will reduce, but never be completely eliminated.

4.4 The Effect of Time

In work presented so far, all of the results were gained by loading the impressor against the specimen for the same dwell time (300s). As has been shown by various authors, diamond creeps at temperatures above its brittle-ductile transition temperature. In this section a series of impressions were made in the same diamond at different dwell times (300, 1000, 2000s and 3000s). This was achieved by first impressing for 300s then moving the impressor to a new part of the crystal and impressing for a 1000s whilst the chamber was still evacuated and the sample at the experimental temperature. The process was repeated until the 3000s impression was completed.

Low temperature creep

It can be seen from figure 4.19 and table 4.2, where series of impressions have been made at different times but otherwise identical conditions, that the observed level of deformation can be drastically altered by the length of the dwell time. The impressions in figure 4.19 show that the deformation produced by the TiB_2 impressor for dwell time of 300s is a category **C** impression (using the nomenclature used in figure 4.17). However, by increasing the time from 300s to 3000s, the impression has changed from a category **C** (slip just outside the contact area) to a category **D** impression (rosette). Increasing the dwell time of impression, therefore, has a dramatic effect on the brittle-ductile schematic diagram shown in figure 4.18

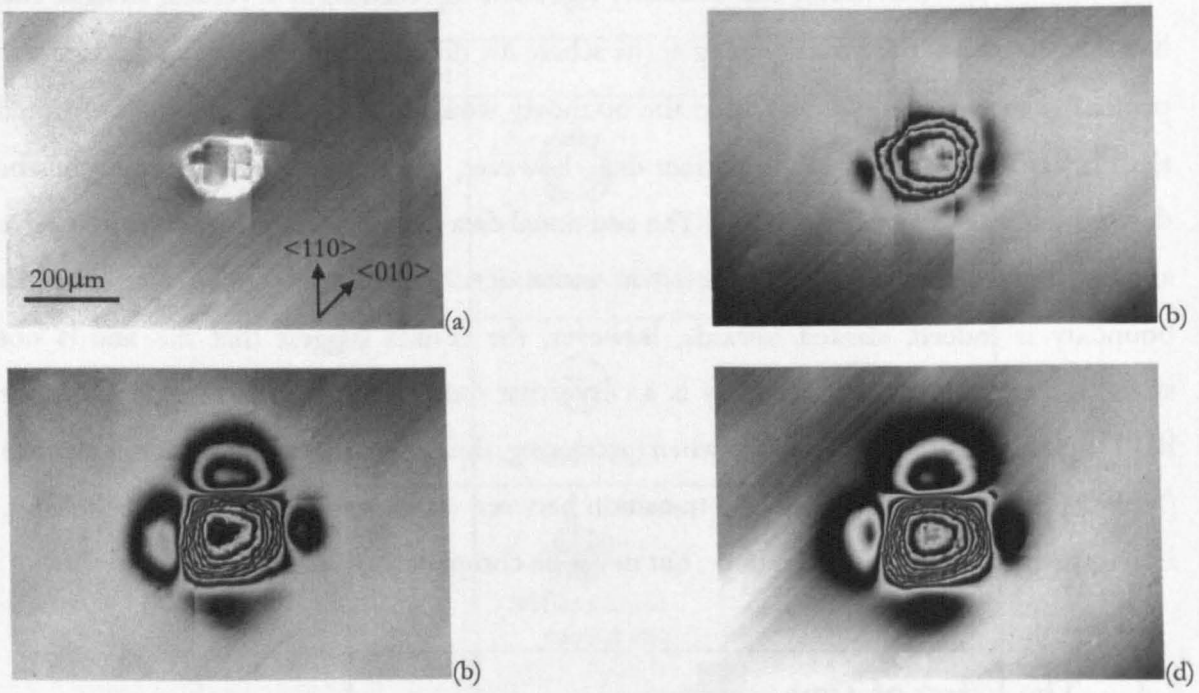

Figure 4.19. Interferograms of impressions produced by a TiB_2 impressor (~4GPa), under a load of 115N, at a temperature of 1000°C for (a) 300s, (b) 1000s, (c) 2000s (d) 3000s on the (001) face of synthetic Ib diamond.

Dwell time (s)	300	1000	2000	3000
Contact Diameter (μm)	150	181	192	194
Contact Pressure (GPa)	6.51	4.47	4.37	3.89
Impression Depth (μm)	0.25	0.75	1.875	2.125
Impression Volume (m^3x10^{-14})	0.034	1.16	4.37	4.61
Pile-up Height (μm)	0	0.25	0.5	0.5

Table 4.2. Measurements of the deformed area of impressions produced by a TiB_2 impressor, under a load of 115N, at a temperature of 1000°C for increasing dwell times.

By increasing the time, the pressure to produce a rosette at 1000°C was reduced from approximately 8.5GPa to approximately 4GPa, *i.e.* the Regime II/III boundary was moved to the left. The effect of time was that, when the diamond was loaded at a given temperature, the intrinsic resolved shear stress of the diamond determined the level of deformation that was achievable. As the dislocations were initiated within the bulk of the crystal rather than the surface, they had to travel to the surface where they could be seen and recorded by the observer. However, if the time under load was not long enough, the dislocations produced terminated at some point beneath the surface where they would not be seen. This effect was more marked when investigating very low levels of deformation, such as would be found at the brittle ductile transition boundary (BDT). The previously recorded data for the BDT relied on the few dislocations produced, travelling to the surface within the 300s time period. However, if the experiments were repeated but using a

longer dwell time (e.g. 3000s), then the recorded levels of deformation would be much higher than would be necessary to decide that plastic deformation had just started. This would have the effect of moving the BDT boundary to the left as well as the Regime II/III boundary. As a consequence of moving the BDT, the brittle ductile transition temperature, will also be reduced (figure 4.20).

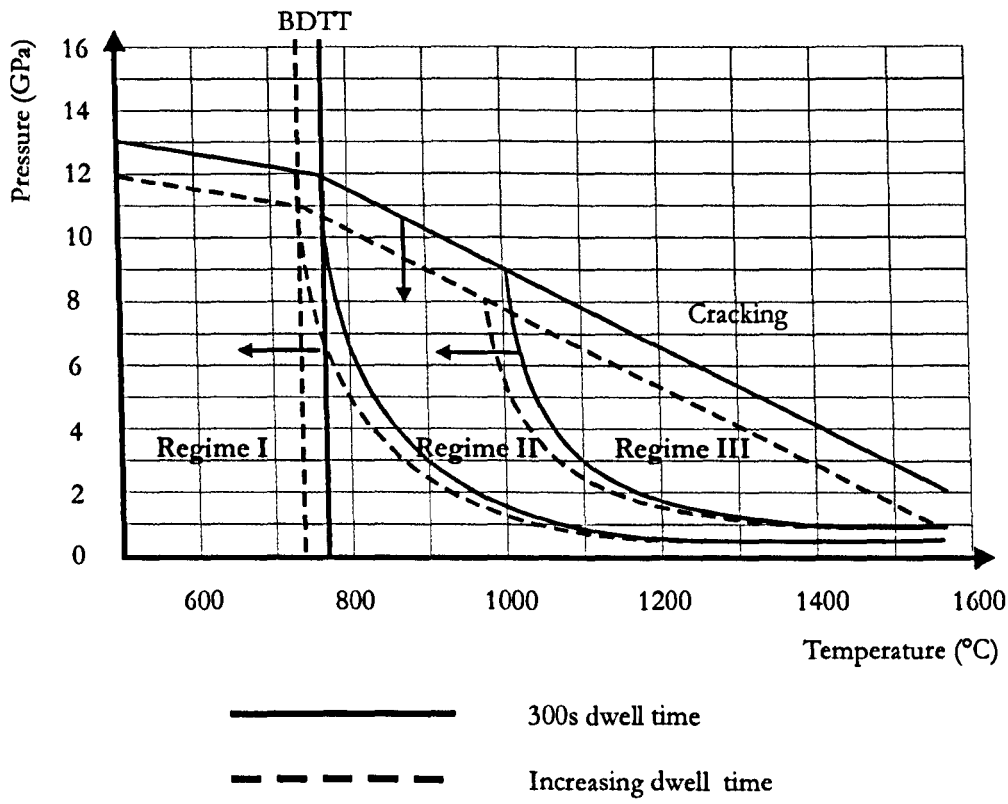

Figure 4.20. Schematic diagram showing the effect of time on the brittle-ductile transition of diamond.

High temperature creep

The effect of time on the plastic deformation of diamond was less marked at temperatures and pressures that were sufficient to produce rosettes. This was because a significant number of dislocations had been produced and travelled to the surface. It can be seen from the series of impressions shown in figure 4.21, that diamond continues to creep, even when a rosette has been formed. Although the form or the area of the impressions has not significantly altered, the depth of the impression increased with time (table 4.3). It can also be seen from measurements of the length of the rosette arms that, as the dwell time is increased, the rosette arms do not increase in length, but decrease. This indicated that the furthest rosette slip line was created by the highest achieved stress, rather than by continued dislocation motion. This suggests that the dislocation rosette size was dependent on the value of the resolved shear stress and was independent of time.

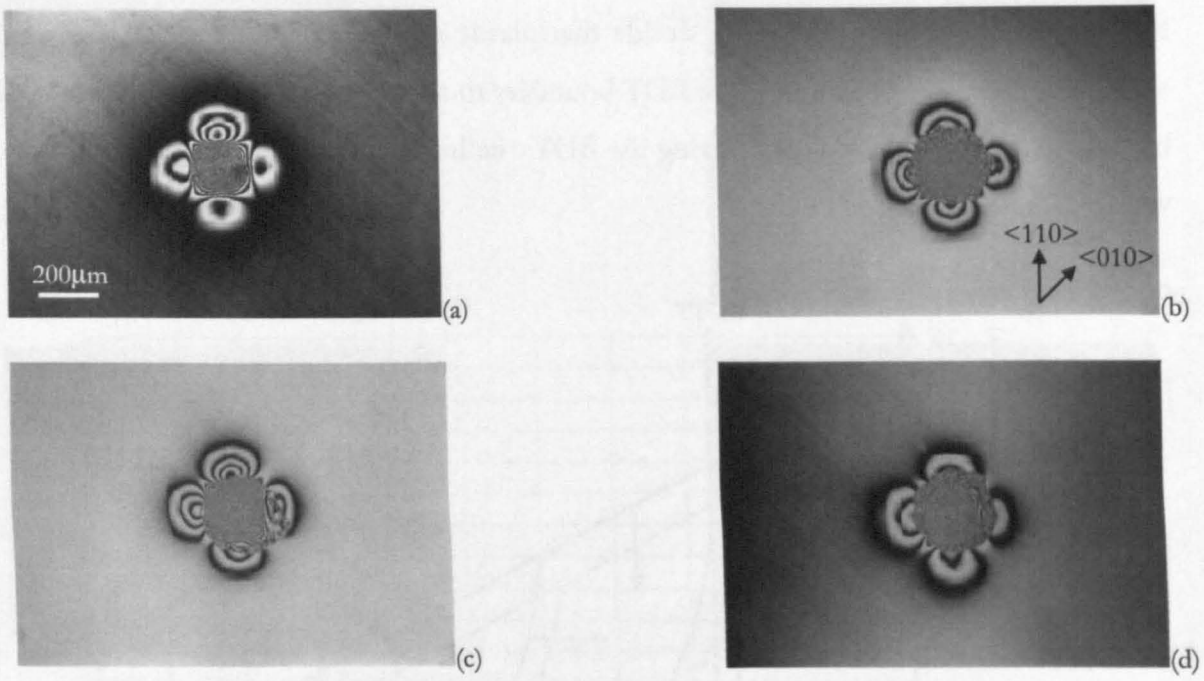

Figure 4.21. Interferograms of impressions produced by a Si_3N_4 impressor, under a load of 115N, at a temperature of 1400°C for (a) 300s, (b) 1000s, (c) 2000s (d) 3000s on the (001) face of synthetic Ib diamond.

Dwell time (s)	300	1000	2000	3000
Contact Diameter (µm)	206	187	201	207
Contact Pressure (GPa)	3.45	4.19	3.62	3.42
Impression Depth (µm)	4.25	6	4.75	5.25
Impression Volume (m^3x10^{-14})	3.8	5.4	4.1	5.2
Pile-up Height (µm)	1	0.75	1	0.5
Average rosette wing length (µm)	106.25	98.25	79.75	92.5

Table 4.3. Measurements of the deformed area of impressions produced by a Si_3N_4 impressor, under a load of 115N, at a temperature of 1400°C for increasing dwell times.

The effect of the continued creep of the diamond at the higher temperatures and pressures was very similar to that seen under the lower temperatures and pressures, *i.e.* the deformation process was still operating, but in a less visible manner. With the lower conditions the manifestation of the creep was the emergence of a rosette of dislocations at the surface. When the rosette is formed during the initial time period, the creep could be seen by an increasing impression volume. Although the impression volume increased in size, the area of the rosette did not grow significantly. Equally, as the deformation depth is dependent on the load not the applied pressure, the deformed volume must also have remained relatively constant. The increase in impression volume with no increase in deformation volume would have resulted in dislocations becoming ever more densely packed. Therefore, the likelihood for sessile dislocations and associated piled up

dislocations was increased. The increased possibility of dislocation interaction and pile-up led to dislocation induced cracking. This behaviour was seen in the deformation caused at dwell times of 300s, but at higher temperatures and pressures, *i.e.*. the conditions to cause dislocation induced cracking are reduced by the increase of dwell time.

4.5 Summary

This section has reviewed the current models that describe the plastic deformation of diamond when loaded under point contacts. A new model explaining the deformation process has been devised, using the previous models and experimentally observed results.

A seven-point deformation story has been devised, where each point represents a visible change in the observed plastic deformation of diamond when using the soft impressor technique. It has been shown that whilst each point is reached consecutively, the onset of each point is dependent on the experimental temperature, pressure and dwell time.

In addition, the schematic diagram of the brittle-ductile transition (BDT) of diamond has been expanded. A second curve has been added to denote the change from localised plasticity to gross plastic deformation, in the form of dislocation rosettes and pile-up. An upper cracking boundary has also been added, below which Hertzian or dislocation induced fracture were not observed.

It has also been shown that the time for which the diamond is impressed plays a significant role in the onset and subsequent plastic deformation of diamond. Although the form of the BDT schematic is not altered the experimental conditions (temperature and pressure) to produce the features represented on the diagram are reduced by increasing the dwell time.

The main results of this chapter are summarised below:

- A seven-point deformation story has been devised.
- A model explaining the observed deformation story, from the onset of plasticity to rosette formation and pile-up has been hypothesised.
- The BDT schematic diagram has been expanded.
- The regime II/III boundary has been added and found to be similar in form to the CRSS curve.

- An upper boundary, below which no cracking was observed, has been added. It was found to deviate significantly from the line theorised by Hertzian fracture mechanics.

- Increasing the dwell time reduces the temperature/pressure conditions for all features on the BDT schematic.

- The effect of dwell time is more marked at lower temperatures and pressures.

Chapter 5

THE EFFECT OF NITROGEN CONTENT

5.1 Introduction

The effect that impurity atoms have on the properties of materials has been extensively studied. It is well known that impurity atoms affect the velocity of dislocations by either pinning them or aiding them to overcome the Peierls barrier. Macroscopically speaking, this means that impurity atoms can change the yield stress and brittle ductile transition temperature of a given material, amongst other properties (Rabier et al, 1983). The detailed understanding of the effect of dispersed impurity elements, as obstacles to dislocations, requires careful study of the "host" material together with the nature of the impurity. For instance, in silicon single crystals, dislocation mobility is increased by the addition of n-type or p-type dopants with n type dopants having a larger effect (Hirsch *et al*, 1985b), but p type dopants retarding the dislocation mobility in germanium (Roberts *et al*, 1985). Indentation testing was used to induce the plasticity at temperatures up to 400°C. No change in indentation hardness as a function of impurity level was recorded.

Although it is widely accepted that impurity elements within a crystal affect the properties, there has been little experimentation to determine the effect on diamond. In fact, in most cases, there still exists the misnomer that diamond's extreme properties make it a "special" material, that is immune to the laws that affect all other materials. This is clearly not the case, as it has been shown in this and previous works that diamond behaves like any other f.c.c. crystal. Brookes, E.J. (1992) showed that nitrogen content had a significant effect on the plastic deformation of diamond and furthermore, the nature of the nitrogen impurity was also important. In that work it was shown that the brittle ductile transition temperature and the critical resolved shear stress for a given temperature were higher for natural IIa diamond than type Ia, which were both higher than synthetic type Ib diamond.

In this work, the effect of nitrogen content on the plastic deformation of synthetic (HPHT) diamonds have been studied more carefully. Synthetic (HPHT) diamonds were selected because this type of diamond is more available, the quality is superior, the

reproducibility is good and the large single growth sectors permit good experimental control within a region of reasonably homogeneous nitrogen concentration. Also, owing to the fact that the nature of the nitrogen impurity has an effect (*i.e.* A, B centres or single substitutional), it was necessary to distinguish between them. It was decided that the role of the single substitutional nitrogen defect would be determined as the only other nitrogen defect that is found in "as produced" HPHT diamonds is the H3 defect. Although this defect is similar to the A centre, the H3 defect is not found in sufficient quantities to significantly influence the results. Assuming that because the H3 defect does not have an IR absorption peak the defect concentration in a sample 3mm thick must be lower than $10^{14}/cm^3$ or 0.001ppm (Mainwood and Newton, 2000). In natural type Ia samples, however, there is always a mixed component of the nitrogen content present. Care must be taken to select samples that are predominantly one type, however, as there is still significant doubt as to the concentration profile within a given area. Even when ignoring the inherent difficulties of experimentation, it is still prudent to investigate the plastic properties of synthetic diamonds with different levels of nitrogen. This is, again, because the majority of interest lies with the industrial, rather than geological communities. When the significant role that nitrogen plays in the plasticity of diamond is better understood, it is conceivable that a range of synthetic diamonds with differing levels of nitrogen concentration could be produced. This would mean that it would be possible to choose the "grade" of single crystal diamond to be used, much in the same way as diamond grit products are separated today.

The investigation of the effect of nitrogen concentration comprised of two parts. The first part involved detailing the macroscopic changes in levels of plastic deformation for a given temperature and pressure, and were displayed in the form of a revised BDT map. The second part concentrated on investigating the reasons why the nitrogen content played such a significant role in plastic deformation. This involved producing large plastic rosettes in several samples containing different levels of nitrogen and detailing the resultant deformation in as many ways as possible, including spectroscopy and AFM.

5.2 Deformation Map

In this investigation, the soft impressor technique was used to create predominantly plastic impressions (whilst avoiding fracture), under controlled experimental conditions, in a range of synthetic (HPHT) type Ib diamonds. The diamonds were carefully selected for form and each diamond contained different concentrations of single substitutional nitrogen within the {100} growth sectors, in the range 0-850ppm N. The temperature and pressure

range for plastic deformation were 700°-1400°C and 0.5-12GPa respectively. All of the samples were polished {001} plates of approximate area ~2mm^2. The impressions were carefully placed, where possible, in {100} growth sectors where the nitrogen content was fairly uniformly dispersed and of "average" concentration. In addition, the cubic growth sectors exhibit only nitrogen related impurity centres as it has been widely reported that other impurities such as the Ni and Co are preferentially incorporated into {111} growth sectors.

The level of plastic deformation for each impression was determined using optical microscopy and categorised using the methodology outlined in chapter 4. Due to the number of impressions needed to produce the plastic deformation versus nitrogen concentration relationship, it was not possible to show examples of every impression. Instead, examples are shown that best show the trends observed.

Figure 5.1 shows interferograms of impressions made in synthetic (HPHT) diamonds containing 0ppm N and 550ppm N, at a temperature of 1100°C using a cBN impressor (~7GPa). It can be seen that the nitrogen containing sample has deformed extensively, producing a deep impression (~6μm), a full rosette pattern and also dislocation induced cracks, whilst the diamond containing no nitrogen has hardly deformed at all with a shallow impression (0.75μm) and no rosette.

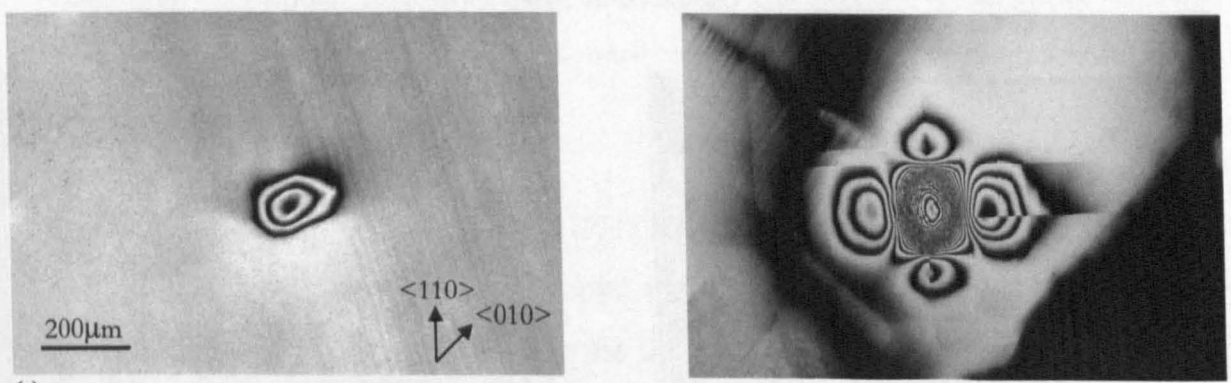

Figure 5.1. Interferograms of impressions produced by a cBN impressor, at a temperature of 1100°C, under a load of 115N, for a dwell time of 300s: (a) 0ppm N and (b) 550ppm N

In figure 5.2 the interferograms of impressions made in the same samples but under different conditions are shown. The experimental temperature was raised to 1300°C and the mean pressure was lowered to ~2.5GPa by using a ZrB_2 impressor. In this case both samples extensively plastically deformed, producing rosettes, however the sample containing the higher nitrogen content produced a deeper impression (~1μm for 0ppm

and ~3μm for 550ppm N) and visibly higher pile-up. Neither impression produced dislocation-induced cracks, which was a reflection of the higher experimental temperature and the lower applied pressure.

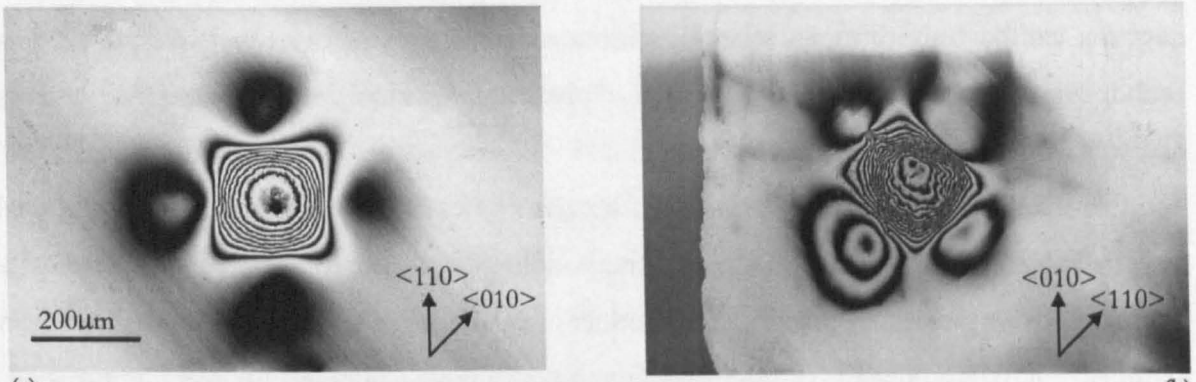

Figure 5.2. Interferograms of impressions produced by a ZrB_2 impressor, at a temperature of 1300°C, under a load of 115N, for a dwell time of 300s: (a) 0ppm N and (b) 550ppm N

Figure 5.3 shows interferograms of impressions in synthetic (HPHT) diamonds containing 550ppm N and 850ppm N respectively, made at the higher temperature of 1400°C whilst maintaining the pressure by using a Si_3N_4 impressor (~2.5GPa). It can be seen that the effect of the nitrogen concentration seems to have been reversed. The sample containing the lower nitrogen level deformed to produce 1.5μm deep impression with a rosette whilst the higher nitrogen level sample has produced an impression of 0.5μm and no rosette. Again, no cracking was observed in either case.

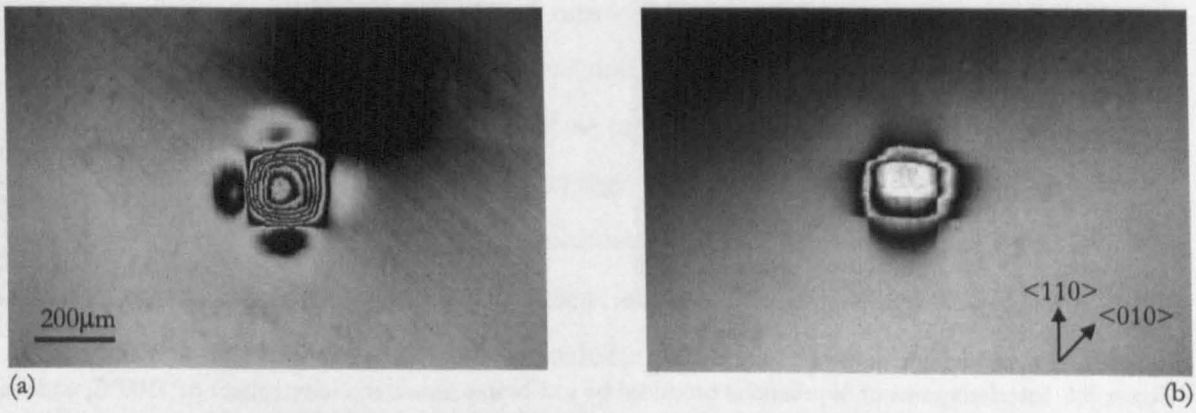

Figure 5.3. Interferograms of impressions produced by a ZrB_2 impressor, at a temperature of 1400°C, under a load of 115N, for a dwell time of 300s: (a) 550ppm N and (b) 850ppm N

The results of this study are summarised in the form of a revised brittle-ductile transition schematic, which is shown in figure 5.4.

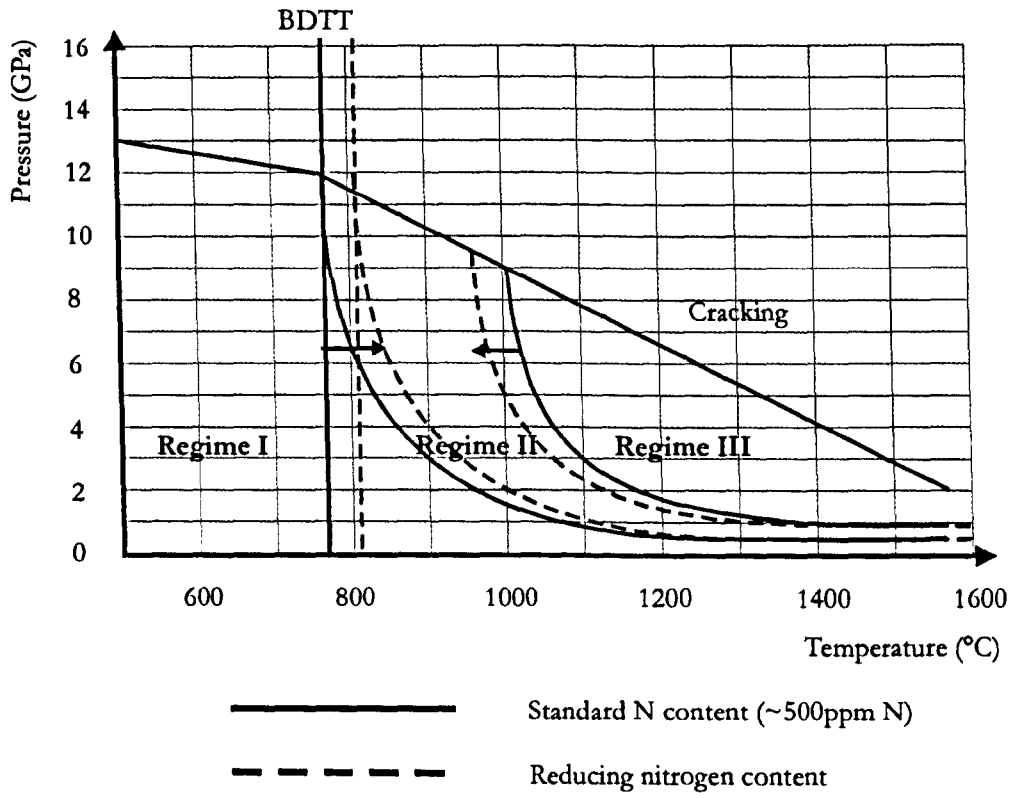

Figure 5.4. Schematic diagram showing the effect of nitrogen content on the brittle-ductile transition of diamond

This map was similar in form to the map shown in figure 4.18, where the nitrogen content was approximately 550ppm N. A number of observations can be made from this map:

- Reducing the nitrogen content of HPHT diamond raises the temperature for the transition from brittle to ductile behaviour, *i.e.* the BDTT.
- Increasing the nitrogen content lowers the flow stress of HPHT diamond, *i.e.* the stress to initiate and multiply dislocations or the CRSS.
- Reducing the nitrogen content lowers the Regime II/III boundary, *i.e.* the boundary between deformation and extensive deformation.

NB. The upper cracking limit shown in figure 5.4 was taken from that shown in figure 4.18, as no cracking was observed during the course of these experiments.

5.3 Deformation Profiles

Impressions were made using a Si_3N_4 impressor at 1400°C under a load of 115N for a dwell time of 300s. The conditions chosen were such that a rosette formation of dislocations was expected for each impression. One impression was placed in each of three synthetic type Ib diamonds with different nitrogen contents (100, 650, 850ppm N) and one natural type IIa sample. In each case, a number of investigative techniques were employed to profile the level and nature of the deformation produced. Optical microscopy in the form of Nomarski DIC, strain birefringence, interferometry, and cathodoluminescent topography was used. In addition, grids of photoluminescence (PL) spectra were taken, analysed and displayed in the form of three-dimensional maps. AFM microscopy was also used to gain high magnification images of the slip lines within the rosette arms and finally the samples were etched in KNO_3 to reveal the dislocation etch pits. The optical results are displayed and discussed in section 1, whilst the photoluminescence results, including the defect intensities and the Raman peak data are displayed and discussed in section 2. Section 3 contains the etching and AFM images.

Section 1, Optical microscopy:

From the Nomarski DIC (figure 5.5), strain birefringence (figure 5.6), and CL micrographs (figure 5.7), the levels of deformation were assessed. The impression depths, areas, volumes and the exact height of pile-up were assessed from the interferometry image measurements (figure 5.8). These values are summarised in table 5.1

	Sample			
	Natural IIa	100ppm N	650ppm N	850ppm N
Contact diameter (μm)	206	192	206	191
Resultant Pressure (GPa)	3.6	4.14	3.6	4.19
Impression Depth (μm)	3	7.5	4.25	1.5
Impression Volume (m^3x10^{-14})	4.5	12.6	3.8	1.4
Pile-up height (μm)	1.5	2	1	0.5

Table 5.1. Measurements of the deformed volume of the impressions, produced by a Si_3N_4 impressor under a load of 115N at a temperature of 1400°C and a dwell time of 300s in diamonds containing different levels of nitrogen.

It is clear from the Nomarski DIC images (figure 5.5) that in each case the contact area was similar, resulting in significant plastic deformation with multiple intersecting slip extending outside the contact areas. The slip steps became more coarse as the nitrogen content was increased. Despite the high levels of plastic deformation, there were no Herztian or dislocation induced cracks.

The strain birefringence micrographs shown in figure 5.6 indicate that the strain field in each case was cruciform in shape along <110> directions. The area of strained material increased as the nitrogen level decreased, indicating the level of strain associated with the impressions placed in the synthetic samples increased as the nitrogen concentration was lowered. The level of strain produced in the natural type IIa samples was lower than that of the 100ppm N sample but higher than the 650ppm N sample. The 100ppm N sample showed a strain pattern that was different from the rest in that it had a <100> strain field superimposed over the <110> one. In the natural type IIa sample, the mosaic of relaxed dislocations inherent in most natural IIa diamonds can clearly be seen.

The cathodoluminescence (CL) images (figure 5.7) show that in each case luminescence was produced, associated with the impressions. The synthetic samples show the characteristic 575nm (N-V) luminescence that is aligned along the slip plane directions. The intensity of the 575nm luminescence increases as the nitrogen level is reduced. In addition the 650 and 850ppm N samples show green luminescence associated with the H3 (N-V-N) defect, whereas the 100ppm N sample shows none. In the 100ppm N sample the fact that the H3 luminescence is not obscuring the weaker 575nm luminescence means that the 575nm luminescence can clearly be seen in the cruciform rosette pattern closely associated with the slip lines.

A measure of the deformed volume can be gained more clearly from the interferograms shown in figure 5.8. Whilst the contact area and, therefore, the resultant pressures, were similar for each impression, the resultant deformation was different. It can be seen that as the nitrogen content increased, the impression depths, volumes and pile-up heights decreased. The natural IIa sample did not follow the trend as the deformed zone was smaller than that of the 100ppm N sample, but higher than that of the 650ppm N sample. The area bounded by the pile-up of the rosette arms followed the previous trend with the largest pile-up area seen in the 100ppm N sample and the smallest in the 850ppm N sample. Again, the results showed different deformation in the 100ppm N sample. Where the rosette pile-up lobes tended to be elongated in the middle along <110> directions, producing teardrop shaped pile-up rather than the elliptical shape seen in the other samples.

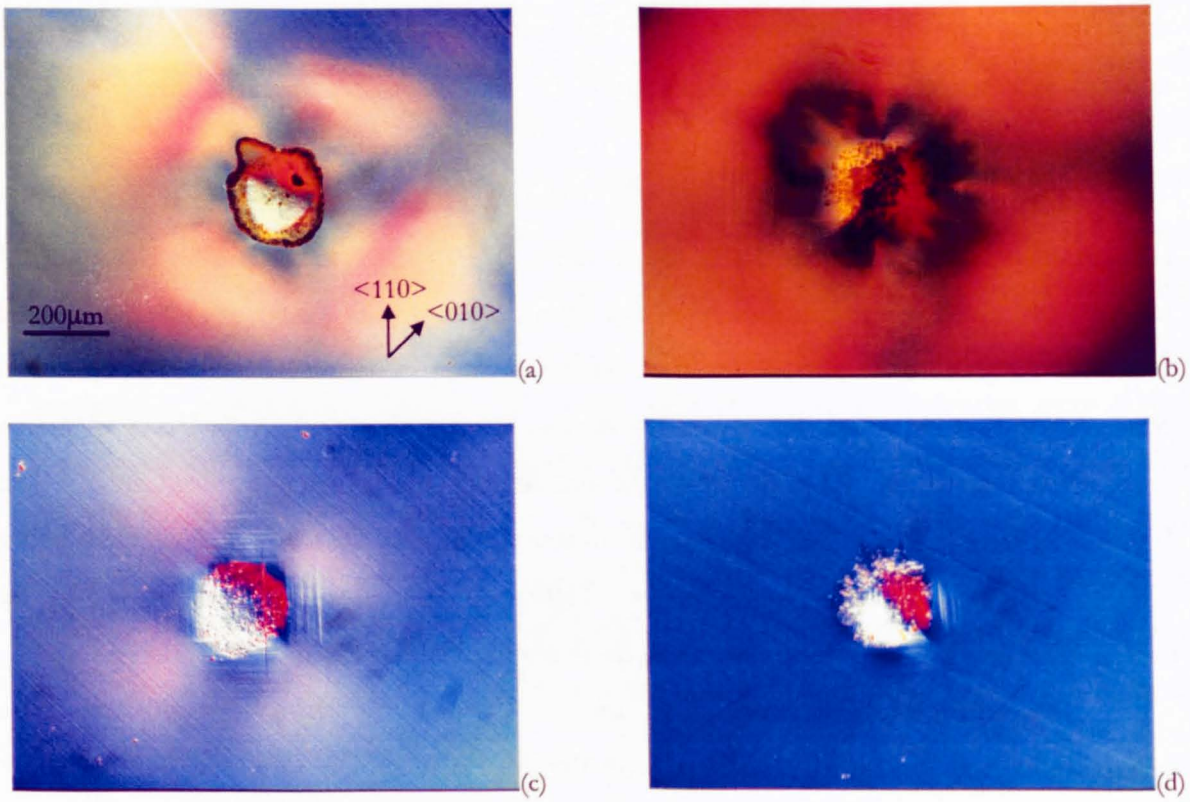

Figure 5.5. Nomarski DIC micrographs of impressions produced by a Si3N4 impressor, at a temperature of 1400°C, load 115N, for a dwell time of 300s: (a) natural IIa, (b) 100ppm N, (c) 650ppm N, (d) 850ppm N

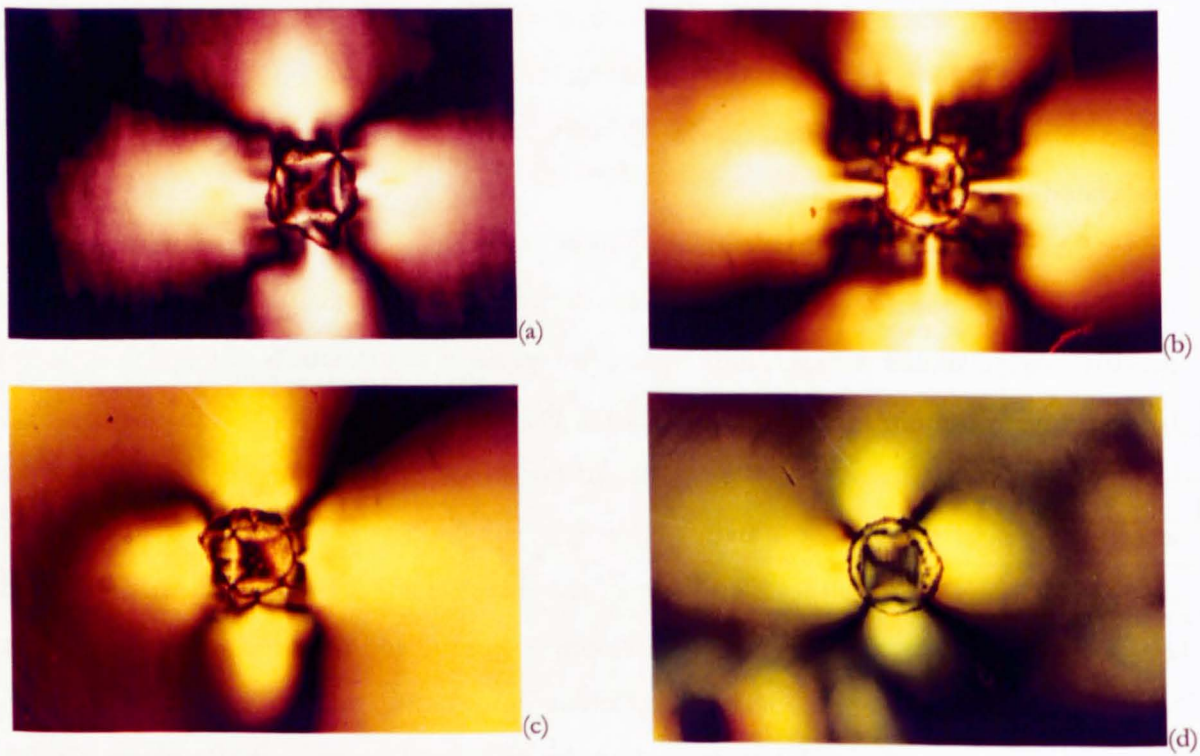

Figure 5.5. Strain birefringence micrographs of impressions produced by a Si3N4 impressor, at a temperature of 1400°C, load 115N, for a dwell time of 300s: (a) natural IIa, (b) 100ppm N, (c) 650ppm N, (d) 850ppm N

No CL image produced for natural IIa sample

(a)

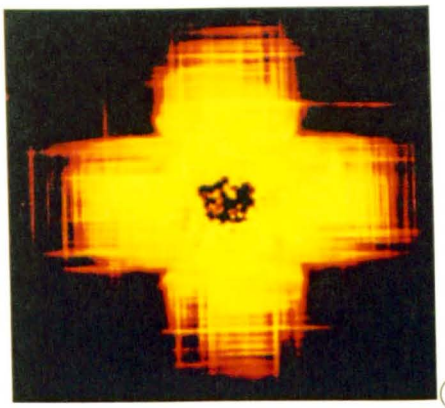

(b)

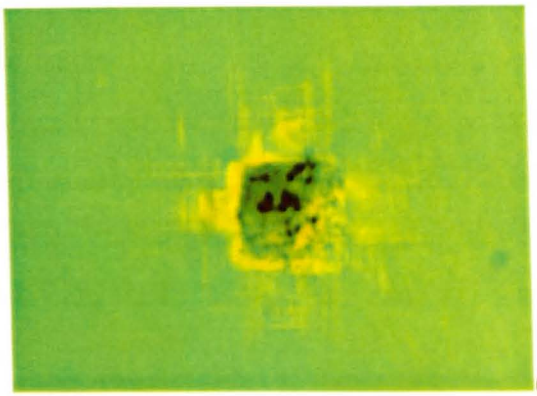

(c)

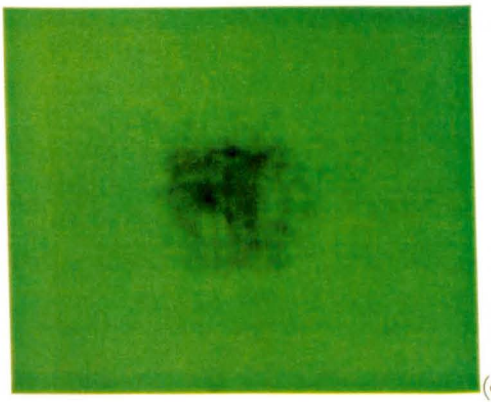

(d)

Figure 5.7. Cathodoluminescence (CL) micrographs of impressions produced by a Si3N4 impressor, at 1400°C, load 115N, for a dwell time of 300s: (a) natural IIa, (b) 100ppm N, (c) 650ppm N, (d) 850ppm N

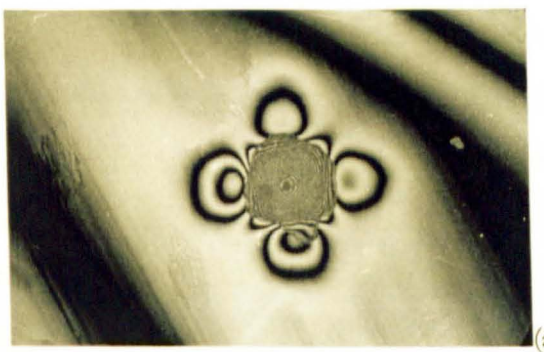

(a)

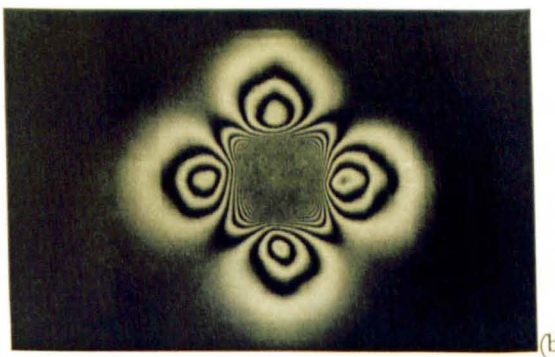

(b)

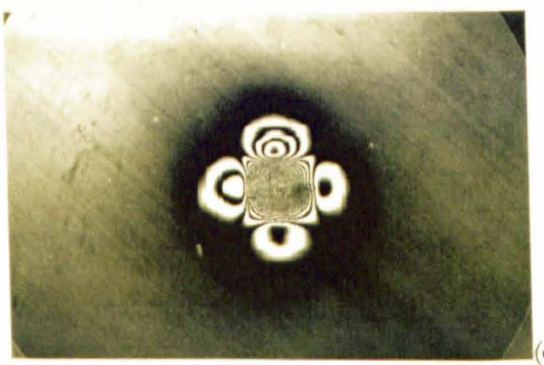

(c)

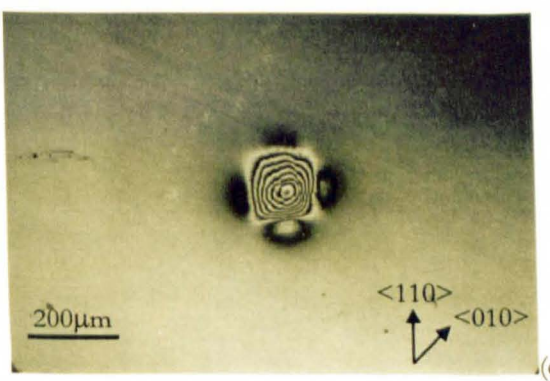

(d)

Figure 5.8. Interferograms of impressions produced by a Si3N4 impressor, at a temperature of 1400°C, load 115N, for a dwell time of 300s: (a) natural IIa, (b) 100ppm N, (c) 650ppm N, (d) 850ppm N

Section 2, Photoluminescence and Raman:

The PL investigation comprised of two components; initially, the emission spectra were analysed for the 1.945ev and H3 defect concentrations, then the Raman peak shift and full width at half maximum (FWHM) were recorded. In each case a grid of PL spectra centred on the impression were taken. The grid size was 800μm square for the 550ppm and IIa samples and 1000μm square for the 100ppm N sample, with a spacing of 100μm, with the exception of the 850ppm N sample where a 400μm square with 50μm spacing was used. The difference in grid sizes between the impressions reflected the difference in deformation area for each impression. The luminescence grids were first taken using the 514.4nm laser line and then repeated using the 488nm laser-line. The laser was focused on the surface of the specimen and produced a spot size of 20μm. For each case, the position and full width at half height (FWHM) of the Raman line (1332 Rcm^{-1}) for each spot in the grid were recorded. In addition, the intensities of the luminescence peaks at 614 Rcm^{-1} from the 488nm line (H3) and at 3745Rcm^{-1} using the 514.4nm line (1.945ev) for each spot were recorded. The H3 and 1.945ev peak intensities were not measured for the natural IIa sample as these defects are nitrogen related and therefore no response was expected. The 100ppm N sample showed no H3 luminescence, therefore a map of H3 luminescence could not be produced.

The Raman line position was converted into values for residual strain (GPa) as described in chapter 3 and in each case, the spectra were baseline corrected. These values were recorded for each spot on the grid and were represented as three-dimensional maps. Table 5.2 gives the peak intensities of the 1.945ev and H3 defects and the values of the Raman peak shift and the FWHM. In each case the maximum and minimum values taken from within the known deformed region are given. For the defect intensities, a value for the background intensity was also calculated by taking a spectrum from a point on each specimen that was known to be undeformed. A background value for the Raman data was not necessary as all of the values were normalised against values taken from a natural IIa diamond sample considered to be strain free.

Intensities (cm^{-1})		Sample			
		Natural IIa	100ppm N	650ppm N	850ppm N
1.945ev defect	Background	/	0	406	1096
	Minimum	/	0	410	386
	Maximum	/	12349	10145	4898
H3 defect	Background	/	0	3411	9942
	Minimum	/	0	0	0
	Maximum	/	0	4616	1625
Raman shift (GPa, comp)	Minimum	1.194	0.908	0.683	-0.057
	Maximum	1.655	1.09	0.907	0.41
FWHM	Minimum	2.391	2.149	2.192	4.112
	Maximum	4.884	3.761	4.048	6.797

Table 5.2. Values for the defect intensities, Raman shift and FWHM of the impressions, produced by Si_3N_4 impressor under a load of 115N at a temperature of 1400°C and a dwell time of 300s in diamonds containing different levels of nitrogen.

Maps of the photoluminescence intensities of the 1.945ev (N-V) and H3 (N-V-N) defects (figures 5.9 and 5.10 respectively) showed that the 100ppm N sample originally had zero populations of either defect. This was in contrast to the higher nitrogen samples, which contained high intensities of H3 but also background 1.945ev. In each case, the 1.945ev defect was higher in intensity towards the middle of the impressions. In addition, an outline, reminiscent of the rosette formation, can be seen. The H3 defect on the other hand was shown to decrease to zero, towards the centre of the impressions.

The Raman shift maps, displayed in figure 5.11, showed that the deformed volume was under a compressive residual stress with the stress becoming less compressive towards the centre of the impressions. In the case of the 850ppm N sample the stress became tensile at the centre of the impression. The residual stress was highest for the natural IIa sample and was reduced as the nitrogen content increased. If the difference between the highest recorded stress and the lowest for each map was taken, it showed that the stress gradient increased as the nitrogen increased, except for the natural IIa sample, which had a residual stress gradient nearly equal that of the 850ppm N sample. Again, the contours on the maps were reminiscent of the rosette formation, especially in the 650 and 850ppm N samples. In the 650ppm N sample the highest residual stresses were along <100> directions, in-between the rosette pile-up lobes, indicating that the material has been displaced outwards and upwards, producing a tensile element towards the centre of the impression.

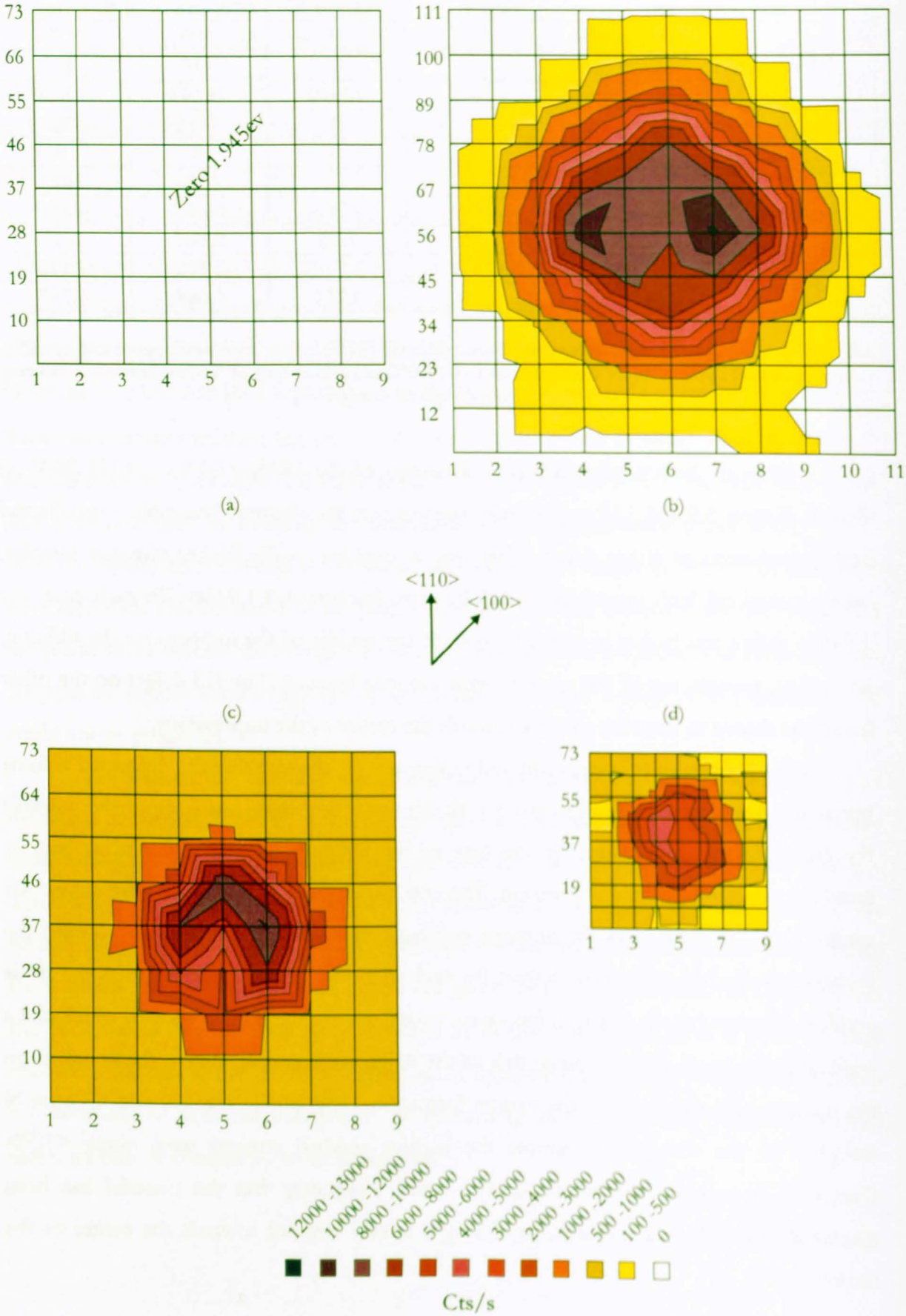

Figure 5.9. Photoluminescence maps showing the intensity of the 1.945ev peak, created by impressions produced by a Si3N4 impressor, at a temperature of 1400°C, under a load of 115N, for a dwell time of 300s: (a) natural IIa (None), (b) 100ppm N, (c) 650ppm N 100µm grid size, (d) 850ppm N, 50µm grid size

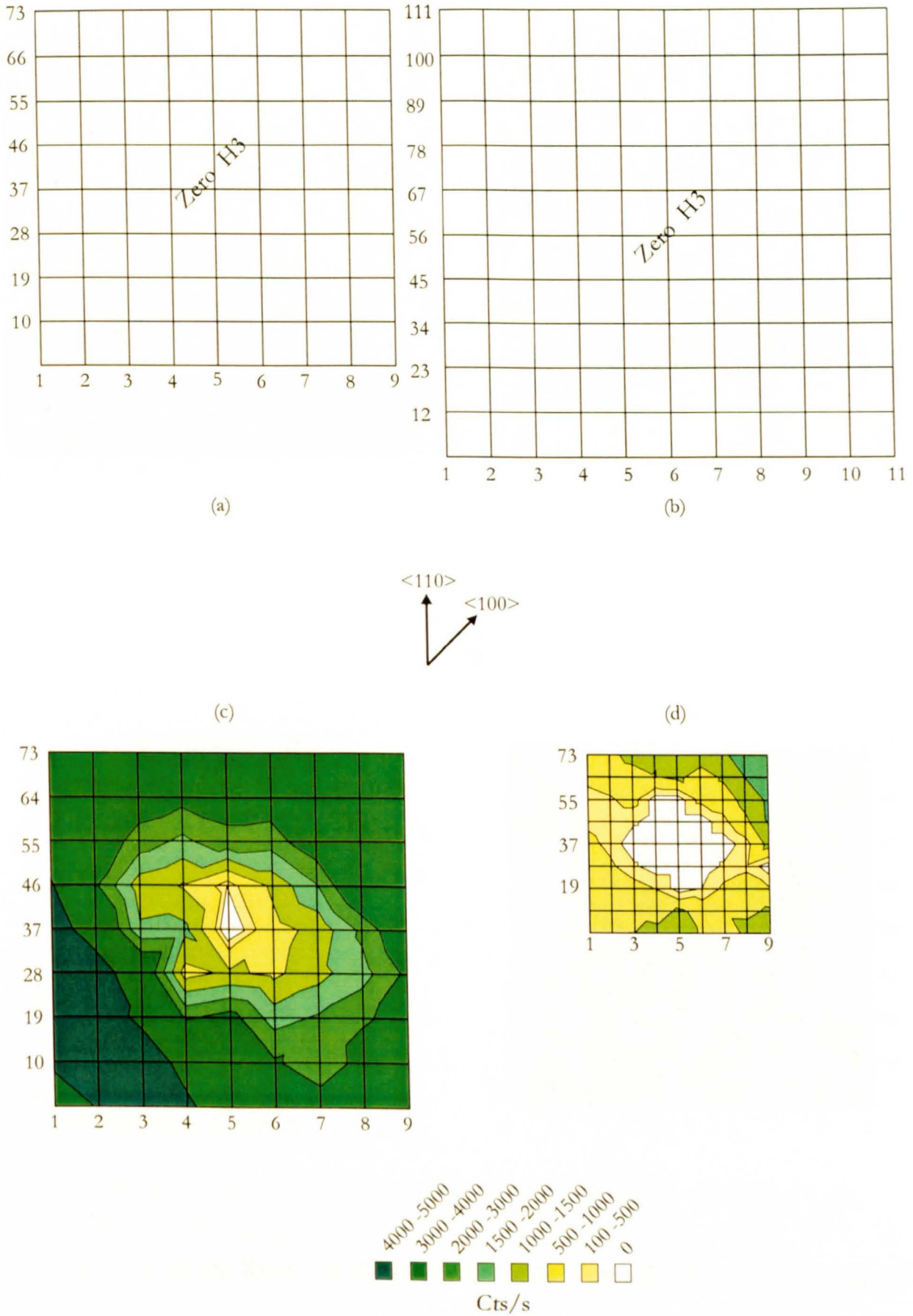

Figure 5.10. Photoluminescence maps showing the intensity of the 2.46ev (H3) peak, created by impressions produced by a Si3N4 impressor, at a temperature of 1400°C, under a load of 115N, for a dwell time of 300s: (a) natural IIa (None), (b) 100ppm N (none), (c) 650ppm N 100µm grid size, (d) 850ppm N, 50µm grid size

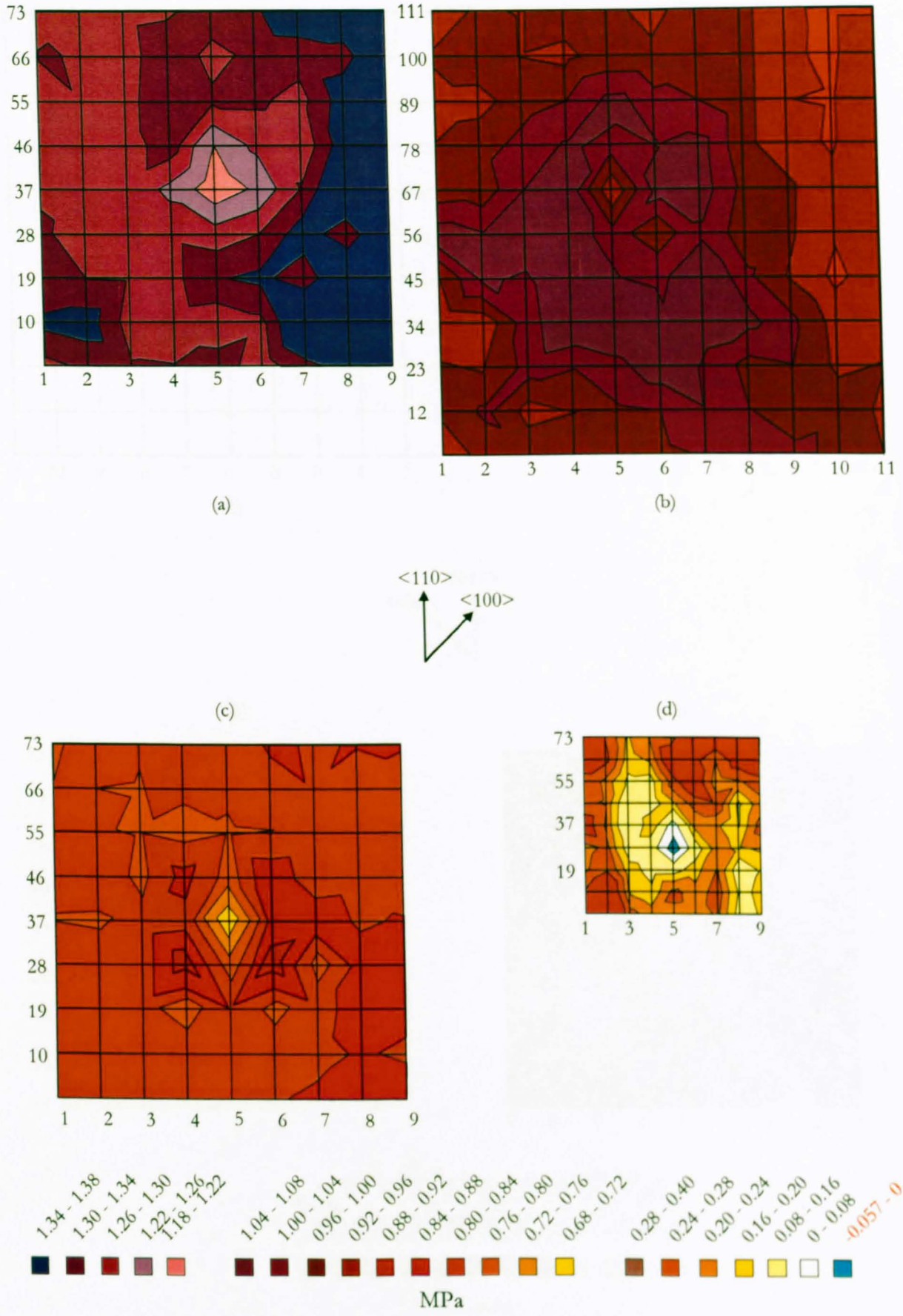

Figure 5.11. Photoluminescence maps showing the Raman shift (GPa), created by impressions produced by a Si3N4 impressor, at a temperature of 1400°C, under a load of 115N, for a dwell time of 300s: (a) natural IIa (b) 100ppm N, (c) 650ppm N, 100μm grid size, (d) 850ppm N, 50μm grid size

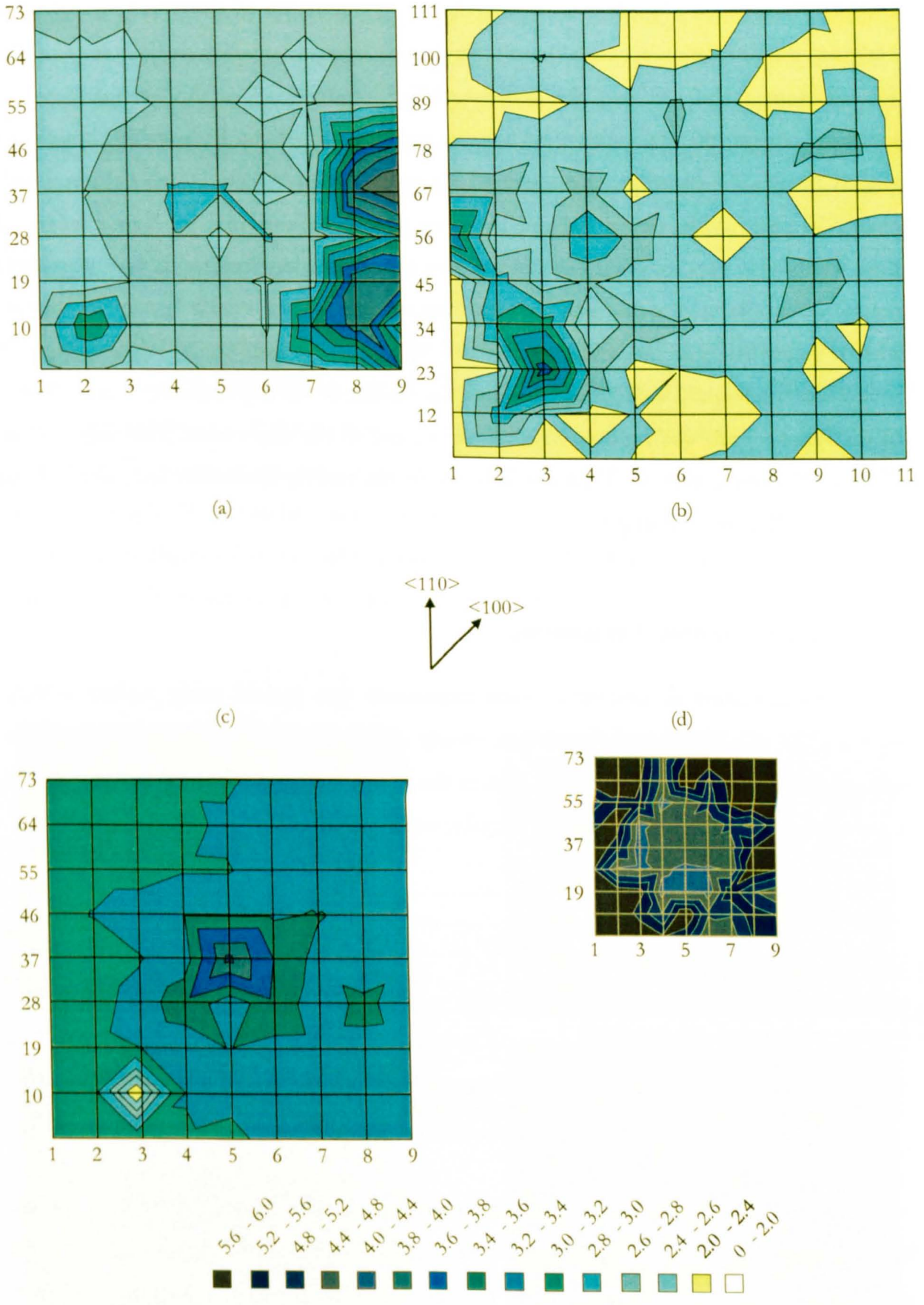

Figure 5.12. Photoluminescence maps showing the FWHM of the Raman peak, created by impressions produced by a Si3N4 impressor, at a temperature of 1400°C, under a load of 115N, for a dwell time of 300s: (a) natural IIa, (b) 100ppm N, (c) 650ppm N 100µm grid size, (d) 850ppm N, 50µm grid size

The full width at half-maximum maps of the Raman peaks (figure 5.12) showed that, as the nitrogen content was increased, the average width of the peaks increased. In addition, the difference between the maximum and minimum values was similar to those for the Raman shift, in that the greatest difference occurred as the nitrogen content increased. Again, the IIa sample had a value near to that of the 850ppm N sample but slightly lower. The contours of the natural IIa and 100ppm N sample maps showed little change in peak width, except for small regions. The small regions with large changes of peak width were very localised and not close to any impression features. It was most likely that these results were either due to impurities on the surface of the specimens or sub-surface inclusions. The maps for the 650 and 850ppm N showed much larger changes in peak width, the highest values being towards the outside of the impressions, *i.e.* the FWHM of the Raman peak was reduced towards the centre of the impression. The map for the 650ppm N sample was the most reminiscent of the rosette formation and, also, of the counterpart Raman shift map.

Section 3, Etching and atomic force microscopy:

As described in chapter 3, each impression was etched using molten KNO_3. Micrographs of each etched impression, clearly showing the extent of the deformation rosette, are displayed below. Table 5.3 gives the results of the AFM step height analyses and measurements of the rosette wing lengths, taken from the etched impressions.

		Sample			
		Natural IIa	100ppm N	650ppm N	850ppm N
Step Height analysis (nm)	Parallel slip	1.063	1.945	17.995	14.744
	90° slip	0.263	0.29	3.973	3.973
Rosette wing length average (μm)		/	310	106	42

Table 5.3. AFM step height analyses and rosette wing length measurements of the impressions, produced by Si_3N_4 impressor under a load of 115N at a temperature of 1400°C and a dwell time of 300s in diamonds containing different levels of nitrogen.

Atomic force microscopy (AFM) micrographs were taken of all of the impressions. In each case, the centre of the impressions could not be scanned, as the AFM is too sensitive to a height change of more than 1μ. For this reason, areas just outside the contact area of the impressions were chosen for scanning. The areas chosen were far enough away from the contact area to prevent saturation but within the area in which the rosette slip had been formed. For each image produced, a simple two-dimensional contrast image showing

the elevation of the surface and a three-dimensional impression created by the software package is given. In each case, the image was levelled by dictating a portion of the image that was deemed a flat, level area (usually away from any deformation). In each case, a schematic diagram accompanies the AFM image so that a sense of position and direction can be gained. The slip and polishing lines have produced images that contain three sets of straight lines. The lines that are perpendicular to each other and diagonal to the picture orientation, are the slip lines whereas those that are at 45° to the others and near vertical are the polishing lines.

Etching the samples (figure 5.15) has revealed that the extent of the deformation is much larger for the 100ppm N sample than for the others. This was determined by measuring the distance of the furthest dislocation etch pit from the edge of the impression. The extra rosette arm length seen in the 100ppmN sample was so large that the micrograph shown in Fig.5.15b had to be taken at a lower magnification. In the case of the natural IIa sample the background mosaic of dislocations produced so many etch pit that the etch pits associated with the slip lines could not be determined.

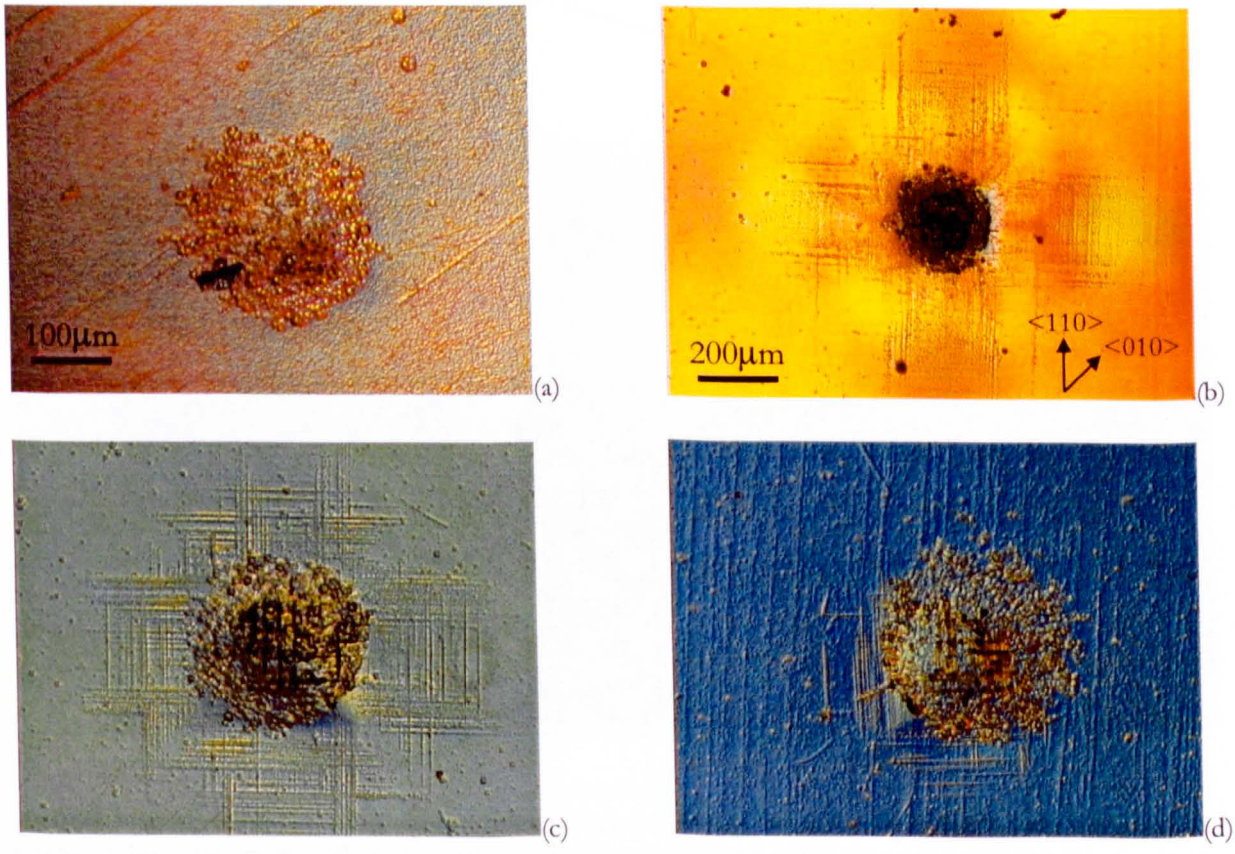

Figure 5.15. Nomarski DIC micrographs of the etched impressions produced by a Si3N4 impressor, at a temperature of 1400°C, load of 115N, for a dwell time of 300s: (a) Natural IIa, (b) 100ppm N, (c) 650ppm N, (d) 850ppm N

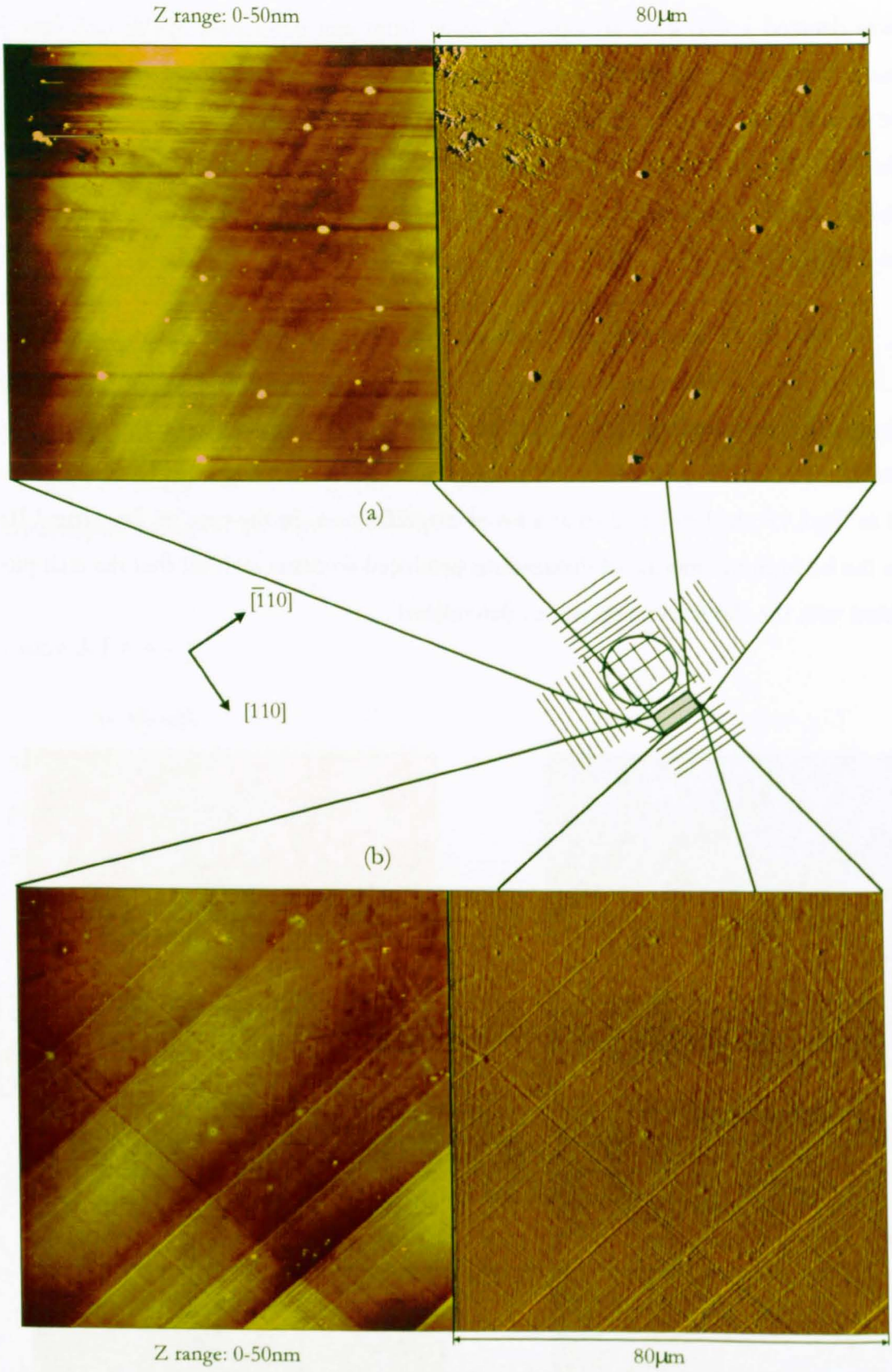

Figure 5.16. AFM micrographs of impressions produced by a Si3N4 impressor, at a temperature of 1400°C, under a load of 115N, for a dwell time of 300s (a) natural IIa, (b) 100ppm N. Where the left-hand image is a 2-D topographic map and the right-hand image is a computer generated 3-D image.

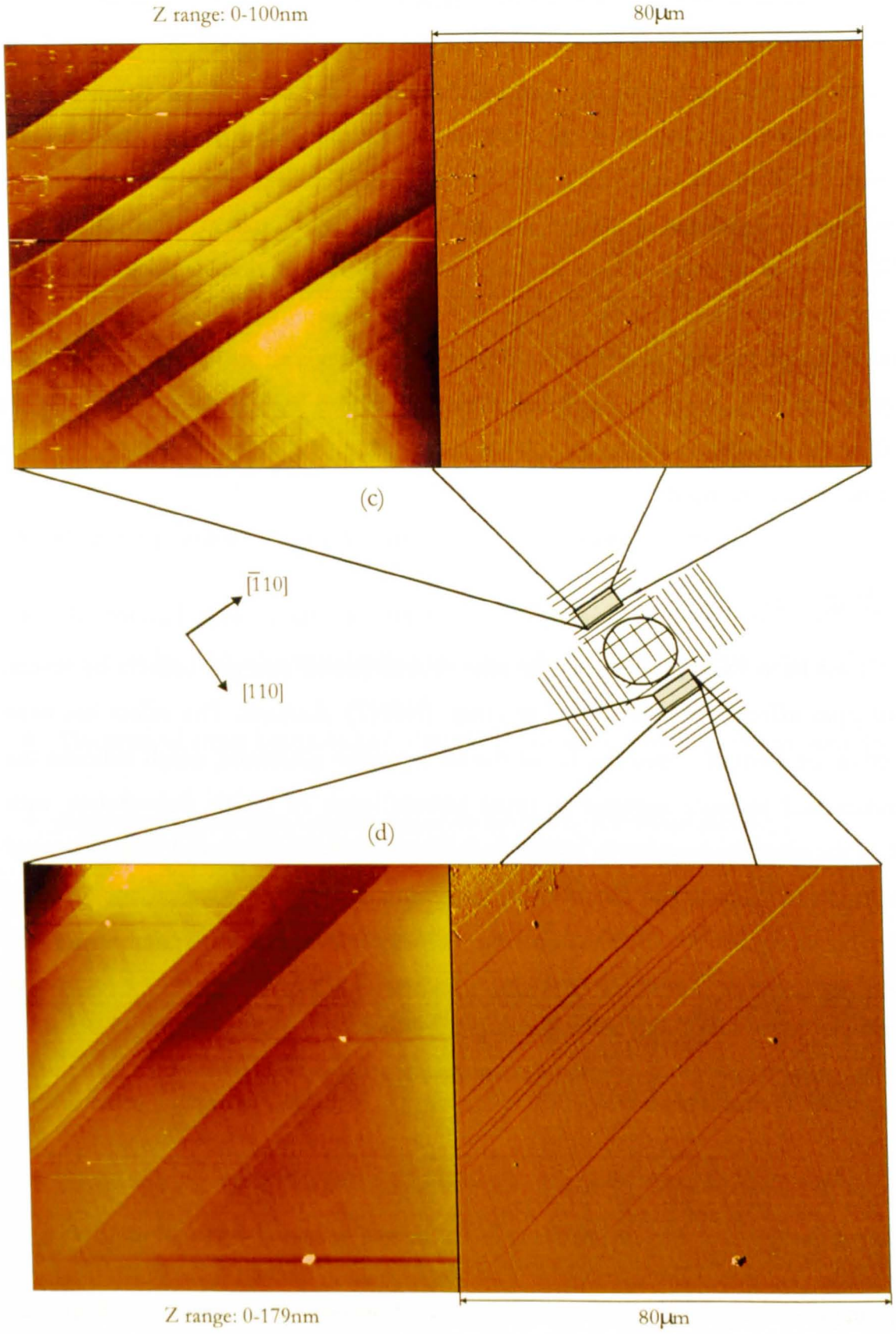

Figure 5.17. AFM micrographs of impressions produced by a Si3N4 impressor, at a temperature of 1400°C, under a load of 115N, for a dwell time of 300s (c) 650ppm N, (d) 850ppm N. Where left hand image is a 2-D topographic map and the right-hand image is a computer generated 3-D image.

The AFM topographs of the slip in each of the rosettes (figures 5.16 and 5.17) produced in each sample revealed that the nature of the slip was very different for each sample. The natural IIa sample shows large numbers of parallel and 90° slip whereas, in the other samples, the number of slip lines, both parallel and at 90°, was reduced as the nitrogen content was increased. In addition to the numbers, the distance between subsequent slip lines was increased as the nitrogen content was increased. For each case the ratio between the number of parallel and 90° slip lines was different, with the IIa have roughly the equal numbers of each and the 850ppm N having virtually no 90° slip lines. The step height analyses and the z-range of each topograph show that as the nitrogen content increased the step height of the slip lines also increased. Moreover, for each case the average step height of the parallel slip lines was higher than that of the 90° slip. In general, as the nitrogen content was reduced the number of slip lines increased, but their average height was reduced.

5.4 Summary

It has been show that varying the single substitutional nitrogen content by several hundred ppm affects the plasticity of synthetic (HPHT) diamond. The effect has been displayed in the form of a modified brittle-ductile transition schematic, which indicates the temperature and pressure required to cause various levels of plastic deformation with respect to the nitrogen content. In addition, dislocation rosettes produced under identical conditions but in samples with different nitrogen contents have been profiled, using a large array of techniques. The results of the different profiling techniques, when combined, allow a unique insight into the reasons why single substitutional nitrogen plays such a significant role in the plasticity of diamond at levels thought previously to be insignificant.

The main results of this chapter are summarised below:

Mapping:

- Reducing the nitrogen content raises the brittle-ductile transition temperature (BDTT).
- Reducing the nitrogen content increases the critical resolved shear stress (CRSS) at low temperatures, *i.e.* regime I/II boundary.
- Reducing the nitrogen content lowers the temperature/pressure conditions to cause gross plasticity (rosettes) *i.e.* lowers the regime II/III boundary.

Profiling:

- Reducing the nitrogen content increases the size of the deformed area, *i.e.* larger rosettes, deeper impressions and higher pile-up.
- 575nm (N-V) cathodoluminescence is strongly associated with the slip lines and dislocations in nitrogen containing diamonds.
- 1.945ev (N_i-V) photoluminescence is produced during plastic deformation and is seen to become more intense towards the centre of the impressions.
- H3 centres are not necessary to produce 575nm cathodoluminescence or 1.945ev photoluminescence.
- H3 photoluminescence is annihilated by plastic deformation processes.
- The residual stress around impression is compressive in nature, and has a cruciform structure by <100> oriented rather than <110> as with the rosette arms and pile-up.
- The residual stress becomes less compressive towards the centre of the impression.
- Reducing the nitrogen content increases the levels of residual stress.
- Reducing the nitrogen content reduces the level of disorder (FWHM) around the impression.
- The level of disorder (FWHM) is reduced towards the centre of the impression.
- Etching with KNO_3 at 750°C produces the best results for dislocation etching.
- Reducing the nitrogen content increases the dislocation rosette wing length.
- Reducing the nitrogen content produces finer, more numerous intersecting slip steps.
- The pile-up is produced by smooth, curved, slip steps for all nitrogen contents.

Chapter 6

DISCUSSION AND CONCLUSIONS

6.1 Discussion

The experimental work described in this thesis has shown that the soft impressor technique can be used to investigate the plastic properties of super hard materials at elevated temperatures. In this work, the study of significant plastic deformation repeatedly introduced into single crystal synthetic (HPHT) diamonds, whilst avoiding brittle failure, has led to a clearer understanding of the temperature and pressure dependence of the plasticity of diamond. It has also been shown that using this method, creep behaviour at temperatures above the brittle ductile transition temperature can be studied. In addition, the application of the soft impressor technique has provided a clearer insight into reasons why it is observed that the plasticity of diamond is sensitive to low levels of single substitutional nitrogen (0-850ppm N).

Discussion of work presented in this thesis can be separated into three main areas. The first area covers modelling and plastic deformation as seen experimentally. The second discusses the extension of the brittle ductile transition schematic diagrams and the effect of dwell time and nitrogen content. The third is concerned with the profiling of the rosette impressions, made in synthetic (HPHT) diamonds with different nitrogen contents.

Modelling:

In this work, a model of elastic stress contours based on single point contacts (Roberts 1988), together with estimates of the critical resolved shear stress (CRSS) of diamond (Brookes, E.J. 1992) and the plastic deformation developed when using the soft impressor technique has been developed to explain the observed deformation in terms of dislocation initiation and movement. The Roberts model provided benchmark levels of stress, whilst the CRSS calculations provided the data necessary to determine where, beneath the contact area, it was possible to initiate and move dislocations. Together with the observed deformation it was possible to hypothesise as to how the dislocations moved and multiplied to produce a macroscopic plastic impression.

The model assumed that the CRSS was the stress necessary to initiate a dislocation, but that the stress necessary to move a dislocation was less than the CRSS. This means that once a dislocation has been created it moves until the stress acting on it is too low for further movement. The subsequent multiplication of dislocations then fills the region in which they are able to expand. To create a larger dislocated volume, the overall stress level applied would need to be raised. However, the nature of the soft impressor technique is such that, to raise the mean pressure, the contact area must be reduced. As the deformation volume is related to the contact area, raising the pressure (*i.e.* lowering the contact area) reduces rather than increases the dislocated volume. However, the resolved shear stress is higher, therefore, a greater number of dislocations can be initiated, producing a greater number of dislocations in a smaller volume. To increase the size of the deformed volume, using the soft impressor technique, it would be necessary to increase the load applied to the impressor, thereby increasing the pressure without decreasing the contact area. Therefore it can be said that (when using the soft impressor technique) the deformed volume and in particular the deformation depth is independent of mean pressure, but dependent on the applied load.

When the resolved shear stress is high enough, the dislocations can expand further than the compressive/tensile boundary created by the edge of the circular contact. Then dislocations expand further into the bulk and emerge at the surface. The model assumes that the dislocations do not significantly alter the stress contours produced by the point contact. By making this assumption, it was possible to hypothesise as to the origin of the dislocations that created the rosette. However, for this to be correct, the dislocations that form the rosette must be full dislocation loops rather than punched out prismatic dislocations. If the rosette dislocations were prismatic in nature, then the length of any slip line would be fixed but its distance from the edge of the contact area (where it was created) would vary with dislocation velocity and the dwell time. However, it has been shown that the slip lines which form the rosette do not have fixed lengths and do not move away from the edge of the impression. This would indicate that the slip lines were manifestations of screw dislocations intersecting the surface.

The AFM studies provided further evidence, revealing that the slip lines were curved, *i.e.* highest at the centre of the slip line and lowest at the edges. Assuming that the slip lines were manifestations of screw dislocations would suggest that the slip lines were several hundred dislocations, all produced at the same point, *e.g.* a Frank-Read source. However, if the slip lines were produced by the prismatic dislocations it is unlikely that the

slip lines be curved. The AFM study also showed that the slip lines did not kink or jog suggesting, again, that they were produced by the same source.

Deformation Maps:

The original deformation map or BDT schematic diagram consisted of two lines (Brookes, E.J. 1992). One indicated the temperature at which plastic deformation was possible (the BDTT) and the other line indicated the pressure and temperature necessary to create plastic deformation above the BDTT (CRSS). Three Regimes of deformation were identified together with a ceiling above which the diamond would crack under these conditions. Regime I was below the BDTT where only elastic behaviour was seen and Regime II was above the BDTT, where a mixture of elastic and plastic behaviour was observed. Regime III indicated the conditions necessary to produce a fully plastic response. The upper cracking limit was calculated using Hertzian fracture mechanics. The numerous impressions made during the course of this investigation has allowed an expansion of the schematic, and a more precise identification of the boundary between Regimes II and III and a better definition of the upper cracking boundary.

To identify the Regime II/III boundary it was first necessary to quantify the term "fully plastic". For the purposes of this work, it was assumed that a fully plastic response was that of a dislocation rosette, with no cracking. As can be seen from figure 6.1 the Regime II/III boundary is similar in shape to that of the CRSS line but at higher temperatures and pressures. Two assumptions were made when producing this boundary. The first assumption was that at the high-pressure end of the line, it followed the form of the CRSS line. The second assumption made was that at high temperatures the pressure to produce a rosette would never equal the CRSS, therefore there would never be a point where Regime I (elastic) had a common boundary with Regime III, *i.e.* there is always some Regime II behaviour, however small.

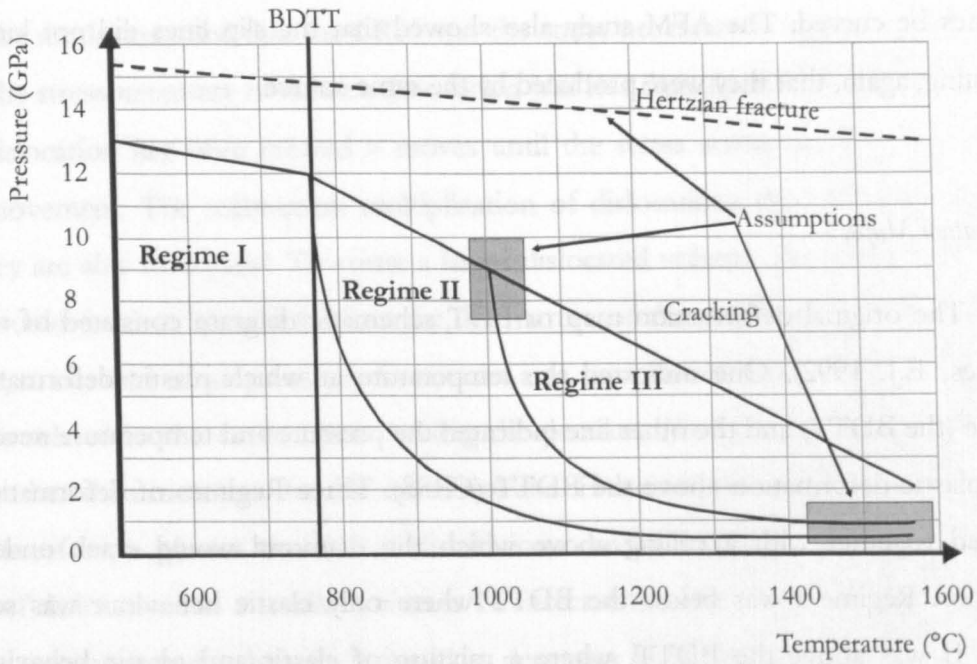

Figure 6.1. The revised brittle-ductile transition schematic, showing areas of assumption.

The upper cracking limit depicted in the diagram was established from experimental results. It was not the aim of this work to investigate the fracture of diamond at elevated temperatures and therefore the line is not exact. However, it does indicate that the line derived from Hertzian fracture mechanics was too high. It also shows that the pressure to produce cracks reduces rapidly as the temperature is increased. This is thought to be due to the interaction of dislocations within the deformed volume, creating sessile and piled-up dislocations, which can act as stress concentrators. It is assumed that as the temperature is lowered the pressure to produce brittle fracture will increase to the figure indicated by Hertzian theory, *i.e.* the two lines will converge at lower temperatures.

Dwell time and impression creep:

During the course of these experiments it became clear that the diamond deformed in set pattern – the deformation 'story'. Regardless of the temperature (providing it was above the BDTT), simply increasing the pressure could induce the whole set of deformation levels. Equally, any deformation level could be achieved by keeping the pressure constant and increasing the temperature. A change in dwell time invoked a similar effect, *i.e.* increasing the dwell time increased the observed deformation level and impression creep was observed. Therefore, the effect of the dwell time on the BDT schematic was to reduce the temperatures and pressure necessary to produce a dislocation rosette and also dislocation induced cracking. The change in deformation with change in dwell time was more marked for lower temperatures and pressures, where only minimal plastic deformation was observed. An increase in dwell time in Regime II produced visibly

higher levels of deformation. For example, if the initial point was a few slip lines in the surface, extending the dwell time from 300s to 1000s produced significantly more slip that extended further than the compressive/tensile boundary around the contact boundary. At higher temperatures and pressures, when the expected response was a dislocation rosette, the effect of increasing the time was a deeper impression with higher pile-up. The overall area of the impression, including the rosette wings lengths was not significantly increased.

On loading, the highest point of resolved shear stress is a certain distance below the surface of the specimen. Therefore, the initial dislocations and all the subsequent dislocations are also at a distance below the surface. This means that with increased time under load, dislocations are able to expand until they reach the surface and can be imaged. In addition, as the observed slip steps are produced by hundreds of dislocations, from the same source, an incubation time is needed before the dislocations are numerous enough to produce a high enough slip step to be seen optically. The reason why the creep process is seen to slow down at the higher levels of strain may be because the dislocations interact with each other to produce a barrier to further deformation. This would suggest significant work hardening of the diamond below the impressor. Considering the number of dislocations that must be initiated to produce the observed levels of strain, it is not surprising that the deformed volume becomes filled with sessile dislocations. If this were the case it would suggest that at 1400°C the dislocations are unable to cross slip *i.e.* at 1400°C stage III work hardening has not been reached. This is further supported by the fact that the slip lines at the surface are not jogged. If the dislocations were able to cross slip they would relieve piled-up dislocations and multiple cross slip would initiate further dislocations, producing more deformation. Equally, by using the deformation modelling in chapter 4, it can be seen that if the volume through which dislocations are able to expand is fixed, then subsequent dislocation initiation would only fill up that volume. On the surface, this would be observed as a reduction in the strain rate as the dislocation area ceases to expand. On the other hand, the amount of strain may only be perceived to slow down as the level of strain is not calculated by the number of dislocations initiated but by the size of the impression.

Nitrogen content:

The effect of nitrogen content on plastic deformation of synthetic diamond is twofold:

- At lower temperatures, reducing the nitrogen content increases the temperature needed to produce plastic deformation (BDTT). Above the BDTT, the trend continues and lowering the nitrogen content results in higher temperatures and pressures needed to cause plastic deformation.

- At higher temperatures (>1300°C) the opposite is observed. Reducing the nitrogen content increases the extent of plastic deformation, for these experimental conditions. Furthermore, the deep impressions introduced into the low nitrogen samples at temperatures above 1300°C have formed very large rosettes, *i.e.* the dislocation rosette covers a greater area and the 'pile-up' is higher.

At the lower experimental temperatures, (≈ 750°C – 1300°C) the presence of nitrogen appears to have the effect of lowering the stress necessary to create and move dislocations. This may be due to the misfit stress concentration created by a nitrogen atom substituted for a carbon atom. Lang et al (1991) carried out investigations into the lattice dilation caused by dispersed single substitutional nitrogen. It was found that the volume occupied by a nitrogen atom was 1.41 times that of the carbon atom. It is possible that the stress concentration caused by this mismatch may be sufficient to act as a nucleation site for dislocations. It has also been shown that when a {110} growth sector, with virtually no nitrogen, is adjacent to a {111} growth sector containing ~88ppm N, the mismatch between lattice parameters is sufficient to produce a residual stress of 7GPa (Lang, 2000). Although the mismatch between growth sectors produces a significant residual stress, there was no evidence of dislocations emanating from growth sector boundaries or that they played a direct role in initiating the deformation observed. However, the residual stress inherent in the crystal may mean that a lower stress is required to initiate slip than would be needed in an otherwise relatively stress free crystal.

At the higher temperatures, the pressure exerted far exceeds the critical resolved shear stress of the crystal regardless of the nitrogen content, and therefore it can be assumed that dislocations have been created and are quite mobile. Here the dispersed nitrogen appears to act as barrier to dislocations as they move through the crystal under the action of the applied stress.

Profiling:

A number of optical techniques were used to map deformation profiles of four different diamond samples to provide a better understanding of the process of plastic deformation and of the effect of nitrogen concentration on that process. Four impressions, made using a Si_3N_4 impressor at 1400°C under a load of 115N for a dwell time of 5 minutes, were mapped. Each sample had a different nitrogen content (natural IIa, synthetic (HPHT) 100, 650, and 850ppm N). These conditions were selected for this study in order to investigate significant plastic deformation without producing any cracks in the specimens.

The impressions were profiled using optical microscopy, spectroscopy, etching and atomic force microscopy (AFM). The optical techniques and dislocation etching techniques were used to quantify the level of deformation produced in each sample. The spectroscopy was used to gain qualitative information about the defect populations, the residual stress and the disorder within the crystal. AFM was used to gain an insight into the mechanism and state of the pile-up in the rosette arms.

The optical micrographs confirmed that in each case, significant deformation was produced without associated cracking. As the nitrogen content was increased the amount of observed deformation was reduced in that the depth of the impression, the height of the pile-up and the length rosette arms were all reduced as the nitrogen content was increased. This result was confirmed by the birefringence studies, where the extent of the strain field clearly showed that the deformed area for the 100ppm N sample was significantly larger than the 850ppm N sample. In the previous section, the effect of nitrogen concentration was discussed with respect to the pinning of dislocations by the nitrogen. Here the same effect can be seen. Clearly the dislocations in the low nitrogen diamond were able to move a greater distance away from the contact area indicating that the pinning ability of the nitrogen was less effective. In the highest nitrogen sample, however, it can be seen that dislocations were created but were unable to move any significant distance away from the contact area, as they appeared to be pinned almost immediately by the dispersed nitrogen atoms.

The level of deformation observed in the 100ppm N sample was certainly the most extensive and the rosette was a different shape to the higher nitrogen content samples. The rosette arms were tear-drop shaped, instead of elliptical, with the long axis parallel to the tangent of the contact area. This may be due to a more even distribution of the intersecting slip that produces the pile-up. In the other samples the pile-up is formed predominantly by slip lines that are parallel to the tangent of the contact area, producing the elliptical shape.

If the slip lines perpendicular to the parallel slip lines were numerous enough it would elongate the ellipse into a teardrop.

In most cases, the natural IIa sample did not fully fit the nitrogen trend observed in type Ib synthetic diamond. The deformation observed was less than the 100ppm N sample but more than the 650ppm N sample. As can be seen from the birefringence micrograph, this was heavily dislocated, with dislocations relaxed into a mosaic formation. The existence of these dislocations prior to impression would have served to inhibit the movement of the dislocations produced by the impression. Indeed it is likely that the mosaic of dislocations had a work hardening effect on the diamond. The effect of increasing the level of nitrogen to 650ppm N or greater clearly exceeds that of the work-hardening effect observed in type IIa diamond.

The cathodoluminescence (CL) micrographs showed that the 575nm (N-V) centre was produced in nitrogen containing diamond and was closely associated with slip. The 100ppm N sample did not show any H3 (N-V-N) CL, therefore, the 575nm CL appeared to be more intense. Although this may be the case, caution must be taken as CL is a competitive process and in the absence of the H3 defect all of the cathode energy is available for the 575nm defect to luminesce. In addition, the green of the H3 defect and the yellow/red of the 575nm defect would mean that it would be difficult to obtain good contrast. The absence of the H3 in the 100ppm N sample on the other hand leaves a black background, which gives a very good contrast to the yellow/red 575nm CL.

The measurements of the 1.945ev and H3 defects using photoluminescence spectroscopy (PL) showed that in the nitrogen containing diamonds the 1.945ev defect was created by the plastic deformation. The area covered by the induced 1.945ev defects follows a rough cruciform shape, which correlate with the areas of deformation calculated using the optical techniques. The H3 defect intensity map did not show the same results and the maps did not reveal a cruciform shape, although the contact area can be seen as roughly circular. The maps also showed that the intensity of the H3 defect was reduced to zero at the centre of the impressions, implying that the H3 has been annihilated or suppressed. The 100ppm N sample did not show any background 1.945ev PL indicating that all of the recorded 1.945ev PL was due to plastic deformation. Both the 650 and 850ppm N samples showed a background intensity, however the PL recorded at the impressions was significantly higher than the background values. The CL result showing that the 100ppm N sample did not have any H3 centres was confirmed by the PL results. As expected, the natural IIa sample did not show any 1.945ev or H3 PL.

The CL and PL results imply that the 575nm and 1.945ev centres are created by plastic deformation, whilst the H3 centre is destroyed. The creation of the 575nm and 1,945ev centres is probably due to non-conservative dislocation motion. When a dislocation climbs it either releases or absorbs a vacancy. At temperatures above 800°C it has been shown that a vacancy can be trapped at a substitutional nitrogen site to produce an N-V, 1.945ev complex (Du Preez, 1965, Davies and Hamer, 1976b). It is assumed that the 575nm defect is created in the same manner, but when a neutral rather than a negatively charged vacancy combines, explaining why the 575nm and 1.945ev defect are so strongly associated with the slip lines. The vacancies produced are highly mobile and highly reactive, therefore they will only be able to move very short distances before either recombining or combining with a nitrogen atom, *i.e.* the 575nm luminescence and 1.945ev defects are an indirect consequence of plastic deformation.

The reason for the H3 annihilation cannot be easily explained. The behaviour of luminescence defects at high temperatures is very complex, with defects combining and separating almost at random. For instance, H3 absorption in type IaA diamonds decreases by a factor of 3 when annealed between 800° and 1500°C, but the H3 intensity is increased by a factor of 6 when the same experiment is carried out on type IaB samples (Collins, 2000). Therefore it is difficult to predict whether the H3 defect has been destroyed by dislocation/vacancy interaction, or by another process. Although the PL maps do strongly suggest that in this case dislocation activity played a large role. Another consideration is that the photoluminescence response has simply been quenched by the heat treatment, as happens with cathodoluminescence in MgO (Chaudhri *et al* 1980).

The implications for the effect of defect populations on the plasticity of diamond are equally ambiguous. If the single substitutional nitrogen atom has such a significant effect on the plasticity of diamond, it is thought that defects that are larger and more reactive should have a larger effect. The ambiguity of the effects of defect populations is borne by the fact that diamond only shows signs of plasticity at temperatures higher than 750°C. At these temperatures, the defects concerned become mobile and interact with one another. The schematic diagram shown in figure 6.2 shows the brittle-ductile transition diagram over laid by lines indicating the mobility and interaction for some of the defects concerning type Ib diamond.

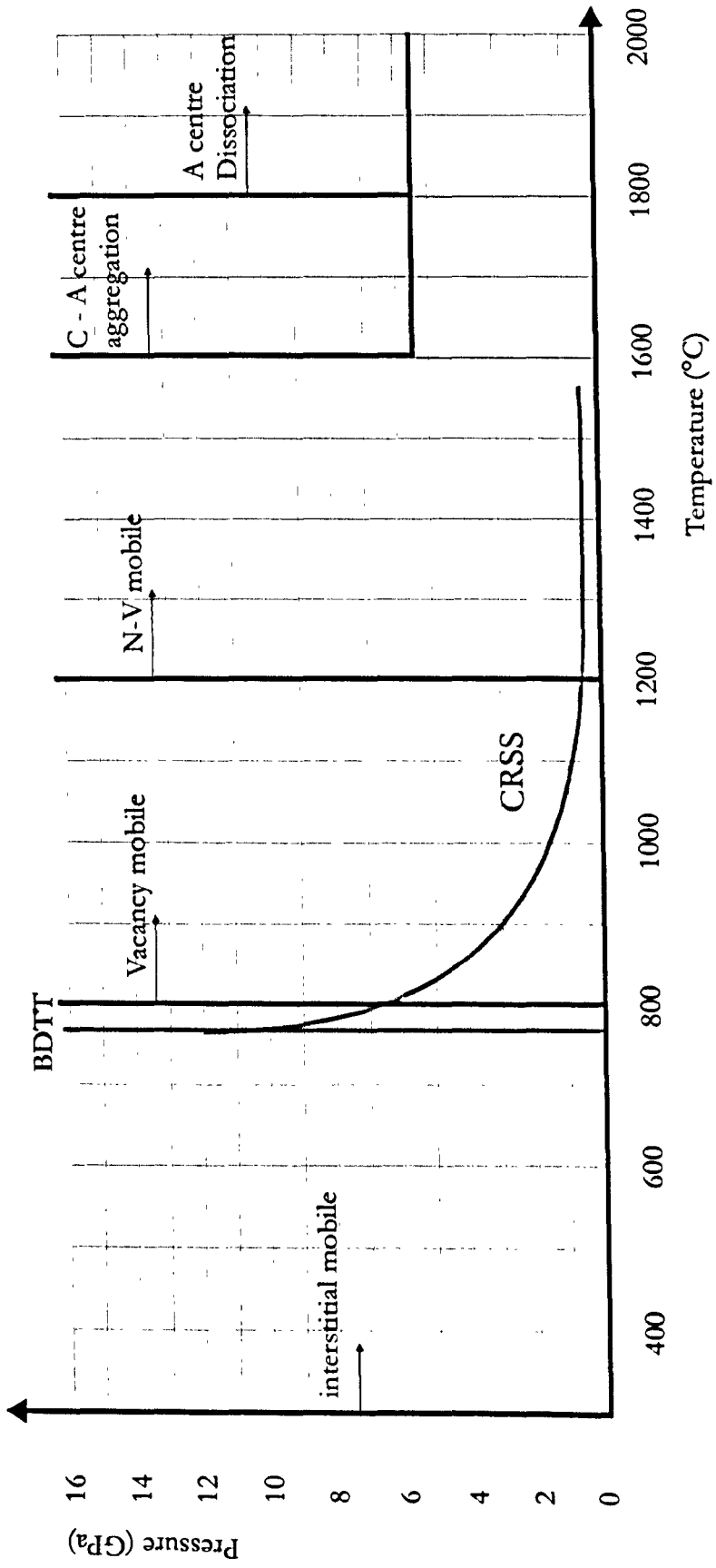

Figure 6.2. Schematic diagram representing the brittle-ductile transition and the mobility/interaction of some of the defects seen in type Ib diamond.

As can be seen from the diagram, in the temperature range where diamond plasticity is possible, both the interstitial and vacancy are mobile. At 1400°C, the N-V defect is also mobile. The mobility of the defects means that there are many possible reactions in addition to the simple interaction with a dislocation. For instance, the creation of Cottrell atmospheres would either drag moving dislocations or relieve the stress surrounding those that are piled-up. There is also evidence to suggest that defect mobility is increased by the presence of dislocations, a confining pressure and other impurities. For instance, it has been shown that the presence of vacancies enhances the aggregation of C centres into A centres, which do not aggregate unless there is a confining pressure of at least 5GPa (Collins, 1980). Furthermore, the aggregation of nitrogen has not been seen in {100} growth sectors of synthetic diamonds at 1600°C but it is readily seen in {111} growth sectors, where there are an appreciable amount of transition metal impurities (Watkins *et al* 2000).

In addition to the defect maps, profiles of the residual stress and the lattice disorder of the impressions were mapped using data taken from the position and shape of the Raman peak. The maps showed that the residual stress around the impressions was compressive, but became more tensile towards the centre of the impressions. The intensity values showed that as the nitrogen content was lowered the overall residual stress was increased. In the 850ppm N sample the residual stress was found to be tensile at the centre of the impression. The FWHM maps showed that the lattice disorder was reduced towards the centre of the impression and with lower nitrogen content. Both the intensity and FWHM contours of the 650ppm N sample map can be seen to resemble the rosette formation, however the high stress lobes are in <100> rather than the <110> directions of the pile-up arms of the rosette.

During deformation, the models show that the stress beneath the impressor is of a compressive nature. However, after the load has been removed and the sample cooled, the values represented by the Raman peak shifts indicated that the residual stress beneath the impressor is tensile. As the crystal was deformed, a deep impression was produced, with a significant amount of material displaced as four pile-up lobes. The residual stress values may indicate that the material was displaced into the pile-up lobes in such a manner that the central portion of the impression was placed in tension. When the diamond was cooled to temperatures below the BDTT the tensile stresses were effectively "frozen in". This is supported by the compressive nature of the surrounding material. The values of highest residual stress are along <100> directions, particularly in the 650ppm N sample. This may

be due to the <110> pile-up lobes compressing the <100> valleys in-between each rosette arm.

In each case it is clear that the level of nitrogen within the lattice has had an effect on the residual stress and on the lattice disorder produced by impression. The highest values of residual stress were observed with the samples lowest in nitrogen. This correlates well with the previous images of the deformation produced showed that the level of deformation observed for the low nitrogen was also highest. These results, however, seem to contradict the FWHM results, which indicated that the lattice disorder was reduced towards the centre of the impression and furthermore, as the nitrogen content of the diamonds was reduced, the level of lattice disorder was reduced. It seems, therefore, that although dislocation movement produces appreciable lattice disorder, the presence of the nitrogen within the crystal produces a larger effect.

To investigate the nature of the pile-up, AFM was used to image small sections of the rosette arms for each sample. The results showed that with lower nitrogen concentration the number of interpenetrating slip lines increased. In fact, the average height of the slip steps increased with nitrogen content, as the number of slip steps decreased.

It is evident from the results that nitrogen plays a significant role in the plastic deformation mechanism. At low levels of pressure and temperature nitrogen atoms may be acting as stress concentrators, which aid the production of Frank-Read style sources. As the pressure and temperature are increased the capacity for dislocation production is also increased. With the nitrogen in the crystal lattice, dislocations are produced at the discrete sources. However, when the nitrogen level in the crystal is negligible there are also negligible numbers of dislocation sources. Therefore the stress level must be raised to a higher level before other, less effective stress concentrators can act as sources. These are more numerous, however, producing a greater number of slip lines. As the pressure and temperature conditions were the same for each level of nitrogen concentration, it can be assumed that the capacity to produce dislocations was also the same. This means that although a greater number of dislocation lines were produced when the nitrogen concentration was low, the number of subsequent dislocations each source could produce was also low. The high nitrogen samples on the other hand had a small number of sources, but each was able to produce a greater number of consecutive dislocations, thereby producing the higher step heights.

6.2 Conclusions

These studies on the plastic deformation of single crystal diamonds containing different levels of nitrogen support the following conclusions:

- Under these experimental conditions, the onset of plastic deformation (BDTT) is influenced by nitrogen content.

- Above the brittle-ductile transition temperature, the critical resolved shear stress is also influenced by nitrogen content.

- The level of nitrogen in the lattice in substitutional sites affects the conditions necessary to produce extensive plastic deformation.

- Impression creep of synthetic type Ib diamond occurs at temperatures just above the brittle-ductile transition temperature.

The way in which single crystal diamond deforms plastically when loaded with a soft impressor at high pressures and temperatures is not yet fully understood. However, work within this thesis has produced results that have provided further evidence that can be used to gain a greater insight into the mechanisms of plastic deformation. The soft impressor technique has allowed experiments to be carried out that have shown that the level of plastic deformation for a given set of results is sensitive to the levels of dispersed single substitutional nitrogen within the crystal lattice. The large range of techniques used to profile the plastic deformation has provided a unique insight into the possible reasons for that sensitivity. Although many results have been gained, it is obvious that the full answers to the questions asked within this thesis would benefit from further experimentation.

6.3 Future Work

- The onset of the BDTT has been shown to be sensitive to nitrogen. Profiles similar to those carried out on impressions made at1400°C are necessary to determine the effect of temperature and pressure on the defect population at low levels of plastic deformation.

- The brittle-ductile transition temperature, as stated in this work, was defined using a dwell time of 300s. However, results on the creep of diamond have indicated that if the experimental dwell times were increased, the temperature at which plastic deformation is observed would be reduced.

- The creep results also indicate that the creep process may change in mechanism as the experimental temperature is increased. More creep results would provide clearer evidence for such a change in mechanism.

- A line indicating the point at which the samples cracked was produced. It was not the intention to create cracks during the course of this experimental work. Further investigation into the brittle behaviour, both Hertzian and dislocation induced, is needed to identify this upper limit more accurately.

- As diamond is susceptible to localised plastic deformation, work-hardening and ultimately fracture under conditions of point loading, cycling the impressor at temperatures just above and just below the BDTT would provide an interesting assessment of mechanisms of fatigue wear in diamond.

- The high level of dislocation initiation with the course of these experiments introduces the question of work hardening. As with many other materials does the presence of dislocations within the crystal structure make it more difficult to produce further plastic deformation?

- It has been shown that the nitrogen content affects the plasticity of single crystal diamond. However, nothing is known about the effect of variation in nitrogen levels on polycrystalline, CVD diamond. In addition, what would be the effect of doping diamonds with an element that is smaller than carbon, such as boron?

References

Alexander, H. and Haasen, P., (1961) *Acta Metal.*, **9**, 1001

Andrade, E.N. da C., (1940) *Proc. Phys. Soc.*, **52**, 1

Bakul, V.N. and Loshak Mal'nev V.I., (1973) *Sint Almazy*, **6**,

Bardeen, J. and Herring, C., (1952) *Imperfections in Nearly Perfect Crystals*, Wiley

Barrett, C.S., (1952) *Imperfections in Nearly Perfect Crystals*, Wiley

Barry, J.C., Bursill, L.A., Hutchison, J.L., Lang, A.R., Rackham, G.M. and Sumida, N., (1987) *Phil. Trans. Roy. Soc. London*, **A321**, 361-401

Beachem, C.D., (1972) *Metall. Trans.*, **3**, 437

Becker, R., (1925) *Phys. Zeit.*, **26**, 919

Bergman, K., Stavola, M., Pearton, S.J. and Lopata, J., (1988) *Phys. Rev.*, **B37**, 2770

Berman, R. and Simon, F.E., (1955) *Zeitschrift fur Electrochemie*, **59**, 333-338

Bernholc, J., Antonelli, A. Del Sole, T. M. Bar-Yam, Y. and Pantelides, S.T., (1988) *Phys. Rev. Lett.*, **61**, 2689-2692

Bi, X.X., Eklund, P.C., Zhang, J.G., Rao A.M., Perry, T.A. and Beetz, C.P., (1990) *J. Mater. Res.*, **5**, 811-817

Bibby, D.M. (1982) *Chemistry and Physics of Carbon*, (ed. Thrower, P.A.) **18**, 1-91

Birnbaum, H.K., Grossbeck, M. and Gahr, S., (1974) *Am. Soc. for Metals*, 303

Bokii, G.B. and Kirova, N.F., (1975) *Sov. Phys. Crystal*,. **20**, 386-388

Bokii, G.B., Kirova, N.F. and Nepsha, V.I., (1979) *Sov. Phys. Dokl.*, **24**, 83-84

Borisenko, V.A., Grigorev, O.N., Mil'man, Yu. V., Trefilov, V.I., Yepifanov, V.I. and Kononenko, V.I., (1973) *Sint Almazy*, **6**

Bragg, W.L. and Nye, J.F., (1947) *Proc. Phys. Soc. London*, **A190** 474

Bragg, W.L. and Lomer, W.M., (1949) *Proc. Roy. Soc. London*, **A196**, 171

Brookes, C.A., (1972) *Nature*, **228**, 660-661

Brookes, C.A., O'Neill, J.B. and Redfern, B.A.W., (1971) *Proc. Roy. Soc. London*, **A322**, 73-88

Brookes, C.A. and Green, P., (1972) *Nature,* **263,** 760-762

Brookes, C.A. and Green, P., (1973). *Nature,* **246,** 119-122

Brookes, C.A. (1979) in *The Properties of Diamond,* (ed. Field J.E.) Academic Press, London 383-402

Brookes, C.A. (1984) in *Proc. Second Int Conf on Science of Hard Materials.* (ed. Almond E.A., Brookes, C.A. and Warren R.) R. Inst. Phys. Conf. Ser. **75,** 207-220

Brookes, C.A. and Ross, J.D.J., (1987) *Euro. App. Res. Reports,* **7,** 1159-1160

Brookes, C.A., Brookes, E.J., Howes, V.R., Roberts, S.G. and Waddington, C. P., (1990) *J. Hard. Mater.,* **1,** 3-24

Brookes, C.A. and Brookes E.J., (1991) *Dia. and Rel. Mater.,* **1,** 13-17

Brookes, C.A., (1992) in *The Properties of Natural and Synthetic Diamond,* (ed. Field, J. E.) Academic Press, London 515-547

Brookes, E.J., *Ph.D. Thesis* (1992) The University of Hull

Brookes, E.J., Collins, A.T. and Woods, G. S., (1993) *J. Hard Mater.,* **4,** 97

Bull, S.J., Page, T.F. and Yoffe, E., (1989) *Phil. Mag. Lett.,* **59,** 281-288

Burgermeister, E.A., (1980) *J. Phys.,* C13 L963-L968

Burgers, J., M., (1939) *Proc. Kon. Ned. Akad. Wetenschap.,* **42,** 293-378

Burnand, R.P., (1974) *Ph.D. Thesis,* The University of Exeter

Burns, R.C., Cvetkovic, V., Dodge, C.N., Evans, D.J.F., Rooney, M.T., Spear, P.M. and Welbourne, C. M., (1990) *J. Crystal Growth,* **104,** 257-279

Burns, R.C. and Davies, G.J., (1992) *Properties of Natural and Synthetic Diamond* (ed. Field, J.E.) Academic Press, London 395-423

Burns, R.C., Hansen, J.O., Spits, R.A., Sibanda, M., Welbourne, C.M. and Welch, D.L., (1999) *Dia. and Rel. Mater.,* **8,** 1433-1437

Castaing, J., Veyssiere, P., Kubin, P. and Rabier, J., (1981) *Phil Mag., A***44,** 6, 1407-1413

Chapman, J.G., (1999) *Diamond Conference,* Oxford

Charette, J.J., (1961) *J. Chem. Phys,.* **35,** 1906-1907

Chrenko, R.M., McDonald, R. S. and Darrow, K. A., (1967) *Nature,* **213,** 474-476

Chrenko, R.M., Strong, H.M. and Tuft, R.E., (1971) *Phil. Mag.* **23,** 313-318

Chrenko, R.M., (1973) *Phys. Rev.* **B7,** 4560-4567

Chrenko, R.M. and Strong, H.M., (1975) *Report No. 75CRD089, General Electric Company*

Chrenko R.M., Tuft, R.E. and Strong, H.M., (1977) *Nature,* **270**, 141-144

Chaudhri, M.M., Hagan, J.T. and Wells, J.K., (1980) *J.Mater. Sci.,* **15**, 1189-1193

Clark, C.D., Ditchburn, R.W. and Dyer, H.H., (1956) *Proc. Roy. Soc. London,* **A234**, 363-381

Cockayne, D.J.H., (1981) *Diffraction and Imaging Techniques in Materials Science,* **1**, 153-183

Collins, A.T., (1980) *J Phys C.,* **13,** 2641-1650

Collins, A.T. and Spear, P.M., (1982) *J. Phys.,* **D15**, L183-L187

Collins, A.T. and Spear, P.M., (1983) *J. Phys.,* **C16**, 963-973

Collins, A.T., Kanda, H. and Burns, R.C., (1990) *Phil. Mag.,* **B61** 797-810

Corbett, J.W., Deak, P., Ortiz, C. and Snyder, L.C., (1989) *J. Nucl. Mater.,* **169**, 179

Cottrell, A.H., (1953) *Dislocations and Plastic Flow in Crystals*, The Clarendon Press, Oxford

Cottrell, A.H., Hunter S.C. and Nabarro, F.R.N., (1953) *Phil Mag.*, **44**, 1064

Custers, J.F.H., (1952) *Physica*, **18**, 489-496

Custers, J.F.H., *Physica,* 20, 183-184 (1954)

Daniels, F. and Dunn, C., (1949) *Trans. Am. Soc. Metals*, **41**, 419-442

Dash, W.C., (1957) *Dislocations and Mechanical Properties of Crystals* Wiley, New York, 57

Davies, G., (1976) *J. Phys.,* **C9**, L537

Davies, G., Nazare, M.H. and Hamer, M.F., (1976a) *Proc. Roy. Soc. London,* **A351**, 245-265

Davies, G. and Hamer, M.F., (1976b) *Proc. Roy. Soc. London,* **A348**, 285

De Theije, F.K., Roy, O., Van der Laag, N.J. and Van Enckevort, W.J. P., (1999a) *Dia. and Rel. Mater.,* in Press

De Theije, F.K., Van der Laag, N.J., Plomp, M. and Van Enckevort, W.J.P., (1999b) *Phil. Mag.,* **A**

De Theije, F.K., (1999) *Personal Communication.* University of Nijmegen, Holland

DeVries, R.C., (1975) *Mat. Res. Bull.,* **10**, 1193-1200

Dodge, C.N., (1986) *Ph.D. Thesis,* University of Reading

Du Preez, L., (1965) *PhD. Thesis,* University of Witwatersrand

Dyer, H.B. and du Preez, L., (1965) *J. Chem. Phys.*, **42**, 1898-1906

Elam, C.F., (1936) *The Distortion of Metal Crystals,* Oxford

Evans, T and Phaal, C., (1962) *Proc. Roy. Soc. London,* **A270** 538-552

Evans, T. and Wild, R.K., (1965) *Phil. Mag.,* **12**, 479-489

Evans, T. and Sykes, J., (1974) *Phil. Mag.,* **29**. 135-147

Evans, T and Qi, Z., (1982) *Proc. Roy. Soc. London,* **A381**, 159-178

Faulkner, E.A., Whippey, P.W. and Newman, R.C., (1965) *Phil. Mag.,* **12**, 413-414

Frank, F.C., (1949) *Physica.,* **15**, 131

Frank, F.C., (1951) *Phil Mag.,* **42**, 809

Frank, F.C. and Read, W.T., (1950) *Symposium on Plastic Deformation of Crystalline Solids,* P.44.

Frenkel, J., (1926) *Zeit. Phys.,* **37**, 572

Friedel, J., Boulanger, C. and Crussard, C., (1955) *Acta Metal,*. **3**, 380

Friedel, J., *Dislocations,* (1964) Pergamon Press

Field, J.E., (1992a) in *The Properties of Natural and Synthetic Diamond,* (ed. Field, J. E.) Academic Press, London, 473-515

Field, J.E., (1992b) in *Properties of Natural and Synthetic Diamond* (ed. Field, J. E.) Academic Press, London

Greenland, K.M., (1937) *Proc. Roy. Soc.London,* **A163**, 28

Greenwood, P., (1998) *Ph.D. Thesis,* The University of Hull

Hall, H.T., (1970) *Rev. Sci. Instrum.,* **31**, 125-131

Hargreaves, F., (1928) *J. Inst. Mater.,* **39**, 301-335

Harris, T.K., (1997) *Ph.D. Thesis,* University of Hull

Harrison, P., (1973) *Ph.D. Thesis,* University of Exeter

Hirsch, P.B., Pirouz, P., Roberts, S.G. and Warren, P.D., (1985a) *Phil. Mag.,* **B52**, 759-774

Hirsch, P.B., Roberts, S.G. and Warren, P.D., (1985b) *Phil. Mag.,* **B52**, 761-786

Hirsch, P.B., Hutchinson, J.L. and Titchmarsh, J. M., (1986) *Phil. Mag.,* **A54**, L49-L54

Hirth, J.P., (1961) *J. App. Phys.,* **32**, 4, 700-707

Howes, V.R. and Tolansky, S., (1955) *Proc. Roy. Soc. London,* **A230**, 287-293, *ibid* 294-300

Hudson, P.R.W. and Tsong, I.S.T., (1977) *J. Mater. Sci.,* **12**, 2389-2395

Humble, P. and Hannink, R.H.J., (1978) *Nature,* **273**, 37-39

Joos, P., (1957) *Z. Angew. Phys.,* **9**, 556

Jones, D.A. and Mitchell, J.W., (1958) *Phil Mag.,* **3**, 1.

Kaiser, W. and Bond, W., (1959) *Phys. Rev.,* **115**, L857-863

Kanda, H., Oshsawa, T. and Fukunaga, O., (1989) *J. Crystal Growth,* **94**, 115

Khruschov, M.M. and Berkovich, E.S., (1951) *Ind. Dia. Rev.,* **11**, 42-49

Kisielowski-Kemmerich, C., Beyer, W. and Alexander, H., (1990) *unpublished*

Knoop, F. and Peters, C.G., (1945) *Ind. Dia. Rev.,* **5**, 103

Lang, A.R., Moore, M., Makepeace, A.P.W., Wierzchowski, W. and Welbourn, C.M., (1991) *Phil. Trans. R. Soc. London,* **A 337**, 497-520

Lang, A.R., (2000) *Diamond Conference, Queens' College, Cambridge*

Lee, M., DeVies, R.C. and Koch, E.F., (1984) in *Proc. Second Int Conf on Science of Hard Materials.* (ed Almond E.A., Brookes, C.A. and Warren R.) R. Inst. Phys. Conf. Ser. **75**, 181-205

Lightowlers, E.C. and Collins, A.T., (1976) *Diamond Research,* 14-21

Lightowlers, E.C. and Dean, P.J., (1964) *Diamond Research,* 21-25

Loladze, T.N., Bokuchava, G.V. and Davydova, G.E., (1967) *Zavododskaya Loaboratoriya,* **33**, 1187-1190

Loubser, J.H.N. and van Rynefeld, W.P., (1966) *Nature,* **211**, 517

Love, A.E.H., (1929) *Proc. Roy. Soc. London,* **A228**, 377-420

Lynch, S.P. (1986) *J. Mater. Sci.,* **21**, 692

Mackenzie, J.K, (1949) *Ph.D. Thesis,* University of Bristol

Mainwood, A., (1994) *Phys. Rev. B-Condensed Matter.,* **49**[12], 7934-7940

Mainwood, A. and Newton, M., (2000) Kings College, London, *Personal Communication*

Mao, H.K. and Bell, P.M., (1978) *Science* 2000, 1145-1147

Miyoshi, K., (1998) *Dia. Films and Tech.* **8**, 153-172

Myers, S.M., Baskes, M.I., Birnbaum, H.K., Corbett, J.W., DeLeo, G.G., Estreicher, S.K., Haller, E.E., Jena, P., Johnson, N.M., Kirchheim, R., Pearton, S.J. and Stavola, M.J., (1992) *Reviews of Modern Physics, Am. Phys. Soc.,* **64**, No.2, 559-617

Novikov, N.V., Sirota, Ju.V. and Malnev, V.I., (1991). *Proc. Int Conf. New Diamond Sci and Tech,.*

Novikov, N.V. and Dub, S.N., (1992) *Sverkhtverdye Materialy,* **14**, 5-11

Novikov, N.V., Dub, S.N. and Mal'nev, V.I., (1993) *J. Hard Mater.* **4**, 19-27

Novikov, N.V., Dub, S.N. Mal'nev, V.I., (1994) *Dia and Rel. Mater.,* **3**, 198-204

Nye, J.F., (1949) *Proc. Roy Soc. London,* **A198**, 191

Orowan, E.Z., (1934) *Phys.,* **89**, 605-634

Pankove, J. ,I., Carlson, D.E., Berkeyheiser, J.E. and Wance, R.O., (1983) *Phys. Rev. Lett.,* **51**, 2224

Pankove, J.I., Berkeyheiser, J.E. and Wance, R.O., (1984) *Appl. Phys. Lett.,* **45**, 1100

Pashley, D.W., Menter, J.W. and Basset, G.A., (1957) *Nature,* **179**, 752

Pfeffer, K.H., Schiller, P. and Seeger, A., (1965) *Phys. Stat. Solidi,* **8**, 517

Pirouz, P., Cockayne, D.J.H., Sumida, N., Hirsch, P.B. and Lang, A. R., (1983) *Proc. Roy. Soc. London,* **A386**, 241-249

Pospiech, J. and Gryziecki, J., (1970) *Arch. Hulm.,* **15**, 267-283

Roberts, S.G., (1988) *Phil. Mag.,* **A58**, 347-364

Robertson, R., Fox, J.J. and Martin A.E., (1934) *Phil. Trans. Roc. Soc.,* **A232**, 463-535

Ross, J.D.J., (1984) *Ph.D. Thesis,* The University of Exeter

Runciman, W.A. and Carter, T., (1971) *Solid State Commun.,* **9**, 315-317

Satoh, S., Sumiya, H., Tsuji, K. and Yazu, S., (1990) *Science and Tech of New Diamond,* 351-355

Schmid, E., (1924) *Proc. Int. Cong. App. Mech. Delft,.* 342

Schmid, E. and Boas, W., (1950) *Plasticity of Crystals* (translation of *Kristallplastizitat*)

Sellschop J.P.F., Renan, M.J., Keddy, R.J. and Mingay, D.W., (1977) *Int. J. Appl. Radiation and Isotopes,* **28**, 277-279

Sellschop, J.P.F., (1992) in *Properties of Natural and Synthetic Diamond* (ed. Field, J. E.) Academic Press, London

Silcox, J. and Hirsch, P.B., (1959) *Phil Mag.,* **4**, 72

Semenova-Tyan-Shanskaya, A.S., (1969) *Mashinovedeniye,* **1**, 120-121

Smallmann, R.E., Westmacott, K.H. and Coiley, J.A., (1959) *J. Inst. Mater.*, **88**, 127

Smith, W.V., Gelles, I.L. and Sorokin, P.P., (1959) *Phys. Rev. Lett.,* 2, 39-40

Sobolev, E.V., Lenskaya, S.V. and Lisoivan, V.I., (1968) *J. Struct. Chem.,* **9**, 917-920

Sobolev, E.V. and Lisoivan, V.I., (1972) *Sov. Phys. Dokl.,* **17**, 1142-1144

Sobolev, E.V., Litvin, Yu.A., Samsonenko, N.D., Il'In, V.E., Lenskaya, S.V. and Butuzov, V.P., (1969) *Sov. Phys.-Solid State,* **10**, 1789-1790

Stephenson, R.F., (1978) *Ph.D Thesis, University of Reading*

Strong, H.M. and Chrenko, R.M., (1971) *J. Phys. Chem.,* **75**, 1838

Sumiya, H., Toda, N. and Satoh, S., (1997) *Dia. Rel. Mater.,* **6**, 1841-1846

Sungawa, I., (1984) *Mater. Sci.of the Earth's Interior,* 303-330

Sunagawa, I., (1995) *J.Gemm.,* **24**, 7

Sutherland, G.B.B.M., Blackwell, D.E. and Simeral, W.G., (1954) *Nature,* **174**, 901-904

Taylor, G.I., (1934) *Proc. Roy. Soc. London,* **A 145**, 362

Taylor, G.I. and Elam, C.F., (1926) *Proc. Roy, Soc. London,* **A 112**, 337

Telling, R.H., (1999) *Ph.D. Thesis,* The University of Cambridge, (1999)

Thompson, N., (1953) P*roc Phys. Soc.,* **66B** 481

Trefilov, V.I., Borisenko, V.I., Grigor'ev, O.N. and Mil'man, Yu.V., (1975) *Sov. Phys. Dokl,* **19**, 464-466

Watkins, M., Mainwood, A.M. and Fisher, D., (2000) *Diamond Conference, Queens' College Cambridge*

Welbourn, C.M., Cooper, M. and Spear, P.M., (1996) *Gems and Gemmology*

Wilks, E. and Wilks, J., (1982) *Properties and Applications of Diamond*

Woods, G.S. and Lang, A.R., (1975) *J. Crystal Growth,* **28**, 215

Woods, G.S., Purser, G.C., Mtimkulu, A.S.S. and Collins, A.T., (1990a) *J. Phys. Chem.,* **51**, 1191-1197

Woods, G.S., van Wyk, J.A. and Collins, A.T., (1990b) *Phil Mag.,* **B62**, 589-595

van Wyk, J.A. and Loubser, J.H.N., (1980) *Diamond. Conference, Bristol*

Zhang, T.Y. Haasen, P., (1989) *Phil. Mag.*, **A60**, 15

PUBLICATIONS

Refereed Journals

T K Harris, E J Brookes and R D Daniel, *Journal of Refractory and Hard Materials*, **17**, (1999) 33-38

E J Brookes, J D Comins, R D Daniel and E M Erasmus, *Diamond and Related Materials*, 8, (1999) 1115

E J Brookes, R D Daniel, J D Comins, E M Erasmus, *Journal of Radiation Effects and Defects in Solids*, accepted for publication

T K Harris, E J Brookes and R D Daniel, *Diamond and Related Materials*, accepted for publication.

Published Conference Papers

T K Harris, E J Brookes and R D Daniel, "The Application of the Soft Impressor Technique to Problems of the Measurement of Creep in Covalent Materials" 6th International Conference on the Science of Hard Materials, Lanzarote, 1998

E J Brookes, J D Comins, R D Daniel and E M Erasmus, "A Study of Plastic Deformation Profiles of Impressions in Diamond" Diamond 99, Prague 1999

E J Brookes, R D Daniel, J D Comins, E M Erasmus, "Impressions in Type Ib Diamond Formed at Elevated Temperatures" International Conference on Defects in Insulating Materials, Johannesburg, South Africa, 2000

T K Harris, E J Brookes and R D Daniel "Comparison of the Creep Properties of Single Crystal and Polycrystalline Diamond Cutting Tool Materials" Diamond 2000, Oporto, 2000

Unpublished papers or posters presented at Conferences

E J Brookes, T Harris and R Daniel, "Dislocation Motion in Diamond" UK Diamond Conference, Bristol, 1997

E J Brookes, R Daniel and T K Harris, "Dislocations in Diamond" 6th International Conference on the Science of Hard Materials, Lanzarote, 1998

E J Brookes, R Daniel and T K Harris, "The Use of the Soft Impressor Technique in Determining the Flow Stress of Polycrystalline Diamond Cutting Tool Materials" UK Diamond Conference, Royal Holloway, London, 1998

E J Brookes, R Daniel and T K Harris, "Deformation in Diamonds Containing Different Levels of Nitrogen" UK Diamond Conference, Royal Holloway, London, 1998

E J Brookes, R Daniel, J D Comins and R M Erasmus, "Characterisation of the Plastic Deformation in Diamonds Containing Different Levels of Nitrogen" UK Diamond Conference, Oxford, 1999

E J Brookes, R D Daniel, J D Comins, and R M Erasmus "A Study of Plastic Deformation Profiles of Impression in Diamond" International Conference on Defects in Insulating Materials, Johannesburg, South Africa, 2000

E J Brookes and R Daniel, "Plasticity in Type Ib Diamond Deformed at Elevated Temperature" UK Diamond Conference, Cambridge, 2000

T K Harris, E J Brookes and R D Daniel, "The Effect of Time and Temperature on the Plastic Deformation of Type Ib Diamond and of a Polycrystalline Diamond Cutting Tool Material" UK Diamond Conference, Cambridge, 2000

L J Brown and E J Brookes and R D Daniel "Cumulative Deformation and Fatigue Fracture of Type Ib Diamond" UK Diamond Conference, Cambridge, 2000

R D Daniel and F K de Theije "Recent Observations on the Nature of Slip Steps in Plastically Deformed Diamonds" UK Diamond Conference, Cambridge, 2000

Papers in preparation

E J Brookes, L Brown, J D Comins, R D Daniel, and R M Erasmus – The Influence of Nitrogen Defect Concentration on Deformation Mechanisms in Synthetic Type Ib Diamond. *Journal of Applied Physics.*